A STUDY OF (p,d) REACTIONS ON THE EVEN Se ISOTOPES

by

Leonidas Odysseus Barbopoulos, M.Sc.

A Thesis submitted for the Degree of Doctor of Philosophy

at the Australian National University, Canberra.

March, 1976.

CONTENTS

ABSTRACT

Deuteron angular distributions from ^{76,78,80,82}Se(p,d) ^{75,77,79,81}Se reactions were measured using detector telescopes, from 15° to 80° at intervals of 2.5°, at an incident energy of 33 MeV.

Distorted wave Born approximation calculations were performed with the program DWUCK using optical parameters obtained from the literature. It was found that the theory can fit reasonably well the experimental angular distributions, especially at forward angles.

Angular distributions were measured for 88 states, from which ℓ assignments were made. Forty of these assignments were made for the first time in the present work. Confident assignments were made to the levels at 1484 keV and 1913 keV in ^{75}Se, 1717 keV in ^{77}Se, 1817 keV, 1964 keV and 2092 keV in ^{79}Se and 1812 keV, 2150 keV in ^{81}Se. Spectroscopic factors and experimental filling coefficients were extracted and compared to the theoretically calculated values. A total of 22 states were observed for the first time. Coriolis coupling calculations were performed and it was found that the model can account reasonably well for the low-lying positive parity states in all of the Se nuclei studied and in particular the $5/2^+$ and $7/2^+$ anomalous states with level spacings and spectroscopic factors that are in reasonably good agreement with the experimental data.

PREFACE AND ACKNOWLEDGEMENTS

The experiments described in this thesis were performed at the Australian National University using the Cyclograaff facility of the Department of Nuclear Physics. The work was done under the supervision of Dr J. Nurzynski and subsequently Dr D. Gebbie when Dr Nurzynski went on study leave in January 1976.

The thesis project was suggested by Dr Nurzynski and the experimental work was equally shared with him, Dr D.W. Gebbie, Dr C. Hollas and Dr M. Borsaru. Mr K. Aniol participated in the collection of half of the experimental data. The reduction of data to obtain experimental cross-sections and angular distributions was performed by the author.

The program code AUTOFIT used in the primary analysis of the experimental data to unfold peaks and determine peak areas was supplied by the Argonne National Laboratory and was adapted to the UNIVAC 1108 computer by Dr Gebbie.

The Coriolis coupling calculations were performed with the program code SNOOPY supplied by the Niels Bohr Institute and written by R.F. Casten and C.S. Newton.

Some of the work reported in this thesis has appeared in the following publications:

(1) One and two neutron pick-up reactions from ^{76}Se and ^{78}Se.

L. Barbopoulos et al. Bull.Am.Phys.Soc. 18 (1973) 1408.

(2) One and two neutron pick-up reactions from ^{80}Se.

L. Barbopoulos et al. Bull.Am.Phys.Soc. 19 (1974) 451.

It is a great pleasure to acknowledge Dr Nurzynski for his constant encouragement and guidance during the course of research. He constantly strove for clarity and insisted on focussing on what was important about the various stages of this research. For the pleasure of knowing him personally I am very fortunate. In addition I am grateful to Dr Gebbie who spent many hours reading the draft of this thesis and made very valuable suggestions and comments.

It is also a pleasure to acknowledge the many people who have provided assistance during the course of this work and especially Dr T. Ophel and Mr R. Ball who came many times at odd hours at night or weekends to help in running the cyclotron. I am also grateful to Mrs N. Campbell for typing the final version of this dissertation.

I would like to thank also my wife Stavriani for her assistance in composing tables and figures from computer outputs, and for her enduring love and encouragement.

Finally, I would like to thank Professors J.O. Newton and Sir Ernest Titterton for the opportunity to use the facilities of the Department of Nuclear Physics, and the Australian National University for the award of the Post-Graduate Research Scholarship without which I would not have been able to do this work.

No part of this thesis has been submitted for a degree in another university.

CHAPTER 1

INTRODUCTION

Information about the single particle structure of nuclear levels can be obtained from the study of one nucleon transfer reactions. In an A(p,d)B reaction the incoming proton picks up a neutron from the target nucleus A, leaving the residual nucleus B either in its ground state or in an excited state. Many of the properties of these states can be determined by studying the angular distributions of the outgoing deuterons. From the shape of the angular distribution which may be strongly dependent on the orbital angular momentum transferred to the nucleus, the shell model orbital from which the neutron originates may be determined.

Given a theory for a direct reaction mechanism such as the distorted waves Born approximation, a comparison can be made between the calculated and the experimental cross-sections. Such a comparison gives the spectroscopic factor $S(\ell,j)$, which is a measure of the extent to which the final state is described by a single particle or hole in a given orbital together with an inert core.

Spectroscopic information obtained from (d,p) reactions can be complemented by analogous measurements from (p,d) reactions. This may give a check on ℓ-transfer determinations and also gives an independent determination of occupational probabilities and centre-of-gravity energies. The precise determination of these quantities depends on the spectroscopic factors $S(\ell,j)$ which in turn are sensitive to the optical model parameters used in the DWBA calculations.

The odd neutron nuclei ^{75,77,79,81}Se are the subject of investigation in the present work, which studies the ^{76,78,80,82}Se(p,d) ^{75,77,79,81}Se reactions at 33 MeV proton energy.

The only spectroscopic information available from single neutron transfer reactions to the odd Se nuclei studied in the present work, comes from the $^{76,78,80}Se(d,p)\ ^{77,79,81}Se$ reactions of Lin [Li 65] at 15 MeV and from the $^{76}Se(d,t)^{75}Se$ reaction by Sanderson [Sa 73] at 18, 19 MeV. Lin also obtained a few levels from the $^{78,80,82}Se(d,t)^{77,79,81}Se$ reaction but did not measure angular distributions.

The level structure of ^{75}Se has also been studied with the $^{75}As(p,n\gamma)^{75}Se$ reaction by Sugimitsu [Su 74], Agarwal et al [Ag 73] and Finckh et al [Fi 70] and from the β-decay of ^{75}Br by Coban et al [Co 72]. Zell et al [Ze 75] studied the level structure and the rotational properties of ^{75}Se from the $^{72}Ge(\alpha,n\gamma)^{75}Se$ and $^{73}Ge(\alpha,2n\gamma)^{75}Se$ reactions. Rabinstein [Ra 71] has provided level information and assigned some spins in ^{79}Se and ^{81}Se from the $^{78,80}Se(n,\gamma)^{79,81}Se$ reactions. Sarantites [Sa 69] and Braga and Sarantites [Br 73] have also provided information on ^{77}Se by studying the γ-rays following the β-decay of ^{77}Br.

In the Se nuclei the valence neutrons and protons (Z = 34, N = 42 - 48) are filling the $2p_{3/2}$, $1f_{5/2}$, $2p_{1/2}$ and $1g_{9/2}$ subshells. The main transitions expected therefore should be those corresponding to the removal of a neutron from one of the above orbitals. States containing configurations from the almost filled $2p_{3/2}$ and $1f_{5/2}$ subshells are expected to be very weakly excited or not observed at all in a (d,p) reaction. For example Lin in his study of the Se nuclei through the (d,p) reaction observed only three $\ell = 3$ transitions in

^{77}Se, one in ^{79}Se, two in ^{81}Se and a doubtful one in ^{83}Se. Such states however have a much higher probability of being observed in a (p,d) reaction. The (p,d) reaction will provide an almost direct measure of the shell model configurations present in the ground state wave function of the target nucleus. Such a study will have an advantage over a similar study performed through a (d,p) reaction, since in the latter the neutron may be left in an unoccupied configuration and therefore more levels are expected to be excited.

Nuclei in the Se mass region cannot be fully described with any known model. Because of the large number of particles (or holes) outside the nearest closed shell and the large number of available orbitals, no full shell-model calculations have yet been reported. It was originally thought that the level structure of the even Se nuclei should be well explained by the vibrational model [Sc 55]. However Barrette et al [Ba 74] have shown that the even Se nuclei are not described well by the simple vibrational picture. The ratios

$$\frac{B(E2; J_i \rightarrow 2^+)}{B(E2; 2^+ \rightarrow 0^+)}$$

are consistently smaller than those predicted by the vibrational model, where $J_i = 0^{+'}$, $2^{+'}$ and 4^+, except in ^{74}Se. There are also easily observable crossover transitions from the second $2^{+'}$ state to the ground state.

During recent years, Lieder and Draper [Li 70], McCauley and Draper [Mc 71], Wyckhoff and Draper [Wy 73] and Nolte et al [No 75] investigated the even-even Ge, Se and Kr nuclei with heavy ion reactions and found quasi-rotational bands up to spin 10^+. The large moment of inertia determined for these bands indicate that the ground states of these nuclei may be deformed. Coupling a neutron to such a deformed core should stabilize the deformation and one could therefore expect the odd nuclei in this mass region to be also deformed.

The anharmonic vibrator model is also able to describe such quasi-rotational bands as have been seen in this region by heavy ion reactions. Holzwarth and Lie [Ho 72, Li 75] used such a model to describe ^{76}Se and ^{78}Se and obtained good agreement between the calculated and experimental levels below 2.5 MeV. They also calculated quadrupole moments and B(E2) values which agree reasonably well with the experimental values. Another problem that remains in the interpretation of the nuclei in this mass region is the low-lying $5/2^+$ and $7/2^+$ levels that appear in all odd N, even Z nuclei throughout the $39 \lesssim N \lesssim 49$ region. These most likely are not single particle states since the $2d_{5/2}$ and the $1g_{7/2}$ orbitals should be filling at $N > 50$. Similar $5/2^+$ and $7/2^+$ low-lying states are also found in odd-Z, even-N nuclei in the $1g_{9/2}$ mass region. The presence of such states in all of these nuclei is somewhat surprising and have led to several theoretical attempts to explain their origins.

The first attempt to explain these states was made by Flowers [Fl 52] using the seniority coupling model. His calculations

predict that the $7/2^+$ level of the configuration $g_{9/2}^{3,5,7}$ is never the ground state. This is in conflict with the experimental findings where, for example, ^{79}Se has a ground state spin of $7/2^+$. This suggests a breakdown in the jj-coupling approximation. Kisslinger and Sorensen [Ki 63] coupled the $1g_{9/2}$ quasi-particle to the neighbouring 2^+ one-phonon state (QPC). The calculations were unable to explain cases such as ^{75}Se and ^{79}Se where the ground state spins are $5/2^+$ and $7/2^+$ respectively. These calculations were then improved by the inclusion of the quasihole-phonon coupling by Sherwood and Goswami [Sh 67] (EQPC) and by the extension of this latter approach by A. Goswami and O. Nalcioglu [Go 68] to include the quadrupole-quadrupole interaction. Again the extended calculations fail to explain fully the $5/2^+$ and $7/2^+$ states which often lie below the $9/2^+$ state. Because of the inability of the spherical shell model with appropriate residual interactions to adequately describe the odd proton nuclei in this region, Scholz and Malik [Sc 68] extended the successful use of the Coriolis coupling model in the $f_{7/2}$ shell to some of these nuclei. The model correctly predicts spins and parities for the low-lying states with the right energy spacing for all the nuclei considered.

Since the situation is analogous to the low-lying positive parity states that occur in the $1g_{9/2}$ odd neutron nuclei, the Coriolis coupling model has been applied with considerable success to ^{75}Se by Sanderson [Sa 73] and a number of odd neutron nuclei in the $1g_{9/2}$ mass region ($73 < A < 87$) by Heller and Friedman [He 75]. Both Sanderson, and Heller and Friedman obtained spins, parities and level spacings for the low-lying positive parity states that are in good agreement with the experimental data. Sanderson also calculated spectroscopic factors and the $5/2^+$ ground state quadrupole moment for ^{75}Se and Heller and Friedman calculated magnetic moments and quadrupole moments for the anomalous states which agree reasonably

well with the experimental values. Their calculations predict a prolate deformation in this mass region.

In the present investigation using 33 MeV protons, deuteron spectra and angular distributions were measured up to an excitation energy of about 3 MeV. From a comparison with DWBA calculations this investigation has confirmed a number of previously known results and in addition has given a large amount of new spectroscopic information including new levels, new ℓ assignments, spectroscopic factors, occupation probabilities and centre-of-gravity energies. The latter two are also compared with theoretically predicted values.

The present study may also help to clarify the origins of the low-lying $5/2^+$ and $7/2^+$ states that are characteristic of the Se nuclei. Available experimental evidence points to the fact that the Se nuclei are deformed and that such states can be interpreted as arising through the Coriolis coupling model. If such is the case then these states may have significant single particle components and should be excited in a (p,d) reaction. A further test of this model will be a comparison between the experimental and theoretical spectroscopic factors. Such a comparison is made in the present study.

Chapter 2 presents the DWBA theory and optical model concepts. The experimental techniques and absolute cross-section measurements are discussed in Chapter 3. Chapter 4 discusses the DWBA analysis, optical parameters used in the calculations and corrections applied. Chapter 5 presents the results from the (p,d) reaction. Angular distributions for new ℓ assignments are also discussed. Spectroscopic factors, filling coefficients and results from Coriolis

coupling calculations are presented in Chapter 6. The summary and conclusions of both the (p,d) reaction and Coriolis coupling calculations are given in Chapter 7. An outline of the Coriolis coupling theory is given in an appendix.

CHAPTER 2

ONE NUCLEON TRANSFER REACTIONS AND DWBA

The mechanism of a transfer reaction may be represented by the diagrams in Fig. 1. In the case of a pick-up reaction the outgoing deuteron carries information on the orbital angular momentum $\ell\hbar$ with which the neutron has left the nucleus.

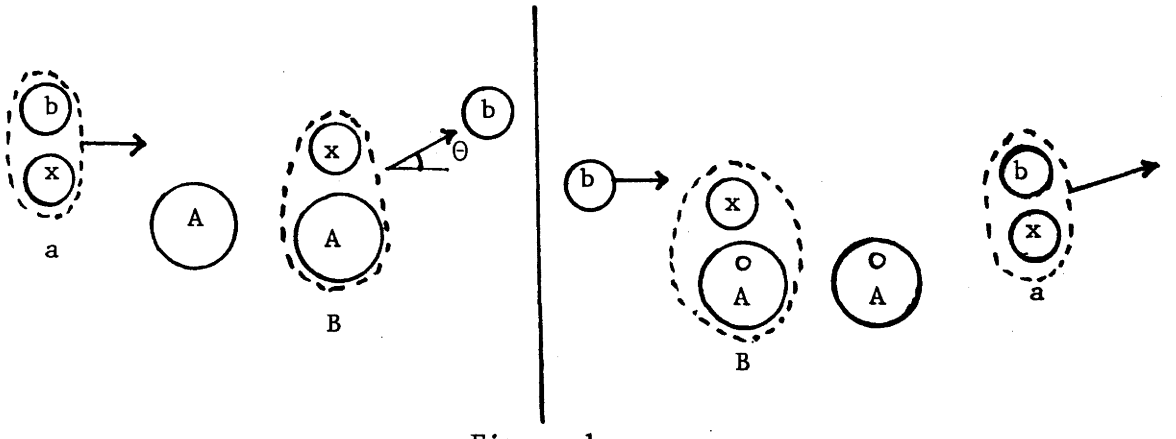

(a) Stripping

Figure 1

(b) Pick-up

The angular distributions of the deuterons display maxima in the forward direction at angles that are characteristic of the angular-momentum transferred to the target nucleus.

From the general theory of scattering the differential cross-section for a transfer reaction is given by

$$\frac{d\sigma}{d\Omega} = \frac{\mu_a \mu_b}{(2\pi\hbar^2)^2} \left(\frac{k_b}{k_a}\right) \sum |S_{ab}|^2 \qquad (2.1)$$

where $d\Omega$ is an element of solid angle about the direction of k_b and S_{ab} is the reaction amplitude. For unpolarized beams, the summation $\sum$ indicates a sum over the z-components of the angular momentum in the final state and an average over those in the initial state such that

$$\frac{d\sigma}{d\Omega} = \frac{\mu_a \mu_b}{(2\pi\hbar^2)^2} \frac{k_b}{k_a} \frac{\sum_{M_A M_B M_a M_b} |S_{ab}|^2}{(2J_A+1)(2S_a+1)} \qquad (2.2)$$

2.1 Distorted Waves Born Approximation

The amplitude of the cross-section S_{ab} is given by the transition matrix from state a to state b as

$$S_{ab} = \langle \Phi_b(k_b) | V_{bx} | \Psi_a(k_a) \rangle \qquad (2.3)$$

where $\Phi_b(k_b)$ and $\Psi_a(k_a)$ are the wave functions in the exit and entrance channels respectively and V_{bx} is the interaction potential responsible for the transition.

If it is assumed that the incident and the emitted particles have no other interaction with the nucleus, they may be represented by plane waves before and after the interaction. Hence, the total initial and final wave functions are

$$\Psi_a(k_a) = \psi_a \exp(i\underset{\sim}{k}_a \cdot \underset{\sim}{r}_a)$$

$$\Phi_b(k_b) = \psi_b \exp(i\underset{\sim}{k}_b \cdot \underset{\sim}{r}_b) \qquad (2.4)$$

where ψ_a and ψ_b are the internal wave functions in the entrance channel (target plus incident particle) and exit channel (residual nucleus plus emitted particle) respectively. However, it was quickly noted that the predicted absolute cross-sections were too large. This is because the plane wave theory ignores other effects of the nuclear and coulomb potentials. These effects are taken into account by the distorted-wave Born approximation (DWBA) which gives a more accurate description of the reaction mechanism by using distorted waves instead of plane waves. The basic assumptions in the application of DWBA to direct transfer reactions are:

1. The projectile moves in the average field of the target. This field can be described by means of an optical potential and leads to a wave function identical to the one describing elastic scattering.

2. A nucleon is picked-up from a single particle orbital of the target or transferred to an empty single particle orbital in the target (stripping).

3. The reaction is treated as a direct process whereby it proceeds from the initial to the final state without passing through any intermediate states; hence, the assumption that the target nucleus or core is passive throughout.

4. The outgoing particle is acted upon by the optical potential of the final nucleus. This again is an elastic scattering problem.

The exact expression for the transition amplitude for the transfer reaction A(a,b) B in the DWBA [Ba 62] is

$$S_{ab} = \int d\underset{\sim}{r}_{aA} \int d\underset{\sim}{r}_{bB}\, \chi^{(-)*}_{bB}(\underset{\sim}{k}_b, \underset{\sim}{r}_{bB}) \langle b,B|V_{bx}|a,A\rangle \Psi_{aA}(\underset{\sim}{r}_{aA}) \tag{2.5}$$

where $\chi^{(-)}_{bB}$ describes the motion of b in the optical potential of B and Ψ_{aA} is the exact total wave function for a particle incident on nucleus A and outgoing waves in all other channels. If we assume that elastic scattering is the dominant process then in the Born approximation we may approximate Ψ_{aA} with $\chi^{(+)}_{aA}(\underset{\sim}{r}_{aA})$, a distorted wave describing the shape elastic scattering of the incident particles. The distorted waves amplitude then becomes

$$S_{ab} = \int d\underset{\sim}{r}_{aA} \int d\underset{\sim}{r}_{bB}\, \chi^{(-)*}_{bB}(\underset{\sim}{k}_b, \underset{\sim}{r}_{bB})\, \langle b,B|V_{bx}|a,A\rangle\, \chi^{(+)}_{aA}(\underset{\sim}{k}_a, \underset{\sim}{r}_{aA}). \quad (2.6)$$

The matrix element $\langle b,B|V_{bx}|a,A\rangle$ expresses those parts of the calculation of S_{ab} which involve the internal states, and which do not concern the scattering wave functions $\chi^{(+)}_a(\underset{\sim}{r}_{aA})$ and $\chi^{(-)}_b(\underset{\sim}{r}_{bB})$. As a result, the calculations of Eq. 2.6 are made easier. The matrix $\langle b,B|V_{bx}|a,A\rangle$ plays the role of the effective interaction between the elastic scattering states $\chi^{(+)}_a(\underset{\sim}{r}_{aA})$ and $\chi^{(-)}_b(\underset{\sim}{r}_{bB})$ and contains all the information on nuclear structure, angular momentum selection rules, and the type of reaction being considered.

Taking the effective operator V_{bx} for the transition to be the interaction between the outgoing particle b and the transferred nucleon x, then the effective matrix element separates into a product of two disjoint form factors such that

$$\langle b,B|V_{bx}|a,A\rangle = \langle B/A\rangle\, \langle b|V_{bx}|a\rangle \quad (2.7)$$

with the nuclear form factor $\langle B/A\rangle$ independent of V_{bx}.

If we introduce coordinates into Eq. 2.6, then the transition matrix element can be written as

$$S_{ab} = \int d\underset{\sim}{r}_{aA} \int d\underset{\sim}{r}_{bB}\, \chi^{(-)*}(\underset{\sim}{k}_b, \underset{\sim}{r}_{bB})\, \phi^*_b(\sigma_b)\, \Phi_B(\xi_B, \sigma_x, \underset{\sim}{r}_{xA})\, V_{bx}(\underset{\sim}{r}_{bx})\, \phi_a(\underset{\sim}{r}_{xb}, \sigma_b, \sigma_x) \times$$
$$\Phi_A(\xi_A)\, \chi^{(+)}(\underset{\sim}{k}_a, \underset{\sim}{r}_{aA}) \quad (2.8)$$

where we denote the internal coordinates, including spin, of the residual nucleus B by ξ_B and its relative coordinate by $\underset{\sim}{r}_{xA}$; the internal coordinate of the reaction product b by σ_b and that of the transferred nucleon x by σ_x. The target nucleus A is then described by ξ_A and the projectile a is described by the internal coordinates σ_b, σ_x and the relative coordinate $\underset{\sim}{r}_{xb}$.

The functions $\chi^{(+)}_a$ and $\chi^{(-)}_b$ are the distorted waves. They are elastic scattering wave functions which describe the relative motion

of the pair (a,A) with relative momentum $\underset{\sim}{k}_a$ before collision, and the pair (b,B) with relative momentum $\underset{\sim}{k}_b$ after collision. They consist of plane waves plus spherically scattered incoming or outgoing waves given by

$$\chi^{(+)}(\underset{\sim}{k},\underset{\sim}{r}) \to e^{i\underset{\sim}{k}.\underset{\sim}{r}} + f(\theta,\phi)\frac{e^{ikr}}{r}$$

and $$\chi^{(-)}(\underset{\sim}{k},\underset{\sim}{r}) \to e^{i\underset{\sim}{k}.\underset{\sim}{r}} + f^*(\pi-\theta,\pi+\phi)\frac{e^{-ikr}}{r} \quad .$$

They are obtained by solving Schrödinger's equation describing the relative motion of the projectile and target, and also of the residual nucleus and the outgoing particle. Hence

$$\left[\frac{-h^2}{2\mu_i}\nabla^2 + U(r)\right]\chi(\underset{\sim}{k},\underset{\sim}{r}) = E\chi(\underset{\sim}{k},\underset{\sim}{r}) \qquad (2.9)$$

where μ_i is the reduced mass of the pair and U(r) is an optical model potential.

In order to evaluate Eq. 2.9 we need to expand the distorted waves in terms of partial waves such that

$$\chi^{(+)}_{aA}(\underset{\sim}{k}_a,\underset{\sim}{r}_a) = \frac{4\pi}{k_a r_a}\sum_{L_a M_a} Y^{M_a}_{L_a}(\hat{r}_a)Y^{*M_a}_{L_a}(\hat{k}_a)u^a_{L_a}(\underset{\sim}{k}_a,\underset{\sim}{r}_a)i^{L_a}$$

and $$\chi^{(-)}(\underset{\sim}{k}_b,\underset{\sim}{r}_b) = \frac{4\pi}{k_b r_b}\sum_{L_b M_b} Y^{M_b}_{L_b}(\hat{r}_b)Y^{*M_b}_{L_b}(\hat{k}_b)u^b_{L_b}(\underset{\sim}{k}_b,\underset{\sim}{r}_b)i^{-L_b} \qquad (2.10)$$

where $u(\underset{\sim}{k},\underset{\sim}{r})$ is a solution of the radial Schrödinger equation with central potential U(r).

2.2 Nuclear Form Factor

In order to evaluate the nuclear form factor <B/A> we make the fractional parentage expansion for the ground state wave function of the residual nucleus in terms of the complete set of wave functions $\Phi^{M_p}_{J_p}(\xi)$ for the parent state J_p. This is written as

$$\Phi^{M_B}_{J_B}(\xi,\sigma_x,r_{xA}) = \sum_{j\ell J_p \mu M_p} \Theta_{J_B J_p}(j\ell)\Phi^{M_p}_{J_p}(\xi)\psi^{\mu}_{j\ell}(r_{xA},\sigma_x) <J_p M_p j\mu|J_B M_B> \quad (2.11)$$

in which the $\Phi^{M_p}_{J_p}(\xi)$ are eigenstates (normalized and totally anti-symmetric) for the j^{n-1} nucleons coupled to J_p and $\psi^{\mu}_{j\ell}(r_{xA},\sigma_x)$ is a normalized single particle wave function. The Clebsch-Gordan coefficient takes care of the angular momentum coupling and $\Theta_{J_B J_p}(j\ell)$ is the fractional parentage coefficient, where

$$\sum_{J_p} \Theta^2_{J_B J_p}(j\ell) = 1 \quad (2.12)$$

and $$\mu = M_B - M_A \text{ and } j = J_B - J_A \quad . \quad (2.13)$$

Substituting Eq. 2.11 into the expression for the nuclear form factor gives

$$< B/A > = \sum_{J_p j_\mu} \Theta_{J_B J_p}(j\ell) <J_p M_p j\mu|J_B M_B> \psi^{\mu}_{j\ell}(r_{xA},\sigma_x) \int \Phi^{M_p}_{J_p}(\xi)\Phi^{M_A}_{J_A}(\xi) d\xi$$

$$= \sum_{j\mu} <J_A M_A j\mu|J_B M_B> \psi^{\mu}_{j\ell}(r_{xA},\sigma_x) \Theta_{J_B J_p}(j\ell) \quad (2.14)$$

which is the overlap integral for the transition to a definite parent state $J_p = J_A$.

If we now assume that the nucleon x moves within nucleus B with total angular momentum j, orbital angular momentum ℓ and spin s, then $\psi^{\mu}_{j\ell}(r_{xA},\sigma_x)$ may be expanded further in terms of shell model single particle wave functions for the orbit (n,ℓ,j) so that

$$\psi^{\mu}_{j\ell}(r_{xA},\sigma_x) = \sum_{\ell s m} <\ell s m\ m_a - m_b|j\mu> R_{\ell j}(r_{xA}) i^{\ell} Y^m_{\ell}(\hat{r}_{xA})\phi_x(\sigma_x) \quad (2.15)$$

where $$m = M_B - M_A + m_b - m_a \quad .$$

Because the parity is given by $(-1)^{\ell}$ only one of the two possible $\ell = j \pm \frac{1}{2}$ values is allowed. Substituting Eq. 2.15 into Eq. 2.14 gives

$$\langle B/A\rangle = \sum_{\substack{j\mu s\\ \ell m}} \Theta_{J_B J_A}(j\ell)\ \langle J_A M_A j\mu | J_B M_B\rangle\ \langle \ell s m\ \mu-m | j\mu\rangle\ x$$

$$R_{\ell j}(r_{\sim xA})\, i^{\ell}\ Y_{\ell}^{m}(\hat{r}_{xA})\,\phi_x(\sigma_x) \quad . \tag{2.16}$$

The fractional parentage coefficient $\Theta_{J_A J_B}(j\ell)$ selects a particular nucleon x. If there are n identical nucleons within nucleus B, the cross-section is proportional to the spectroscopic factor

$$S(\ell sj) = n[\,\Theta(\ell sj)\,]^2 \tag{2.17}$$

where $\sqrt{S}$ is called the spectroscopic amplitude. The spectroscopic factor is the probability that the wave function for the residual nucleus $\Phi^{M_B}_{J_B}(\xi,\sigma_x,r_{\sim xA})$ can be expressed as a core in state (J_A,M_A) plus the particle x in a given single particle state $\psi^{\mu}_{\ell j}\ (r_{\sim xA},\sigma_x)$.

A similar expansion can be carried out for the projectile a such that

$$\phi_a(r_{\sim xb},\sigma_b,\sigma_x) = \phi_b(r_{\sim xb})\ \langle s_b m_b s_x m_x | s_a m_a\rangle\ \phi_x(\sigma_x)\phi_b(\sigma_b)a(s). \tag{2.18}$$

Substituting Eq.2.16 and 2.19 into Eq. 2.7 and integrating over $d\sigma_b$ and $d\sigma_x$ gives

$$\langle b,B|V_{bx}|a,A\rangle = \sum_{j\ell sm\mu} \langle J_A M_A j\mu | J_B M_B\rangle\ \langle \ell sm\mu-m | j\mu\rangle\ \langle s_b m_b s_x m_x | s_a m_a\rangle\ \times$$

$$R_{\ell j}(r_{\sim xA})\left[\, i^{\ell}\ Y_{\ell}^{m}(\hat{r}_{xA})\,\right]^{*} D(r_{\sim bx})\sqrt{\nu}\, a(s)\ \sqrt{S}\,(\ell sj) \tag{2.19}$$

where $D(r_{\sim bx}) = V_{bx}(r_{\sim bx})\phi(r_{\sim bx})$.

In the zero-range approximation $D(r_{\sim bx}) = D_o\delta(r_{\sim b}-r_{\sim x})$, which gives

$$D_o = \int dr_{\sim bx}\ V(r_{\sim bx})\phi(r_{\sim bx}) \,. \tag{2.20}$$

The zero range assumption has the physical meaning that the light reaction product b is assumed to be emitted at the same point at which particle a is absorbed. As a result Eq. 2.19 is reduced to a three-dimensional integral and this greatly facilitates the calculations. A

more complete calculation [Au 64] uses a "finite-range" function for D_o instead of the approximation in Eq.2.20. This reveals that the cross-sections have similar shapes to those given by the zero-range calculations but they differ in magnitude by approximately 20 percent for stripping reactions.

Substituting Eq.2.19 and 2.10 into Eq.2.6 and integrating over $d\underset{\sim}{r}_{aA}$ and $d\underset{\sim}{r}_{dB}$ [Ba 62] the reaction amplitude is given by

$$S_{ab} = \langle J_B M_B, s_b m_b, k_b | V_{bx} | J_A M_A, s_a m_a, k_a \rangle$$

$$= \frac{\sqrt{4\pi}}{k^2_b} \left(\frac{M_B}{M_A}\right)^2 \sum_{\ell s j m} \langle J_A j M_A M_B - M_A | J_B M_B \rangle \langle s_a s_b m_a - m_b | s m_a - m_b \rangle \times$$

$$(-1)^{s_b - m_b} \langle \ell s m \; m_a - m_b | j M_B - M_A \rangle \sqrt{2\ell+1} \quad \sqrt{v}\, a(s)\, D(\underset{\sim}{r}_{bx}) \times$$

$$\sqrt{S(\ell s j)}\; \beta^{\ell m}_{sj}(\theta) \qquad (2.21)$$

where $$\beta^{\ell m}_{sj}(\theta) = 4\pi \left(\frac{M_A}{M_B}\right) \frac{k_b}{k_a} \sum_{L_a L_b M_b} \langle L_b \ell M_b - m | L_a M_b - m \rangle$$

$$\langle L_b \ell 00 | L_a 0 \rangle i^{L_a - L_b - \ell} \left(\frac{2L_b+1}{2L_a+1}\right)^{\frac{1}{2}} Y^{M_b}_{L_b}(\underset{\sim}{k}_b)\; Y^{m-M_b *}_{L_a}(\underset{\sim}{k}_a) \times$$

$$\int d\underset{\sim}{r}\; U^b_{L_b}(k_b, r_b)\; R_{\ell s j}(r_{xa})\; U^a_{L_a}(k_a, r_a) \quad .$$

Substituting Eq. 2.21 into Eq. 2.2 then the differential cross-section for a stripping reaction becomes [Ba 62]

$$\frac{d\sigma}{d\Omega} = \frac{2J_B+1}{2J_A+1} \sum_{\ell s j} S(\ell s j) \frac{v a(s)^2}{2s+1} \left| \frac{D_o^2(r_{bx})}{1.018 \times 10^4} \right| \sigma_{\ell s f}\theta) \qquad (2.22)$$

where $$\sigma_{\ell s j}(\theta) = \frac{M_B^5 m_b m_a}{M_A^3 (m_a + M_A)(m_b + M_B)} \frac{9.268}{k_b^3 k_a} \sum_m \left| \beta^{\ell m}_{sj}(\theta) \right|^2 . \qquad (2.23)$$

The quantity $\sigma(\theta)$ involves all the radial integrals which contain all the angular and kinematic dependence of the reaction being studied. For a pick-up reaction B(b,a)A the cross-section is related to the corresponding stripping reaction A(a,b)B by the principle of

detailed balance such that

$$\left(\frac{d\sigma}{d\Omega}\right)_{\text{pick-up}} = \left(\frac{k_a}{k_b}\right)^2 \left(\frac{2s_a+1}{2s_b+1}\right) \left(\frac{d\sigma}{d\Omega}\right)_{\text{strip}} \tag{2.24}$$

which gives

$$\left(\frac{d\sigma}{d\Omega}\right)_{\text{pick-up}} = \left(\frac{2s_a+1}{2s_b+1}\right) \left[\frac{D_o^2(r_{bx})}{1.018\times10^4}\right] \sum_{\ell sj} \frac{\nu a(\ell s)}{2s+1} S(\ell sj)\sigma_{\ell sj}(\theta) \ . \tag{2.25}$$

For a (p,d) or (d,p) reaction D_o^2 can be estimated by taking the interaction potential $V_{pn}(r_{pn})$ to be the binding energy of the deuteron, $\phi_d(r_{pn})$ then satisfies the Schrödinger equation

$$(\nabla^2-\alpha^2)\phi_d(r_{pn}) = \frac{2\mu}{\hbar^2} V(r_{pn})\phi_d(r_{pn}) \tag{2.26}$$

where $\varepsilon = \alpha^2\hbar^2/2\mu$ is the binding energy of the deuteron and μ is the reduced mass in proton units. If we choose the correct asymptotic form for $\phi_d(r_{pn})$ such as

$$\phi_d(r_{pn}) = \sqrt{\frac{\alpha}{2\pi}} \frac{e^{-\alpha r}}{r} \tag{2.27}$$

then the solution of Eq. 2.26 gives

$$D_o^2 = \frac{8\pi\varepsilon^2}{\alpha^3} = 8\pi\left(\frac{\hbar^2}{2\mu}\right)^{3/2} \varepsilon^{1/2} = 2.38 \times 10^3 \ \frac{\varepsilon^{1/2}(\text{MeV})}{\mu^{3/2}} \ . \tag{2.28}$$

For ε = 2.23 MeV and μ = ½ (p.m.u.)

$$D_o^2 = 1 \times 10^4 \ \text{MeV}^2 \ \text{fm}^3 \ . \tag{2.29}$$

Alternatively, an improved estimate of D_o is obtained with the use of the Hulthén wave function

$$\phi_d(r) = \left[\frac{\alpha\beta(\alpha+\beta)}{2\pi(\alpha-\beta)^2}\right]^{1/2} \left[\frac{e^{-\alpha r} - e^{-\beta r}}{r}\right] \tag{2.30}$$

which gives

$$D_o^2 = \frac{8\pi\varepsilon^2}{\alpha^3} \left(\frac{\alpha+\beta}{\beta}\right)^3 \tag{2.31}$$

for $\beta = 7\alpha$, $D_o^2 = 1.56 \times 10^4$ MeV^2 fm^3.

2.3 Information obtained from the reactions

Nuclear structure information may be obtained using the conservation of angular momentum

$$\underset{\sim}{J}_B = \underset{\sim}{J}_A + \underset{\sim}{\ell} + \underset{\sim}{s} \tag{2.32}$$

where $\underset{\sim}{J}_B$ is the total angular momentum of the residual nucleus, $\underset{\sim}{J}_A$ is the total angular momentum of the target, $\underset{\sim}{\ell}$ is the orbital angular momentum transferred to the outgoing particle and $\underset{\sim}{s}$ its intrinsic spin. In the case of an even-even target $J_A = 0$ and

$$\underset{\sim}{J}_B = \underset{\sim}{\ell} + \underset{\sim}{s} \ . \tag{2.33}$$

The orbital angular momentum $\underset{\sim}{\ell}$ of the transferred nucleon may be determined from the shape of the angular distribution. The conservation of parity also imposes the restriction

$$\Pi_A \Pi_B = (-1)^{\ell} \tag{2.34}$$

on the parity Π_B of the residual states.

The relation in Eq. 2.33 restricts the value of the transferred $\underset{\sim}{j} = \underset{\sim}{\ell} + \underset{\sim}{s}$ to

$$|J_B - J_A| \leqslant j \leqslant |J_B + J_A| \ . \tag{2.35}$$

Assuming that a single neutron is transferred Eq. 2.22 can be re-written in the form

$$\frac{d\sigma(\theta)}{d\Omega} = S(\ell s j)\sigma_D(\theta) \ . \tag{2.36}$$

By measuring the differential cross-section for a pick-up or stripping reaction, and comparing it to the theoretically calculated factor $\sigma_D(\theta)$ which depends on the detailed mechanism of the reaction and contains all the angular and energy dependence, the factor $S(\ell sj)$ may be determined.

2.4 The Optical Potential

The optical potential U(r) used is given by

$$U(r) = -V(r) - iW(r) + V_c(r) - V_{so}(r)\, \underset{\sim}{L}.\underset{\sim}{\sigma} \qquad (2.37)$$

where r is the distance between the incident particle and the centre of the target nucleus in the centre of mass system, $V_c(r)$ is the Coulomb potential, V(r) and W(r) are the real and imaginary central potentials respectively, $V_{so}(r)$ is the spin-orbit potential, and $\underset{\sim}{L}$ and $\underset{\sim}{\sigma}$ are the orbital angular momentum and the spin of the incident proton in units of $\hbar$.

The Coulomb potential $V_c(r)$ is taken as the potential due to a uniformly charged sphere of radius R_c, i.e.,

$$\begin{aligned} V_c(r) &= \frac{Ze^2}{r} && r \geqslant R_c \\ V_c(r) &= \frac{Ze^2}{2R_c}\left(3 - \frac{r^2}{R_c^2}\right), && r \leqslant R_c \end{aligned} \qquad (2.38)$$

where Z is the charge of the target nucleus.

The real potential is generally chosen to be approximately proportional to the density of nucleons in the nucleus. It has the form of $V\,\rho(r,r_o,a)$ where V is negative and energy and mass dependent and $\rho(r,r_o,a)$ is chosen to approximate the measured nuclear charge density which is assumed to be proportional to the nucleon density. The most common form is the Woods-Saxon form

$$\rho(r,r_o,a) = \frac{1}{1 + \exp[(r-R)/a]} \qquad (2.39)$$

where R is the nuclear radius generally chosen to be $R = r_o A^{1/3}$, a is the surface diffuseness and r_o is taken to be 1.25 fm.

The imaginary or absorptive potential was initially chosen to be a volume potential like the real potential. Because the deuteron is weakly bound a surface absorption potential is generally used.

A widely used surface absorption potential is obtained by using the derivative of the real potential. If, for example, a Woods-Saxon form is employed as the real potential, then the imaginary potential may be expressed as

$$4iW_D a.\frac{d\rho}{dr}(r',r'_o,a') = 4iW_D\rho^2(r',r'_o,a')\exp\left(\frac{r'-R}{a'}\right) . \quad (2.40)$$

It is well known experimentally that the scattered nucleons from an interaction can be partially polarized. This can be accounted for, at least qualitatively, by the inclusion of a spin dependent term in the optical potential. Nuclear theoretical analysis indicates that this potential should have the form

$$V_{so}(r) = V_{so}\left(\frac{\hbar}{m_\pi c}\right)^2 \frac{1}{r}\frac{d}{dr}\rho(r',r'_{so},a'_{so})\underset{\sim}{L}\cdot\underset{\sim}{\sigma} \quad (2.41)$$

where V_{so} is the depth of the potential and $(\hbar/m_\pi c)^2 \simeq 2fm^2$ is the square of the Compton wave-length of the Π meson.

2.5 Non-Local Potential

The interaction of a particle with all the other nucleons in the nucleus is described reasonably well by a potential operator U(r) which is a function only of the coordinates of the projectile (apart from spin-orbit coupling). However, one would expect the motion of the projectile to be affected by the dynamical variables of the other nucleons. The simplest way of including this effect in the two body description is to use the generalization of the Schrödinger equation written as

$$\left(\frac{\hbar^2}{2m}\nabla^2 + E\right)\psi(r) = \int dr'^3\, V(r,r')\psi(r') . \quad (2.43)$$

The function V(r,r') is called a non-local potential. It can be shown that the non-local potential is equivalent to an energy-dependent local potential V(r,p). The potential V(r,r') is symmetric in r and r' and can be represented phenomenologically by

$$V(r,r') = V\left\{\left(\frac{r+r'}{2}\right)\right\} \frac{1}{\pi^{3/2}\,\beta^3} \exp\left\{-\left(\frac{r-r'}{\beta}\right)^2\right\} \qquad 2.44$$

where β is a measure of the range of the non-locality. The effect of the non-local potential is to damp the wave function in the nuclear interior.

2.6 Deuteron Breakup

As the deuteron passes close to the nuclear surface one may expect it to suffer considerable internal distortion. Much of this distortion leads to deuteron breakup, and consequently absorption into other channels is described by the imaginary part of the optical potential. Nevertheless, a fraction of these deuterons may contribute to pick-up without contributing to the elastic amplitude. Originally it was argued that this deficiency could be accounted for by neglecting contributions to the pick-up amplitude from the nuclear interior, with the use of a radial cutoff. It was later found that in order to fit the measured angular distributions with the conventional DWBA a radial cutoff at a large radius was required; such a cutoff is not needed when the adiabatic model is used [Jo 70]. In this model the deuteron optical potential is modified with the use of the following equation

$$\bar{U}(\underset{\sim}{R}) = \frac{1}{D_o}\int\left[\, U_n(\underset{\sim}{R}+\tfrac{1}{2}\underset{\sim}{r}) + U_p(\underset{\sim}{R}-\tfrac{1}{2}\underset{\sim}{r}) \,\right] V_{np}(\underset{\sim}{r})\phi_d(\underset{\sim}{r})d\underset{\sim}{r} \qquad (2.45)$$

where $D_o = 1.53 \times 10^{-4}\,\text{meV}^2\text{fm}^3$, $V_{np}(\underset{\sim}{r})$ is the neutron proton interaction, $\phi_d(\underset{\sim}{r})$ is the wave function for the ground state of the deuteron and U_n, U_p are the neutron and proton optical potentials respectively corresponding to one half the incident deuteron energy. The Hulthén wave function is normally used for $\phi_d(\underset{\sim}{r})$.

CHAPTER 3

EXPERIMENTAL TECHNIQUES AND ABSOLUTE CROSS-SECTION MEASUREMENTS

3.1 Accelerator Beam

The beam of 33 MeV protons was obtained from the Australian National University cyclograaff facility by injecting 26 MeV H^- ions from the CNI-30 cyclotron into the EN tandem.

The beam was analysed in a 90° magnet with defining slits before and after the magnet. It was then deflected by a switching magnet into the beam line on which the scattering chamber was situated. Before entering the scattering chamber the beam was focussed again by a set of quadrupole lenses, and was then defined at the entrance of the chamber by a set of 6mm thick carbon collimators with apertures of 1.5mm, 2.3mm, 1.5mm and 3mm diameter respectively. Carbon collimators were used, because of the low neutron cross-section of carbon. A beam spot of less than 2mm diameter was observed on the irradiated targets. A long, unsuppressed Faraday cup 178cm long and 7.6cm in diameter was placed at 189cm from the target to collect the 33 MeV protons. The beam current from the Faraday cup was integrated by an Ortec 439 current integrator.

3.2 Scattering Chamber

The scattering chamber shown in Fig. 3.1 is 51cm in diameter and 29cm deep. The lid can be lifted to provide access to the chamber. The bottom of the chamber consists of a rotatable table upon which the detector blocks are mounted and positioned to within ± 0.1°. The detector blocks were clamped to a copper cooling ring which was cooled by a freon expansion refrigerator down to -25° C.

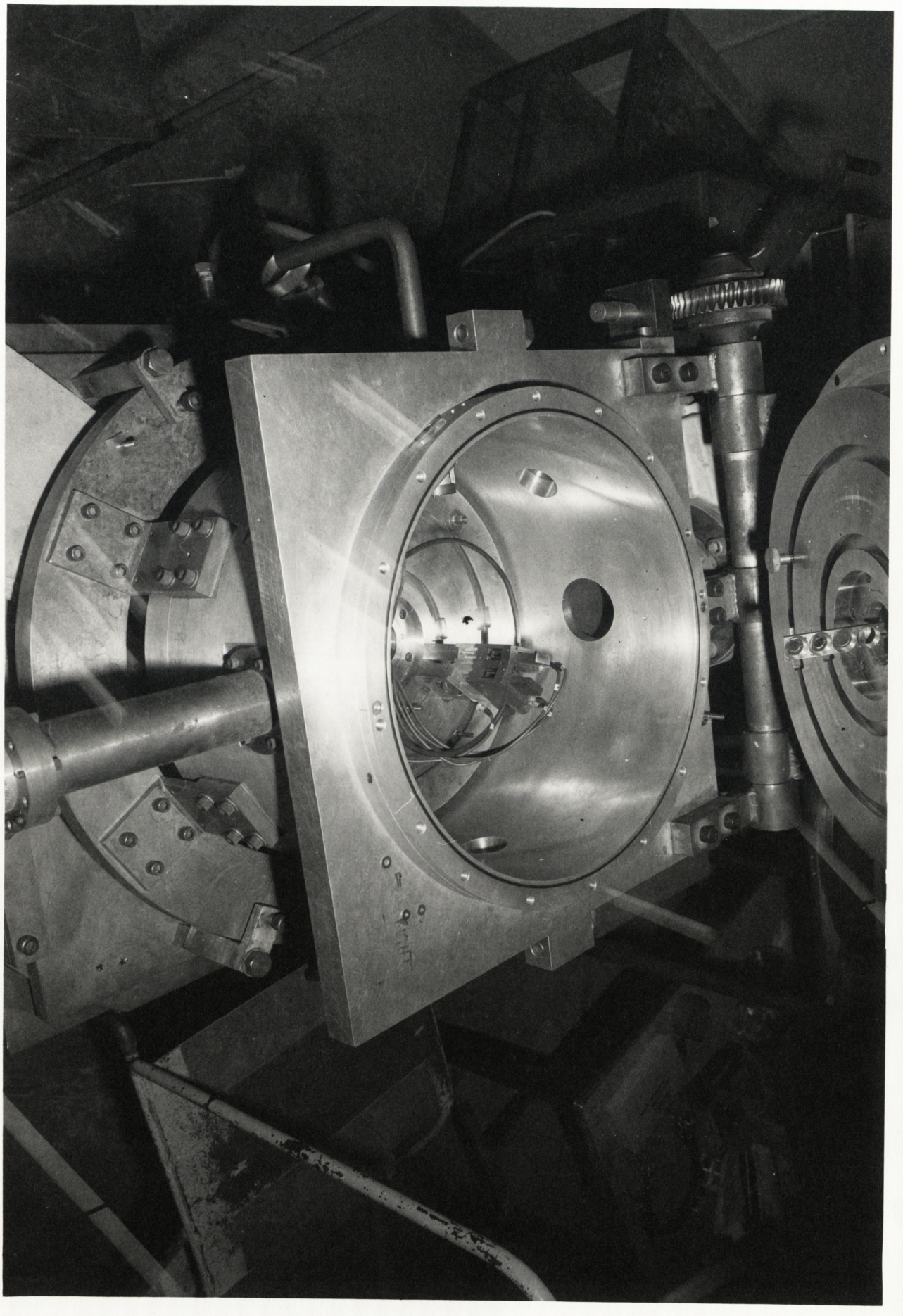

Fig. 3.1 General view of the scattering chamber and detector mounting blocks used in the present experiments.

The blocks also held the defining slits which were placed between two permanent magnets of about 450 oersted . The purpose of these magnets is to suppress electrons knocked out of the target by the beam and thus to prevent them from reaching the detector. The solid angle seen by the detectors was defined by a 2 x 5mm tantalum slit of 2.5mm thickness. Two more slits were used in front of the defining slit to prevent multiple scattered protons from reaching the detectors.

3.3 Detectors

Two counter telescopes placed 22.5° apart were used to detect the scattered deuterons. Each telescope consisted of two surface barrier detectors. Because spectra for (p,d) and (p,t) reactions were collected simultaneously, the first of the two detectors forming the telescope was chosen just thick enough to reduce the energy of the scattered tritons by about 60%. The second detector had to be thick enough to stop completely the scattered deuterons and tritons.

Both the ΔE and E detectors used throughout this work were n-type silicon surface barrier detectors manufactured in the laboratory [En 71]. They were operated 10% above the maximum necessary bias to compensate for any voltage changes across the detector due to leakage current fluctuations with temperature. Several ΔE and E detectors were used during the experiments, the normal thickness being 0.5mm for the ΔE detectors and 1.8mm for the E detectors. The resistivity was of the order of 10K ohm-cm and the resolution was about 25 keV for 8.78 MeV α-particles from a Th B-source. In order to reduce leakage current and thus to improve the resolution, the detectors were cooled to -25° C. The energy resolution obtained

during the measurements varied from 55 to 85 keV depending on the detectors used and the kinematic broadening.

3.4 Particle Identification

In order to separate the deuterons from protons and the rest of the reaction products particle-identification telescopes were used. The method is based on the simultaneous measurement of the total energy of the particle and its rate of energy loss. There is however, a slight loss in energy resolution with this method.

Two detectors are used; a thin $\left(\frac{dE}{dx}\right)$ transmission detector through which the particle passes, followed by a thicker E detector in which the particle is completely stopped. For a non-relativistic particle the product $\left(\frac{dE}{dx}\right)$ x E is almost independent of energy, but depends on the product MZ^2. This is readily seen from the standard Bethe energy loss equation

$$\frac{dE}{dx} = \frac{C_1 MZ^2}{E_T} \log C_2(E_T/MZ^2) \qquad (3.1)$$

where C_1 and C_2 are constants and E_T is the incident energy of the particle of mass M and charge Z. The product $E_T\left(\frac{dE}{dx}\right) = C_1 MZ^2 \log C_2 \frac{E_T}{MZ^2}$ depends on MZ^2 but is not a sensitive function of E_T.

Many particle identification systems have been used to identify light reaction products such as deuterons and tritons. The particle identifier used in this work to identify the (p,d) and (p,t) reaction products was built at A.N.U. [En 70] and is based on Eq. 3.1 expanded in the form [St 58]

$$[E_T + k_0 - k_1 \Delta E + k_2 \Delta E^2 - k_3 \Delta E^3 + ..]\Delta E = \text{const x } MZ^2 \qquad (3.2)$$

Using the energy loss tables of Skyrme [Sk 67], it was determined emperically for a wide range of energies and ΔE detector thicknesses

that $k_0 = +7.0 \pm 0.5$ and $k_1 = +0.5 \pm 0.01$ [En 70]. The other constants k_2 and k_3 are of the order of 0.02 ± 0.02 and $+0.00 \pm 0.002$ respectively. Higher terms in ΔE make a very small contribution to Eq. 3.2 and can be neglected.

The following three functions are performed by the particle identifier:

$$F_1 = (E_T + 7.0)\Delta E$$

$$F_2 = (E_T - 0.5\Delta E + 7.0)\Delta E$$

and $$F_3 = (E' + 0.5\Delta E + 7.0)\Delta E \qquad (3.3)$$

where E' is the E detector signal, ΔE is the signal obtained from the transmission detector and $E_T = E' + \Delta E$. A typical mass spectrum is shown in Fig. 3.3. The elastic and most of the inelastically scattered protons were not stopped in the E detectors which were too thin for the 33 MeV proton energy used in this experiment.

3.5 Associated Electronics

A block diagram of the electronics associated with each counter telescope is shown in Fig. 3.2. The output pulses from the ΔE and E detectors were fed into charge sensitive preamplifiers which were located as close to the scattering chamber as possible to minimize capacitance associated with the connecting leads. The preamplified signals were then fed into linear amplifiers with RC shaping using differentiating and integrating time constants of 0.5μs. The unipolar pulses from the linear amplifiers were fed into two linear gates and the gate outputs were stretched and then summed to give the total energy pulse E_T.

Both E' and ΔE unipolar pulses were also fed into the particle identifier set on the F_3 function.

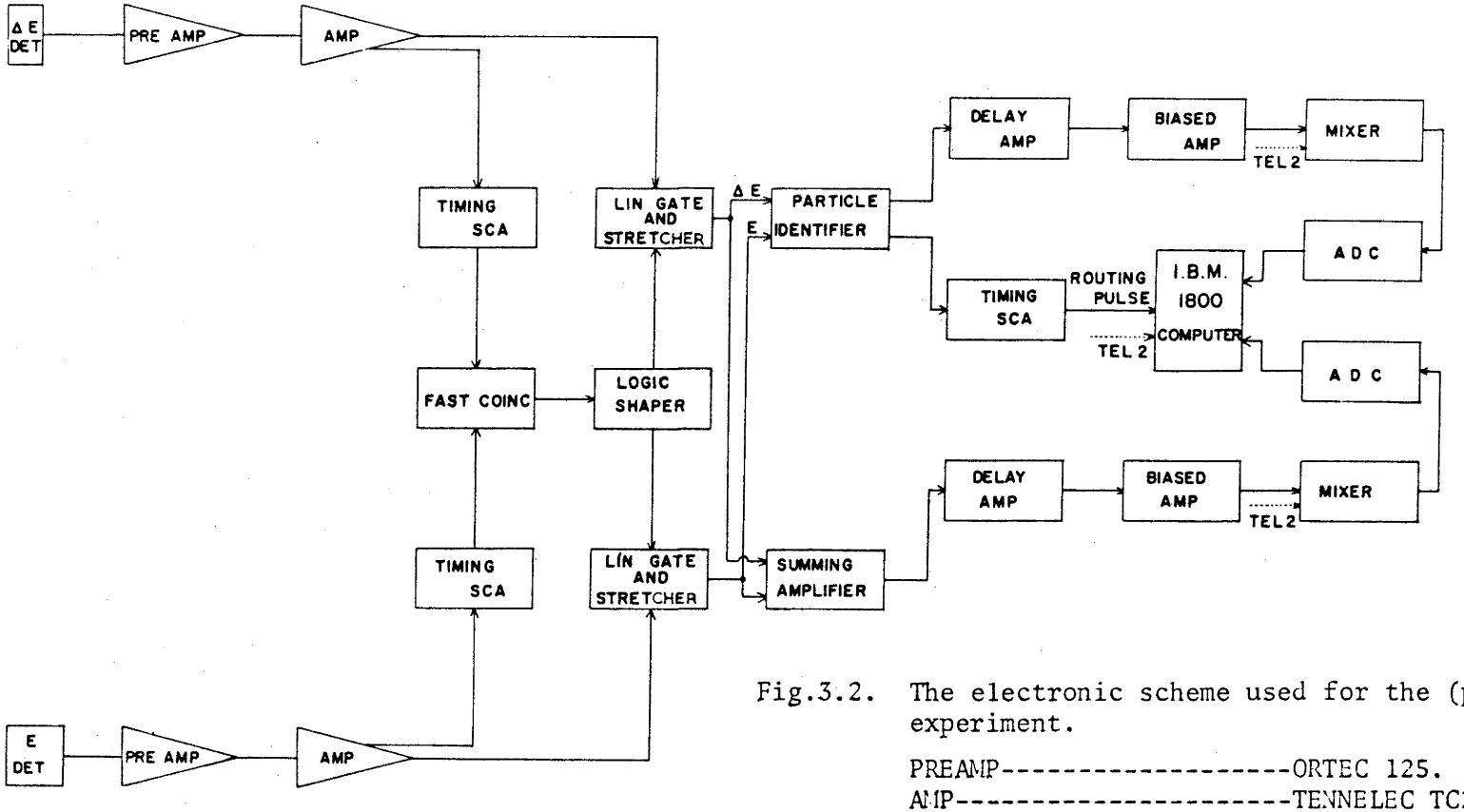

Fig.3.2. The electronic scheme used for the (p,d) experiment.

PREAMP----------ORTEC 125.
AMP----------TENNELEC TC203.
TIMING SCA----------CANBERRA 1437.
LIN GATE AND STRETCHER---CANBERRA 1454.
LOGIC SHAPER----------CANBERRA 1455A.
DELAY AMP----------CANBERRA 1457
SUMMING AMPLIFIER--------ANU.
PARTICLE IDENTIFIER------ANU.
BIASED AMP----------ORTEC 408A.
ADC ----------NUCLEAR DATA INC.
FAST COINC----------ORTEC 414.

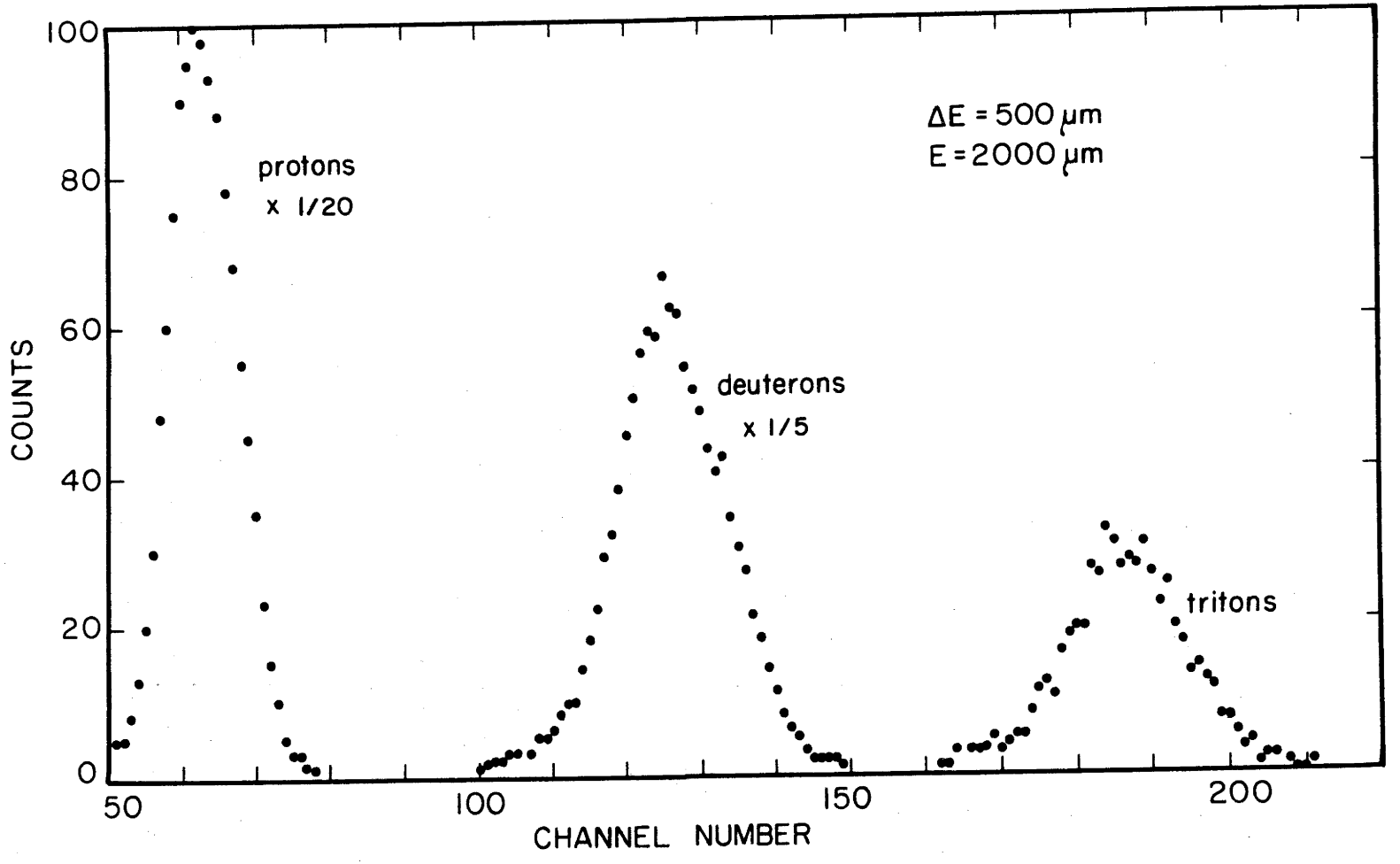

Fig.3.3. Typical mass spectrum from the $^{78}Se(p,d)^{77}Se$ reaction.

It is a necessary condition that the E' and ΔE signals represent the same event; this was ensured by requiring coincidence between the E' and ΔE signals. The bipolar outputs of the linear amplifiers were fed into two T.S.C.A.'s, whose outputs after being very accurately timed were then used to operate a fast leading edge coincidence unit. The unit had a variable resolving time of 10-110 ns. This was to reduce the chance coincidence rate at the most forward angles. The output from the coincidence unit, after being stretched in a logic shaper, was used to open the linear gates.

The bipolar output from the particle identifier was fed into a T.S.C.A. to provide the routing pulse, with the unipolar pulse representing the mass spectrum. The mass and energy pulses were fed into separate A.D.C.'s where coincidence between them was required. The A.D.C.'s were interfaced to the IBM1800 computer. Spectra from the (p,d) and (p,t) reactions were recorded simultaneously by setting digital windows on the deuteron and triton peaks in the mass spectrum. The total energy pulses were then separated according to their associated routing signals and stored in different memory locations of the computer.

3.6 Targets

The targets used were thin foils varying in thickness from 300 $\mu g/cm^2$ to 700 $\mu g/cm^2$, and were prepared from enriched Se metal. Table 3.1 gives the isotopic composition of each of the targets used in this experiment. The method of preparation involved the heating of the Se metal in a tantalum boat with an rf coil at pressures of 10^{-5} torr. The metal was evaporated directly onto glass slides coated with a suitable releasing agent. Because of its low evaporating point a thin carbon layer of about 20 $\mu g/cm^2$ was evaporated onto the Se to prevent sublimation when bombarded

TABLE 3.1

The isotopic composition of target materials as given by the supplier*

	Isotopic Composition in (%)					
Target	^{74}Se	^{76}Se	^{77}Se	^{78}Se	^{80}Se	^{82}Se
^{76}Se	0.2	86.1	2.0	4.4	5.9	1.6
^{78}Se	0.1	0.44	0.98	96.02	2.34	0.21
^{80}Se	0.15	0.94	1.55	2.69	93.65	1.05
^{82}Se	0.16	0.29	0.33	0.59	1.96	96.66

* Oak Ridge National Laboratory, Tennessee, U.S.A.

TABLE 3.2

The Q-values for the (p,d) reaction on the nuclei involved in the present work.

Nucleus	Q-Value MeV
^{76}Se	- 8.9369
^{78}Se	- 8.2726
^{80}Se	- 7.6718
^{82}Se	- 7.0474
^{12}C	-16.4953

with the beam. They were then floated off in deionized water and folded so as to have Se between two thin carbon films. No target thickness loss was detected during the course of the experiments for beam currents less than about 70 nA. This was checked constantly by monitoring the Se elastic peak at 90° by a 5mm SiLi detector.

3.7 Absolute Cross-Sections

The number of deuterons $I_s(\theta)$ scattered into the detector at an angle θ is given by

$$I_s(\theta) = kI_o \, \sigma(E,\theta)_{Abs} \tag{3.4}$$

where k represents the detector solid angle $d\Omega$ and the target thickness and I_o is the number of particles in the incident beam. In order to convert relative to absolute cross-sections it is necessary to know the constant k. This is calculated from the ratio of experimental to theoretical Rutherford cross-sections, i.e.,

$$k = \frac{[I_s(\theta)/I_o]_{Meas}}{\sigma(E,\theta)_{Ruth}} \tag{3.5}$$

The experimental Rutherford cross-section was measured by keeping the same target and detector geometry and target as in the (p,d) reaction but lowering the beam energy to 4.5 MeV. Having measurements for the relative differential cross-sections at the same angle as the Rutherford cross-section, a normalization factor was extracted which was then used to convert all relative cross-sections to absolute values. The relative cross-sections were obtained by dividing the number of deuterons for each state by the integrated charge. The elastically scattered protons monitored at 90 degrees were also used to obtain relative cross-sections. Results which were in good agreement were obtained from these two procedures. This also gave a good check on the reliability of the Faraday cup. An average value of k was obtained by measuring Rutherford scattering at angles of 25° to 40° in steps of 2.5°.

3.8 Primary Data Analysis

The primary data analysis was performed with the program code AUTOFIT [AT 65]. This program instead of using an analytical

function, such as a skewed Gaussian to fit the data, uses in its place the experimental line shape. A well-defined and well-resolved peak was chosen from the spectrum to be used as this reference peak.

The information extracted by the program is listed below:

(a) Peak position (channel number).

(b) Q-value for the peak (MeV).

(c) Error in the peak position (keV if Q-values are listed or channels if channel numbers).

(d) Number of counts in the peak.

(e) Sum of the background underneath the peak.

(f) Unfolding of overlapping peaks.

In using the program the following information had to be supplied:

(a) Approximate peak positions - the program can also automatically search for the existence of peaks but this option is not the best. Two hundred peaks can be analysed at a time.

(b) Reference peak, which in most cases was the ground state with the background subtracted.

(c) Background points.

The user has also the option of forcing the program to fit a peak at a fixed energy. This proved very useful in the unfolding of partially resolved multiplets.

3.9 Energy Resolution

The overall energy resolution varied between 55 keV and 85 keV (FWHM). The major contributions to the resolution were:

(1)	Electronic noise	$\leqslant$ 20 keV
(2)	Energy resolution of the "Cyclograaff" beam	$\gtrsim$ 35 keV
(3)	Energy loss and straggling in the target	15 keV
(4)	Detector resolution (each)	25 keV
(5)	Kinematic broadening	20-30 keV .

The above contributions when added in quadrature gave an energy resolution of $\gtrsim$ 55 keV.

The electronic noise was measured by injecting a pulser into the system at the preamplifier input and measuring the analyzed peak width.

The contribution to the resolution from energy loss and straggling in the target was taken from tables [Ma 67].

3.10 Uncertainties

The uncertainties in the differential cross-sections can be divided into two categories.

In the first category we list:

(a) possible systematic error in the beam integration;

(b) the error in obtaining the normalization constant k of Eq. 3.4;

and in the second category the statistical error and the fitting error. The error in the beam integration network consists of the error in the charge integrator which is given by the manufacturer to be of the order of ± 1% and any error introduced from the multiple scattering of 4.5 MeV protons from the 200 $\mu gm/cm^2$ target.

Multiple scattering has been estimated using the theory by Nigam et al [Ma 67]. Assuming the angular distribution of the multiple scattered protons to be Gaussian, the angle of the cone that contains 98% of the multiple scattered beam is estimated to be

0.028°. Using the angle of 0.84° subtended by the Faraday cup, the theory then shows that multiple scattering results in negligible error.

An uncertainty in the scattering angle also introduces an error in the normalization constant k of Eq. 3.4 which was determined at angles between 25° and 40° assuming pure Rutherford scattering.

An error is introduced into the absolute cross-section from the fact that θ is measured from the centre of the detector slit assuming that $\sigma(E,\theta)$ varies linearly across the slit. The uncertainty in θ introduced from the above assumption for a 2mm slit is estimated to be $\pm$ 0.0033 radians. This introduces an error in k of about 2%.

The energy loss of the beam particles in the target introduces an additional uncertainty into the absolute cross-section, which for 4.5 MeV protons and a 0.7 $\mu g/cm^2$ target thickness is about 2%.

The uncertainty in the yield is normally taken to be the statistical error and the fitting error, which for the extraction of yields for overlapping peaks can be larger than the statistical error.

All peak areas in this work have been extracted with the computer code AUTOFIT discussed in Section 3.8. The program gives the statistical error and estimates the fitting error which, for closely spaced and weakly excited peaks, can be as high as 15%. Only statistical errors are shown in the angular distributions. For most cases the size of the error bar is smaller than the data points.

The upper limit error in the absolute cross-section for most cases is estimated to be about 10%.

The uncertainty in the measurement of the excitation energies of the states involves the uncertainty in determining the channel position of the peak and the error in the calibration and the ground

state Q-value which is normally given in the literature. The Q-values of well-known and well-resolved states in the odd selenium nuclei studied in the present work were used as calibration points in a least squares fit program to extract excitation energies. The error in the channel peak positions were determined by AUTOFIT and varied from ± 0.5 channels for well-resolved peaks to ± 2 channels for multiplets and peaks with poor statistics. The error in the excitation energies is of the order of 10 keV for strongly excited states, but could be as high as 15 to 20 keV for weakly excited and partially resolved states at high excitation.

CHAPTER 4

DWBA ANALYSIS

The DWBA calculations were carried out on the A.N.U. UNIVAC 1108 computer using the code DWUCK [Ku 66]. The optical model parameters used to calculate the distorted waves in the entrance and the exit channels are given below.

4.1 Proton Parameters

The proton optical model parameters used in this analysis are shown in Table 4.1. They were calculated from the set of formulae given by Becchetti and Greenlees [Be 69] in which

$$V = 54.0 - 0.32E + 24(N-Z)/A + 0.4Z/A^{1/3} \text{ MeV},$$

$$r_o = 1.17\text{fm}; \quad a = 0.75\text{fm},$$

$$W = 0.22E - 2.7 \text{ MeV or zero whichever is greater},$$

$$W_D = 11.8 - 0.25E + 12(N-Z)/A \text{ MeV or zero whichever is greater},$$

$$r_o' = r_w = r_D = 1.32\text{fm},$$

$$a' = a_w = a_D = 0.51 + 0.7(N-Z)/A \text{ fm}.$$

$$V_{so} = 6.2 \text{ MeV}, \quad r_{so} = 1.01\text{fm} \text{ and } a_{so} = 0.75 \text{ fm}.$$

4.2 Deuteron Parameters

The deuteron optical parameters used to calculate the distorted waves are those of Perey and Perey [Pe 66] set B given in Table 4.1. These parameters were obtained from the elastic scattering of deuterons on Zn at 25.9 MeV and included a spin-orbit term which was not derived from polarization measurements.

A set of global deuteron optical parameters given by Childs and Daehnick [Ch 75] with energy and mass dependent central

TABLE 4.1

Summary of Optical Parameters used in this work

Particle	Target	V MeV	r_o fm	a fm	W_D MeV	W MeV	r'_o fm	a'_o fm	V_{so} MeV	r_{so} fm	a_{so}	Ref.
P	^{76}Se	49.18	1.17	0.75	4.813	4.56	1.32	0.5836	6.2	1.01	0.75	[Be 69]
	^{78}Se	49.7	1.17	0.75	5.088	4.56	1.32	0.5997	6.2	1.01	0.75	"
	^{80}Se	50.2	1.17	0.75	5.34	4.56	1.32	0.616	6.2	1.01	0.75	"
	^{82}Se	50.67	1.17	0.75	5.599	4.56	1.32	0.629	6.2	1.01	0.75	"
d	$^{76,78,80,82}Se$	114	0.986	0.883	14.60		1.283	0.802	6.90	0.986	0.883	[Pe 66]

potential depths and a spin-orbit term became available after this analysis was completed. These parameters gave a slightly better fit to the $\ell = 1$ data at angles greater than 40°, but the fits to the data with other ℓ values remained about the same. There was a 15 percent difference between the spectroscopic factors extracted from these two sets. This set of parameters is given by

$$V = 90.5 - 0.21E + 0.8ZA^{-1/3} \text{ MeV},$$

$$r_o = 1.15\text{fm}, \quad a = 0.79\text{fm}, \quad W_D = 14.9 - 0.05E \text{ MeV},$$

$$r_o' = 1.33\text{fm}, \quad a' = 0.395 + 0.088A^{1/3} \text{ fm},$$

$$W = 0.0483(E-17) \text{ MeV only for } E > 17 \text{ MeV}$$

and $V_{so} = 6.7\text{fm}, \quad r_{so} = 0.98\text{fm}, \quad a_{so} = 1.0\text{fm}.$

4.3 Finite - Range Correction

Corrections for the finite range of the interaction were carried out using a value of FNRNG = 0.650 in the function

$$W(r) = \left[1 + \frac{2}{\hbar^2} \frac{M_p M_n}{M_d} (\text{FNRNG})^2 (U_d(r) - U_p(r) - U_n(r) - S_{pn})\right]^{-1}$$

which is calculated by DWUCK, where S_{pn} is the separation energy of the neutron from the deuteron, $U_{d,p,n}(r)$ are the optical potentials of the corresponding particles and M_p, M_n and M_d are the masses of the proton, neutron and deuteron respectively. This term then multiplies the transition amplitude.

4.4 Non-Locality Correction

In this correction, the distorted waves for a non-local potential are given by the local potential U(r) multiplied by a correction factor f(r) such that

$$\chi_{NL}(r) = f(r)\chi_L(r)$$

where $$f(r) = \left[1 - \frac{\beta^2}{4} \cdot \frac{2\mu}{\hbar^2} U(r)\right]^{-\frac{1}{2}}$$ and

μ is the reduced mass of the projectile or the outgoing particle and β is the range of the non-locality. Since the shell model single particle potential is also believed to be non-local, the same correction is applied by multiplying the bound state wave function by f(r) and then renormalizing it to unity since $|f(r)| \leq 1$.

The following values for the parameters β have been used in this work:

$$\beta = 0.85\text{fm for nucleons}$$

and

$$\beta = 0.54\text{fm for deuterons.}$$

4.5 Form Factor

The form factor for the pick-up reaction, namely $\psi^{\mu}_{j\ell}(\underset{\sim}{r}_{xA}, \sigma_x)$ in Eq. 2.14, is the wave function of the neutron bound in a spherical potential well of radius R and diffuseness a. The form factor is obtained from the solution of the Schrödinger equation by adjusting the depth of the potential well so as to match the binding energy $E = -(S_n + E_x)$, where S_n is the neutron separation energy and E_x is the excitation energy of the state concerned.

The neutron parameters used throughout the present DWBA calculations are:

$$r_o = 1.25\text{fm}, \quad a = 0.65\text{fm and } U_L = 25 \text{ MeV}$$

where U_L is the strength of the spin-orbit term.

4.6 Deuteron Breakup

Early in this work an attempt was made to account for possible deuteron breakup by incorporating Eq. 2.45 into the DWBA calculations. It was found however, that there was no general improvement to the DWBA fits. For this reason this method of accounting for deuteron breakup was not pursued any further.

CHAPTER 5

EXPERIMENTAL RESULTS

This chapter presents the deuteron spectra and angular distributions of the differential cross-sections observed in the (p,d) reaction together with DWBA calculated curves. Only new information obtained from the present work is extensively discussed. States previously observed in particle transfer work and for which ℓ values are now well established, will not in general be discussed.

Typical deuteron energy spectra from the ^{76,78,80,82}Se(p,d) ^{75,77,79,81}Se reactions obtained with solid state detector telescopes are shown in Figs. 5.1, 5.5, 5.8 and 5.11 respectively. The energy resolution in the present work varied from 55 keV to 85 keV FWHM, and the excitation energies were determined using the spectra which had the best energy resolution. All levels presented in this study were observed, in general, at more than three angles.

The deuteron angular distributions were measured from 15° to 80° at intervals of 2.5°. However, owing to poor statistics at larger angles, most angular distributions extend only to about 60°.

In general the agreement between the deuteron angular distributions for well resolved peaks with adequate statistics and the predicted DWBA curves is reasonably good. This is indicative of the direct reaction mechanism. To those angular distributions where the DWBA fits were not as convincing tentative ℓ assignments were made. An attempt was made to extract angular distributions for some of the remaining peaks in the spectrum, but no satisfactory DWBA fits could be obtained for any values of ℓ. This occurred

mainly at high excitation. Because of the fact that the DWBA seems to work well for well resolved peaks, this may perhaps indicate that they are unresolved multiplets.

A common characteristic of most $\ell = 1$ transitions is that they have shallow minima when compared to the DWBA calculated curves. A set of global optical model parameters determined by J. Childs and W.W. Daehnick [Ch 75], which became available after this analysis was completed, gave better fits with deeper minima for the $\ell = 1$ transitions, but the fits to the data with other ℓ values remained about the same.

5.2 $^{76}Se(p,d)^{75}Se$

The odd mass nucleus $^{75}Se_{34}$ has been studied previously through the $^{75}As(p,n\gamma)^{75}Se$ reaction by Sugimitsu [Su 74] who obtained energy levels up to an excitation energy of 1666 keV. Agarwal et al [Ag 73] have studied the same reaction and provided energy levels and made spin and parity assignments to all states up to 748 keV. They have also observed for the first time the $\frac{1}{2}^-$ state at 293.2 keV. Finckh et al [Fi 70] have also studied ^{75}Se through the $^{75}As(p,n\gamma)^{75}Se$ reaction and obtained energy levels up to an excitation energy of 2297 keV. Zell et al [Ze 74] have studied ^{75}Se from the $^{72}Ge(\alpha,n\gamma)^{75}Se$ and $^{73}Ge(\alpha,2n\gamma)^{75}Se$ reactions. They obtained energy levels and observed for the first time a number of high spin states which were interpreted as members of quasi-rotational bands. Spins were assigned from the study of γ-ray angular distributions. Coban et al [Co 72] obtained energy levels and made some spin assignments from the investigation of γ-rays following the β-decay of ^{75}Br.

The only particle transfer work which has been done is that of Sanderson [Sa 73]. This became available only after the commencement

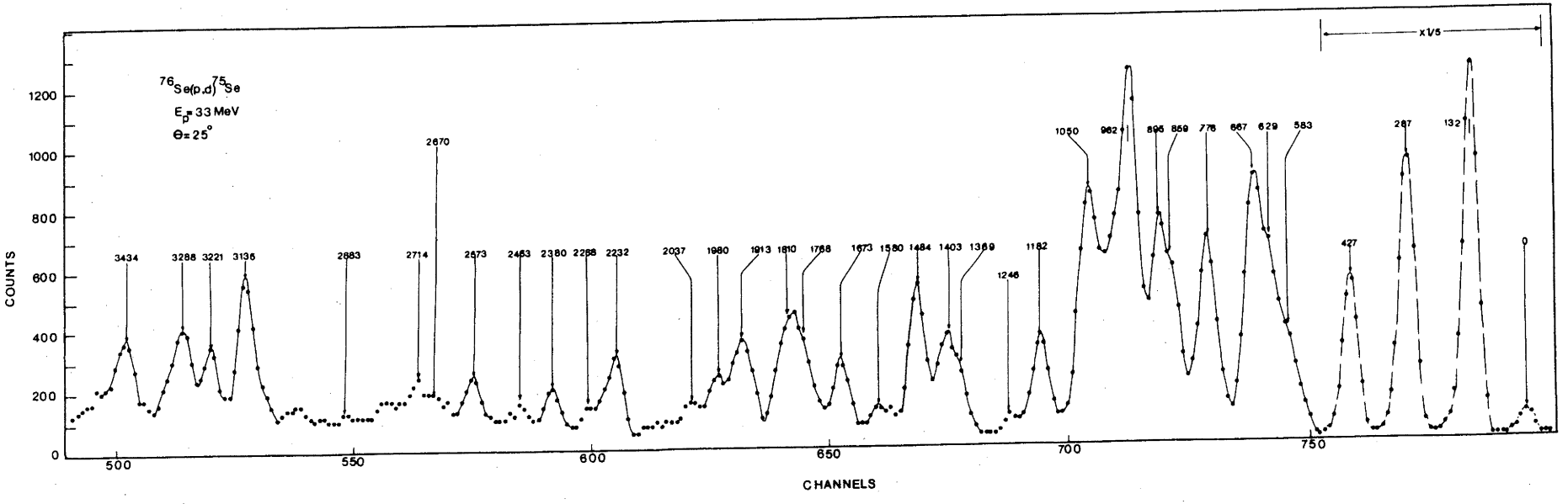

Fig.5.1. Deuteron spectrum from the ^{76}Se(p,d)^{75}Se reaction.

of the present work. Sanderson studied the $^{76}Se(d,t)^{75}Se$ reaction at 18 and 19 MeV using a magnetic spectrograph. He measured angular distributions and extracted spectroscopic factors for states up to a maximum excitation energy of 1246 keV. He used the Coriolis coupling model and made calculations which were able to account for the occurrence of the anomalous positive parity states in ^{75}Se.

Studying this nucleus through the (p,d) reaction, we were able to resolve a total of 36 levels, ten of which have been observed for the first time. This can be ascertained from table 5.1 which shows all the new assignments to be above the highest excitation energy that had previously been observed.

Angular distributions and spectroscopic factors were extracted for 25 of these states. Because of experimental limitations, angular distributions could not be extracted for the remaining states. Eleven new ℓ assignments were made in the present work.

A summary of the results is given in table 5.1.

5.2.1 $\ell = 1$ Transitions

Angular distributions for ten $\ell = 1$ transitions are shown in Fig. 5.2. The four $\ell = 1$ assignments to levels at 1673 keV, 1810 keV, 1913 keV and 2573 keV and the two $\ell = 1 + 3$ assignments to levels at 2037 keV and 2288 keV were made for the first time in the present work.

Two levels at 287 keV and 293.2 keV have been observed by Agarwal et al [Ag 73], to which they assigned spins of $3/\bar{2}$ and $1/\bar{2}$ respectively. Because of the nature of the (p,d) reaction, it is expected that both of these states are excited in the present work and that the angular distribution for the $\ell = 1$ transition at 287 keV is that of an unresolved doublet. The spectroscopic factor of 1.6 which

TABLE 5.1

Summary of results for states in ^{75}Se

E(keV) This Work	E(keV) Ref. [Sa 73]	E(keV) Ref. [Fi 70]	E(keV) Ref. [Su 74]	ℓ This Work	ℓ Ref. [Sa 73]	J^{π} Ref. [Ag 73]	S This Work	S Ref. [Sa 73]
0	0	0	0	2	2	$5/2^+$	0.08	0.19
	112	115	112		4(3)	$7/2^+$		0.08
132	133			4	4	$9/2^+$	2.72	3.8
287	287	286	286	1	1	$3/2^-$	1.6	1.7
			293.6[b]			$1/2^-$		
427	427	525	427.9	3	3	$5/2^-$	1.47	1.4
			579.4					
583	586	584	585.6	1	1		0.09	0.12
	611				0			0.019
629	629	627	628.5	2	2	$(5/2)^+$	0.10	0.15
667	664	660	663.9	3	3	$5/2^-$	0.6	0.33
	747	745	747.6		1) 3 +4)			0.135
			770.9					
776	777	779	777.3	3	3	$5/2^-$	0.36	0.29
			789.6					
		832						
		852	853.5					
859*	859		859	1	1		0.10	0.08
		890	888.7					
895*	895		895.9	1	1		0.10	0.08
962	963	958	962.6	1	1		0.4	0.47
	1004	996	1003.9		2			0.11
	1021		1020.6		1			0.05
1050	1048	1044	1047.4	3	3		0.44	0.16
	1074	1072	1067.2		3			0.21
	1145	1143	1144.7		2			0.006
	1161		1177.9		(4)			0.002
1182[n]	1183	1190	1184.7	3	1+4		0.18	0.1
			1198.9					
			1239.0					
1246	1246	1250	1245.3	1	1		0.03	0.019
		1302	1301.9					

b) Ref.[Ag 73]; * These energies were fixed in the code AUTOFIT; (cont'd)
n) New ℓ assignments; (a) New states;

Angular distributions to which more than one ℓ value has been assigned correspond to unresolved multiplets, and are not the result of nuclear interference as this is not allowed by the Selection rules.

TABLE 5.1 (cont'd)

E(keV) This Work	E(keV) Ref. [Sa 73]	E(keV) Ref. [Fi 70]	E(keV) Ref. [Su 74]	ℓ This Work	ℓ Ref. [Sa 73]	J^{π} Ref. [Ag 73]	S This Work	S Ref. [Sa 73]
1369[n]		1378	1369.2	(4)			0.1	
1403[n]		1407	1411.3	3			0.15	
		1441						
1484[n]		1480	1490.6	3			0.22	
			1550.2					
		1556	1554.4					
			1561.1					
1580[n]		1592	1588.2	(2)			0.02	
		1650						
1673[n]		1668	1666.1	1			0.07	
		1733						
1768[n]		1764		3			0.17	
1810[n]		1813		1			0.16	
1913[n]		1903		1			0.1	
		1947						
1980[n]		1976						
2037		2032		(1+3)			0.03) 0.05)	
		2072						
		2093						
		2117						
		2159						
2232		2235						
		2266						
2288[n]		2297		(1+3)			0.03) 0.04)	
2380								
2463[a,n]								
2573[a]				1			0.06	
2670[a]								
2714[a]								
2883[a]								
3135[a]								
3221[a]								
3288[a]								
3434[a]								

agrees with [Sa 73] is the largest seen for an $\ell = 1$ transition in all of the Se nuclei studied.

Angular distributions for the $\ell = 1$ transitions at 859 keV and 895 keV were obtained by fixing the peak position in the code AUTOFIT at the above energies and forcing the prgram to fit peaks at these positions. The energies were obtained from Sanderson [Sa 73] and the spectroscopic factors agree well with those obtained in that work.

An $\ell = 1$ assignment was made by Sanderson to a weakly excited level at 1021 keV. This state was not seen in the present work but our energy resolution would not be good enough to resolve this state from the strongly excited state at 1050 keV. Sanderson also observed levels at 1004 keV and 1074 keV. He made an $\ell = 2$ assignment to the former and $\ell = 3$ to the latter.

The level at 1673 keV is weakly excited. Its angular distribution does not agree as well with the predicted DWBA curve as other $\ell = 1$ transitions. Levels nearby have been reported at 1650 keV and 1680 keV [Fi 70] and 1666.6 keV [Su 74] and 1660 keV [Ze 75]. However, the energy resolution in the present work was not good enough to distinguish between these levels, if excited at all in the (p,d) reaction. An attempt was made to fit more than one ℓ value, but the best fit to the data is given with $\ell = 1$.

The new $\ell = 1$ assignments to the levels at 1810 keV and 1913 keV agree reasonably well with the predicted DWBA curves at forward angles. Finckh et al [Fi 70] also observed levels at 1813 keV and 1903 keV.

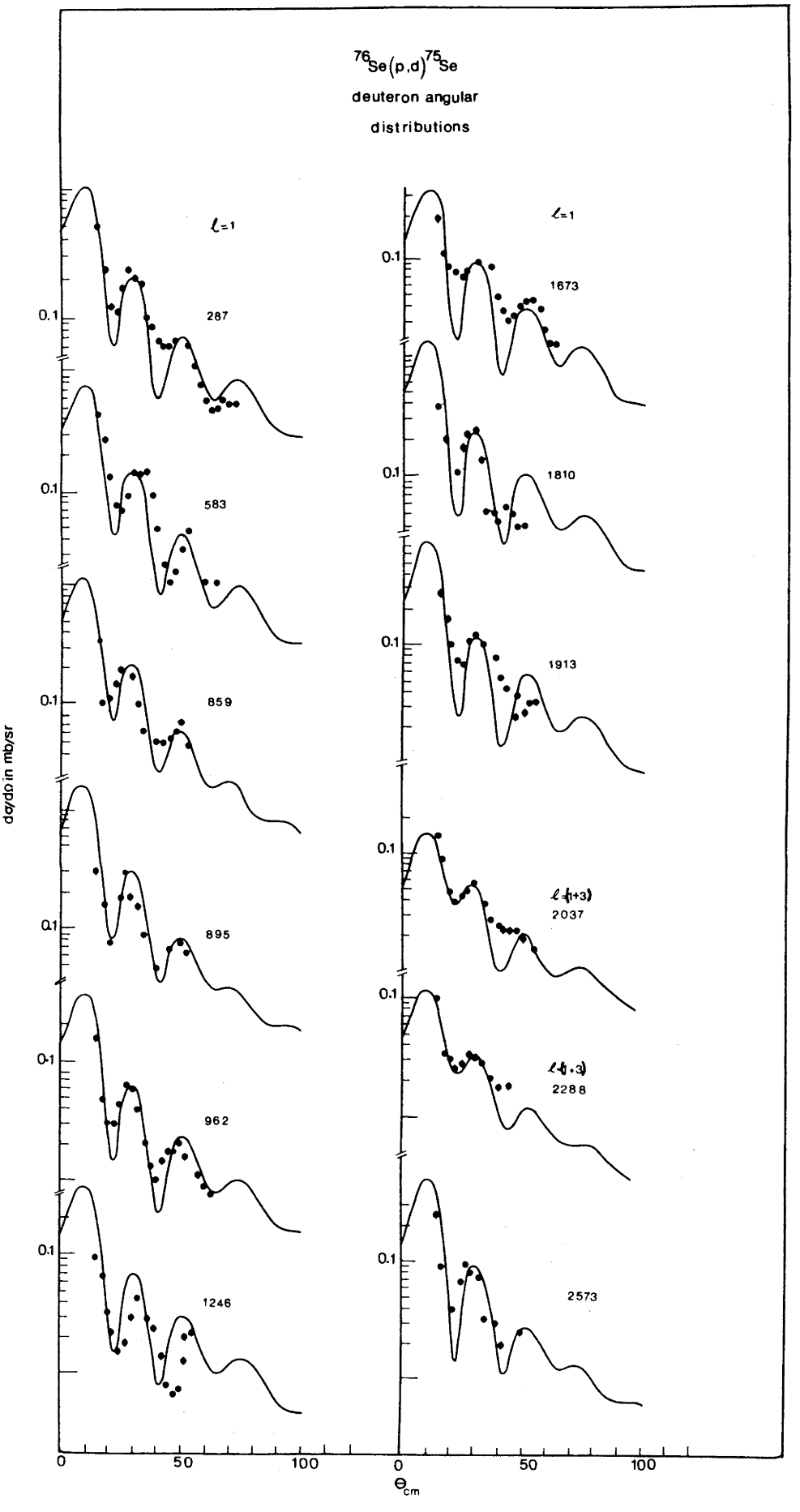

Fig.5.2 Deuteron angular distributions from the $^{76}Se(p,d)^{75}Se$ reaction compared with the DWBA predictions.

The two levels at 2037 keV and 2288 keV appear on the shoulders of other peaks. In order to fit the two ℓ values to these states, a least squares fit was performed with possible linear combinations of ℓ values and it was found that the best fit to the data was given, for both levels, by $\ell = 1 + 3$. The component of each ℓ value was used to calculate the spectroscopic factors shown in table 5.1. Finckh et al also observed levels at 2032 keV and 2297 keV.

The level at 2573 keV was observed for the first time in the present work. As can be seen from the deuteron spectrum in Fig. 5.1 this level is very well resolved and its deuteron angular distribution agrees very well with the DWBA calculation. An $\ell = 1$ assignment has been made to this level.

5.2.2 $\ell = 3$ Assignments

Angular distributions for eight $\ell = 3$ transitions are shown in Fig. 5.3. Four new $\ell = 3$ assignments were made to states at 1182, 1403, 1484 and 1768 keV respectively.

An $\ell = 3$ has been assigned to the level at 776 keV. As can be seen from Fig. 5.3 the agreement between the data and the DWBA calculated curve is not very good at angles greater than 40°. Sanderson [Sa 73] also assigned an $\ell = 3$ to this level. He also observed a level at 747 keV to which he fitted $\ell = 1 + 4$, with the $\ell = 1$ component very small. Zell et al [Ze 75] observed levels at 741, 749 and 778 keV and made spin and parity assignments of $7/\bar{2}$ to the level at 749 keV and $(5/\bar{2})$ to the level at 778 keV. Sugimitsu [Su 74] also reported levels at 747.6 keV, 770 keV, 777.3 keV and 789.6 keV.

An $\ell = 3$ assignment has been made to the level at 1050 keV with a spectroscopic factor of 0.4. This level was also observed by

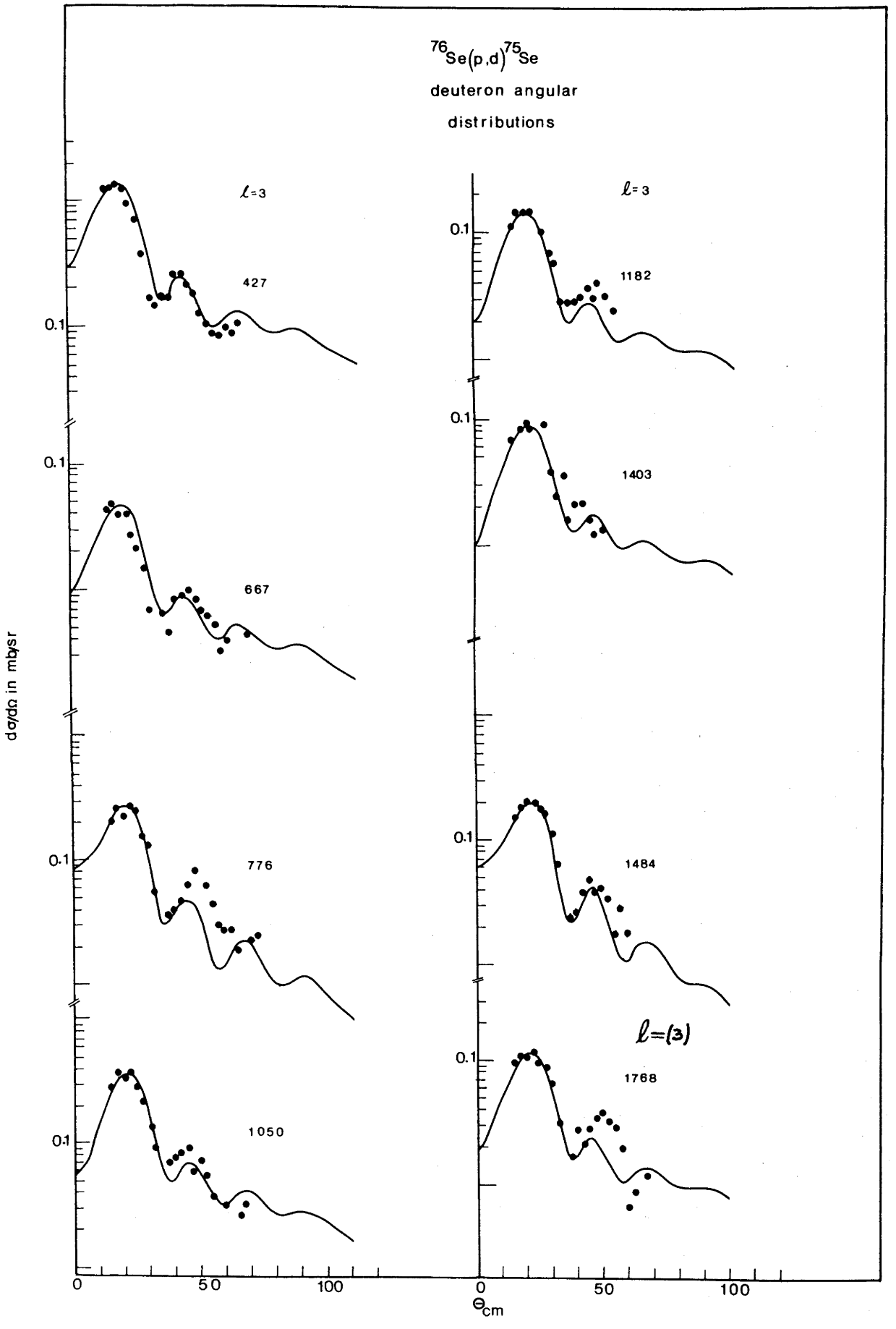

Fig.5.3. Deuteron angular distributions from the $^{76}Se(p,d)^{75}Se$ reaction compared with the DWBA predictions.

Sanderson [Sa 73] to which he made an $\ell = 3$ assignment with a spectroscopic factor of 0.16. He also observed another $\ell = 3$ level at 1074 keV with a spectroscopic factor of 0.21. This level was not resolved in the present work.

The level at 1182 keV was fitted by Sanderson with $\ell = 1 + 4$, while the best fit to the present data was given with $\ell = 3$. Sanderson also observed an impurity close to this level which may have contributed to his angular distribution. Finckh et al [Fi 70] observed a level at 1190 keV and [Su 74] reported levels at 1190 keV, 1184.7 keV and 1198.9 keV.

The $\ell = 3$ assignments to the levels at 1403 keV and 1484 keV agree reasonably well with the predicted DWBA curves. These assignments were made for the first time in the present study.

Because of the poor agreement between the data and the predicted DWBA curve at angles greater than 40°, a tentative assignment of $\ell = 3$ has been made to the level at 1768 keV. The fit with $\ell = 1 + 3$ was also acceptable perhaps because this level sits on the edge of the $\ell = 1$ 1810 keV transition. Levels have also been reported at 1733 keV and 1764 keV by [Fi 70] and by [Ze 75] at 1744 keV.

5.2.3 $\ell = 2$ and $\ell = 4$ Assignments

Fig. 5.4 shows angular distributions for three $\ell = 2$ and two $\ell = 4$ transitions. Two new tentative assignments were made to states at 1369 and 1580 keV.

The ground state of ^{75}Se is known from the previous work of Coban et al [Co 72] and Agarwal et al [Ag 73] to be a $5/2^+$ anomalous state. As can be seen from Fig. 5.4 there is a very good agreement between the experimental deuteron angular distribution and the predicted DWBA curve. An unambiguous $\ell = 2$ assignment has been made

to this state in the present work. An $\ell = 2$ assignment was also made to this state by Sanderson from the $^{76}Se(d,t)^{75}Se$ reaction. This state has also been observed by Sugimitsu [Su 74] and by Finckh et al [Fi 70].

The $\ell = (2)$ assignment to the level at 1580 keV is not very convincing but, as can be seen from Fig. 5.4 the data displays characteristics of an $\ell = 2$ transition at forward angles. The $\ell = 2$ assignment gives the best DWBA fit to the data. This level is very weakly excited. Finckh et al [Fi 70] observed levels at 1556 keV and 1593 keV and Sugimitsu [Su 74] observed four levels at 1550 keV, 1554.4 keV, 1561.1 keV and 1588.2 keV. The angular distribution of the strongly excited level at 132 keV which was fitted with $\ell = 4$ in the present work may be that of an unresolved doublet with a large spectroscopic factor of 2.72. Sanderson [Sa 73] observed a strongly excited level at 133 keV in the (d,t) reaction with a spectroscopic factor of 3.8 to which he made an $\ell = 4$ assignment. He also observed a weakly excited level at 112 keV with a spectroscopic factor of 0.08 to which he also made an $\ell = 4$ assignment. The 112 keV level was also observed by Finckh et al [Fi 70], Sugimitsu [Su 74] and by Agarwal et al [Ag 73] who assigned a spin of $7/2^+$ to this level.

The $\ell = 4$ assignment to the level at 1369 keV is a very weak assignment, but again the best DWBA fit to the data is for an $\ell = 4$ transition. This state is separated by only 34 keV from another state at 1403 keV to which an $\ell = 3$ has been assigned and could contain a small contribution from this state. Levels have also been reported by [Fi 70] at 1378 keV and at 1369.2 by [Su 74].

Sanderson also observed a very weakly excited level at 1145 keV to which he made an $\ell = 2$ assignment. This level was not resolved in the present study. Levels were also reported by Finckh et al at 1143 keV and by Sugimitsu at 1144.7 keV.

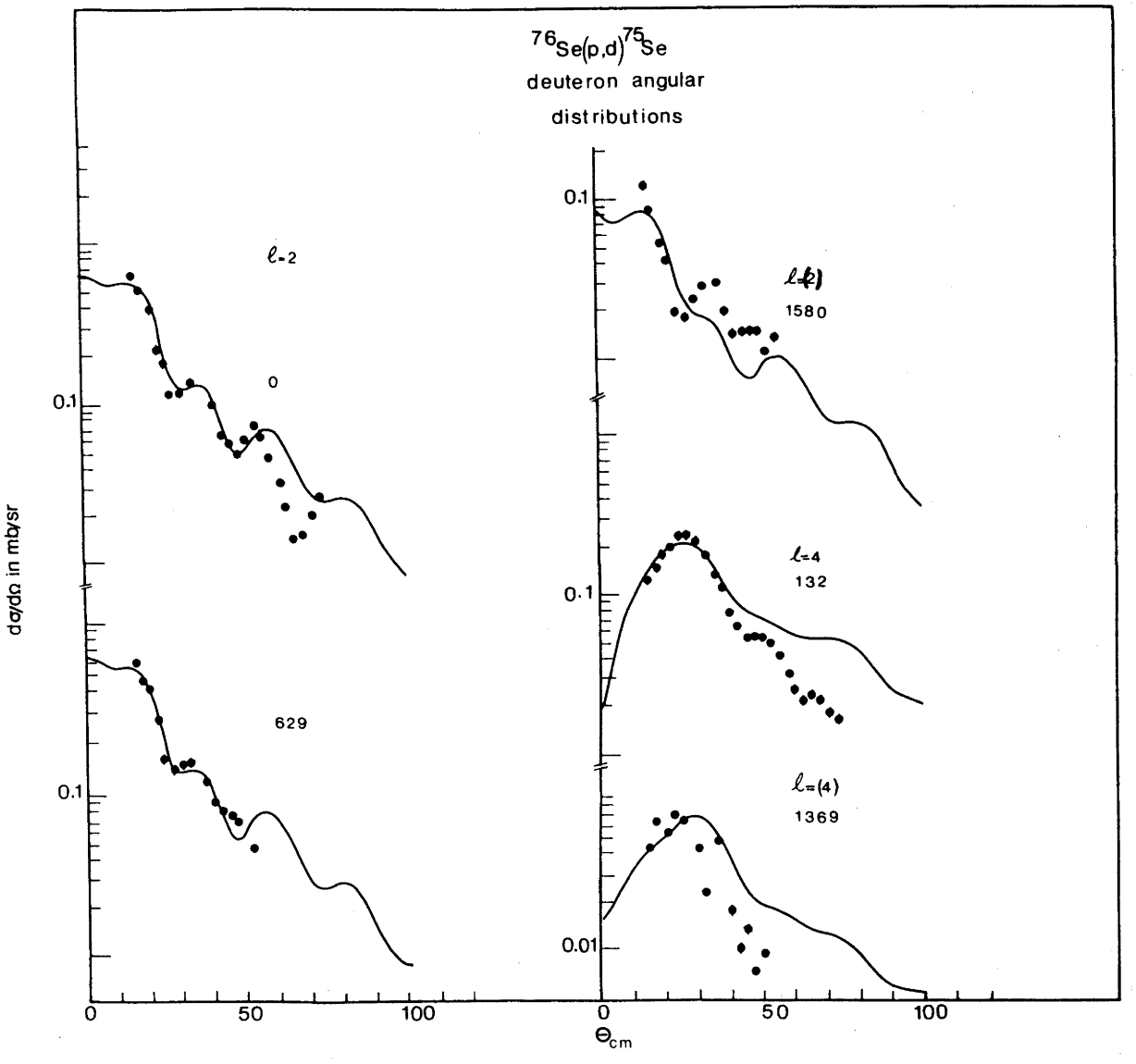

Fig.5.4. Deuteron angular distributions from the $^{76}Se(p,d)^{75}Se$ reaction compared with the DWBA predictions.

Zell et al [Ze 75] have observed yrast levels at 1490 keV, 1907 keV, 1912 keV and 2395 keV and assigned spins of $11/2^-$, $13/2^-$, $(17/2^+)$ and $(15/2^-)$ respectively. The energies of these levels are very close to levels at 1480 keV, 1913 keV and 2380 keV observed in the present work. In view of the above spin assignments these states are expected to be different from those seen by Zell et al, since such high spin states are not expected to be excited in a (p,d) reaction.

5.3 $^{78}Se(p,d)^{77}Se$

The ^{77}Se nucleus has been studied previously through the $^{76}Se(n,\gamma)^{77}Se$ reaction by Rabinstein [Ra 71] who provided energy levels up to an excitation energy of 2872.5 MeV together with some spin assignments. Sarantites [Sa 69] has obtained energy levels and made some spin assignments from a study of the γ-rays that follow the β-decay of ^{77}Br. Additional information on spin and parity assignments was also obtained by Braga and Sarantites [Br 74] from a study of γ-γ directional correlations following the ^{77}Br β-decay.

No spectroscopic information has previously been obtained from neutron pick-up reactions. To date the only particle transfer work which has been done is a study of the $^{76}Se(p,d)^{77}Se$ reaction by Lin [Li 65]. He observed a total of 39 states up to an excitation energy of 4.75 MeV, assigned ℓ values to 38 states and extracted spectroscopic factors.

From this study through the (p,d) reaction additional information was obtained. A total of 30 states were observed and angular distributions measured and spectroscopic factors extracted for 16 of these states. Because of insufficient data, especially at

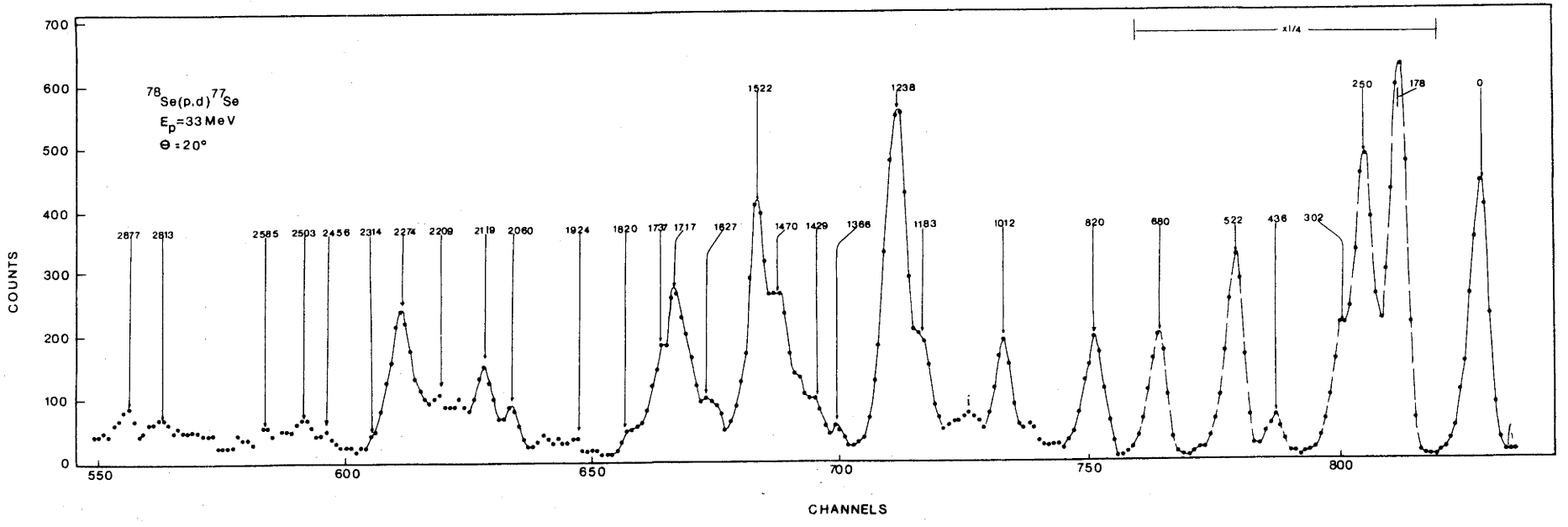

Fig.5.5. Deuteron spectrum from the $^{78}Se(p,d)^{77}Se$ reaction.

higher excitation, angular distributions were not extracted for some of these states. In general the quality of the data obtained for the ^{78}Se(p,d) reaction was not as good as that for the other three isotopes.

There were seven new ℓ assignments made to states at 1183 keV, 1238 keV, 1366 keV, 1470 keV, 1522 keV, 1717 keV and 2209 keV.

A summary of the results is given in table 5.2.

5.3.1 $\ell = 1$ Transitions

Angular distributions for eight $\ell = 1$ transitions are shown in Fig. 5.6. There were four new $\ell = 1$ asignments made to states at 1366 keV, 1470 keV, 1717 keV and 2209 keV in the present work.

As can be seen from the deuteron spectrum in Fig. 5.5, the state at 1366 keV is very weakly excited and is partially resolved from a group of levels at 1429 and 1470 keV. There is also an impurity from ^{75}Se close to this state, but its contribution is estimated to be less than 1%. The angular distribution at forward angles resembles an $\ell = 1$ transition with the first minimum occurring at the right position, while the other maxima and minima are displaced. A tentative $\ell = (1)$ assignment has been made to this state. Rabinstein [Ra 71] has observed a level at 1367.1 keV to which he made a tentative spin and parity assignment of $(3/2^-)$ and Lin [Li 65] observed a level at 1390 keV to which he made no ℓ assignment.

An $\ell = 1$ assignment has been made to the level at 1470 keV. This assignment has been made for the first time in the present work. As can be seen from Fig. 5.6 the agreement between the data and predicted DWBA curve is very good.

An $\ell = 1$ assignment has been made to the level at 1717 keV. As can be seen from Fig. 5.6 the agreement between the calculated

TABLE 5.2

Summary of results for states in ^{77}Se

E(keV) This Work	E(keV) Ref. [Li 65]	E(keV) Ref. [Ra 71]	ℓ This Work	ℓ Ref. [Li 65]	J^π Ref. [Br 74]	S This Work
0	0	0	1	1	$1/2^-$	0.35
		161.8			$7/2^+$	
178	170	175	4	1 + 4	$(9/2^+)$	2.54
		239			$3/2^-$	
250	250	249.7	3	1 + 3	$5/2^-$	2.38
302*	310	300.9	2	(2)	$(5/2^+)$	0.09
436	430	439.6	3	3	$5/2^-$	0.37
522	530	520.6	1	1	$3/2^-$	0.98
		580.8				
680	690	680.1	2	2	$5/2^+$	0.097
		808.4				
820	830	817.9	1	1	$1/2^-$	0.26
		824				
		911.5			$3/2^+$	
		946.9				
1012	1020	1005.2	1	1	$3/2^-$	0.15
	1150	1128.2		0		
1183[n]		1186.7	3		$3/2^-$	0.25
1238[n]		1230.5	3		$3/2^+, 5/2^-$	0.54
	1270	1252.6		2		
1366[n]	1390	1367.1	(1)			0.1
		1402.6				
1429	1450	1411.7		2		
1470[n]		1488.4	1			0.28
1522[n]		1511.4	(3)			0.47
1627		1623.2				
1717[n]		1715.6	1			0.26
1737 ?[a]						
	1760			1		
1820	1830	1818.3		1		
		1888.8				
1924		1915.6				
2060	2060			2		
2119		2142.3				

(Cont'd)

TABLE 5.2 (cont'd)

E(keV) This Work	E(keV) Ref. [Li 65]	E(keV) Ref. [Ra 71]	ℓ This Work	ℓ Ref. [Li 65]	J^{π} Ref. [Br 74]	S This Work
2209[n]	2200	2212.3	1	2		0.11
		2249.2				
2274	2290	2263.9		2		
2314		2319.3				
		2339.1				
		2373.7				
		2392.7				
2456		2456.6				
2503	2500	2490.6		(2)		
		2551				
2585	2570			2		
	2640	2641		(2)		
		2717				
	2770	2776.8				
		2808.4				
2813		2817.6				
		2853.6				
2877		2872.5				
		2892				

a) New states

n) New ℓ assignments

* This energy was fixed in the code AUTOFIT

Angular distribution to which more than one ℓ value has been assigned correspond to unresolved multiplets, and are not the result of nuclear interference as this is not allowed by the Selection rules.

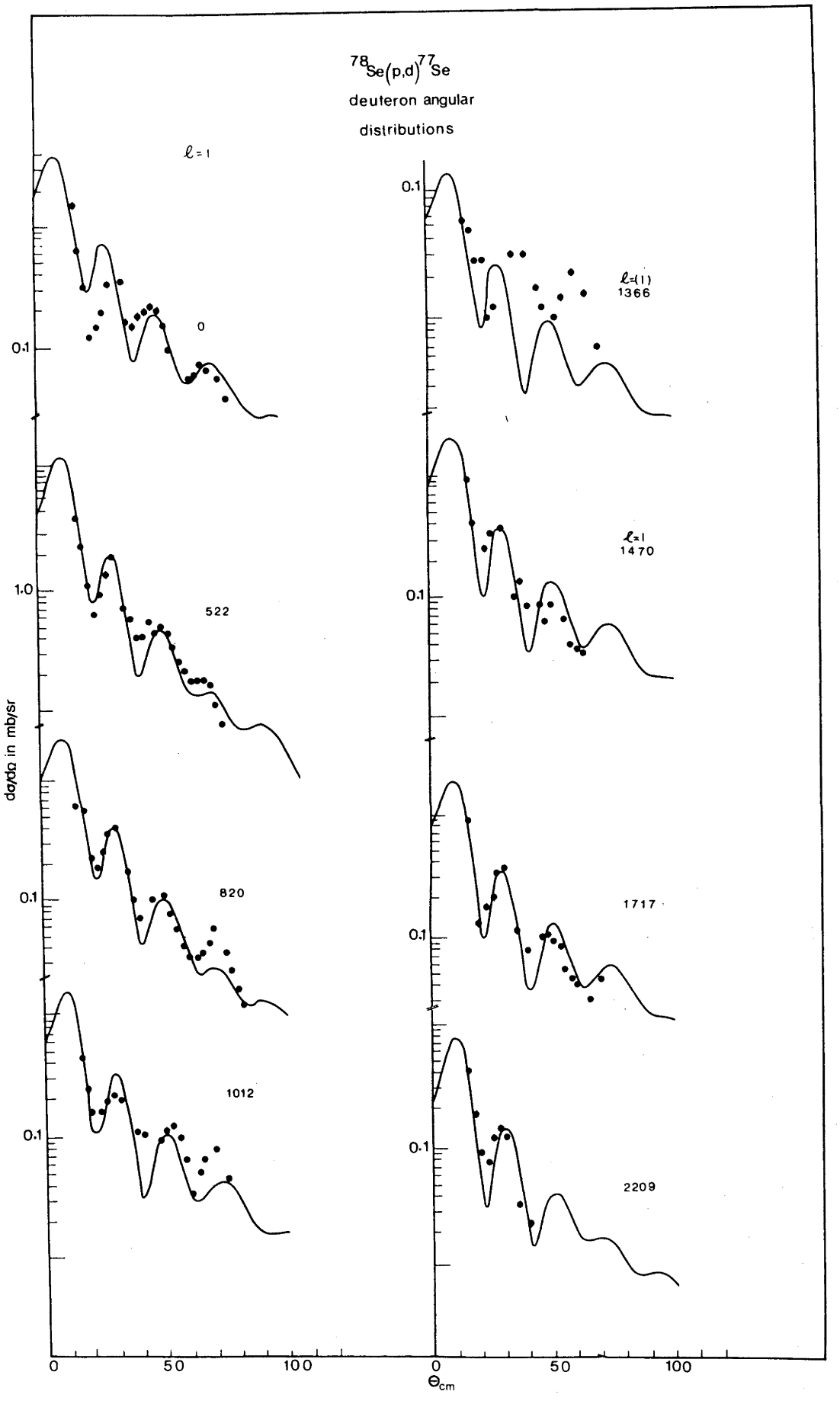

Fig.5.6. Deuteron angular distributions from the $^{78}Se(p,d)^{77}Se$ reaction compared with the DWBA predictions.

DWBA curve and the data is reasonably good. Rabinstein observed a level at 1715.6 keV to which he made no spin assignment. No angular distribution could be extracted for the levels at 1737 keV and 1820 keV. The 1737 keV level has only been resolved at two angles. Lin observed levels at 1760 keV and 1830 keV to both of which he made an $\ell = 1$ assignment.

The $\ell = 1$ assignment to the level at 2209 keV agrees reasonably well with the DWBA calculated curve. Lin observed a level at 2200 keV with a spectroscopic factor of 0.067 to which he assigned an $\ell = 2$ value.

5.3.2 $\ell = 3$ Assignments

Fig. 5.7 shows angular distributions for the $\ell = 3$ assignments made in the present work. There were three new assignments made to states at 1183 keV, 1238 keV and 1522 keV.

The $\ell = (3)$ assignment to the level at 250 keV is not very convincing at forward angles. As can be seen from the spectrum in Fig. 5.5, this state is only partially resolved from the much more strongly excited state at 178 keV and from the state at 302 keV. Being the middle member of the triplet, it is more difficult to determine the area of the peak without a large uncertainty, especially at forward angles where the 178 keV state is very strongly excited. Peak areas in all such difficult cases where the energies of the states could be obtained from the literature, were determined by forcing the program AUTOFIT to fit peaks at these fixed energies. The energies used in the present case were those of Rabinstein [Ra 71]. Braga and Sarantites [Br 74] have assigned $J^{\pi} = 5/2^{-}$ to this state. They also observed another state at 238.9 keV to which a spin of $3/2^{-}$ was assigned. Lin treated the 250 keV state as a doublet and fitted it with $\ell = 1 + 3$. An attempt was made in this study to fit the 250 keV level with more than one ℓ value, but the best fit to the data was

given with ℓ = (3).

To the $\ell = 3$ transition at 1183 keV the agreement between the data and the predicted DWBA curve is reasonably good at forward angles. Braga and Sarantites [Br 74] have assigned a spin of $3/2^-$ to a level at 1186.5 keV. Rabinstein [Ra 71] also observed a level at 1186.7 keV to which he made a spin and parity assignment of $1/2^-(3/2^-)$. This suggests that the angular distribution for the 1183 keV level from the present work may belong to an unresolved doublet.

An $\ell = 3$ assignment has been made in the present work to the level at 1238 keV. Braga and Sarantites have made a spin and parity assignment of $3/2^+$ or $5/2^-$ to a level at 1230.62 keV. Assuming that these two levels are the same; in view of our $\ell = 3$ assignment the $3/2^+$ spin can be eliminated. Rabinstein also observed levels at 1230.5 keV and 1252.6 keV and made tentative spin assignments of $(5/2^-, 3/2^+)$ to the former and $5/2^+$ $(3/2^+)$ to the latter.

The $\ell = (3)$ transition at 1522 keV is close to the 1511.4 keV level excited in (n,γ) by Rabinstein to which he made a tentative spin and parity assignment of $(3/2^+)$. A tentative ℓ assignment has been made to this level from the present work.

5.3.3. $\ell = 2$ and $\ell = 4$ Transitions

Angular distributions for two $\ell = 2$ and one $\ell = 4$ transitions are shown in Fig. 5.7.

The $\ell = 2$ state at 302 keV belongs to a group of states with well known J^π which are expected to be excited in the (p,d) reaction. The 302 keV state is partially resolved from the $\ell = 3$ state at 250 keV which made it difficult to extract peak areas accurately. As can be seen from Fib. 5.7 the $\ell = 2$ assignment is not very convincing at forward angles. Beyond 20° the angular distribution agrees reasonably well with other experimental $\ell = 2$ angular distributions and the agreement with the DWBA calculated curve is reasonably good.

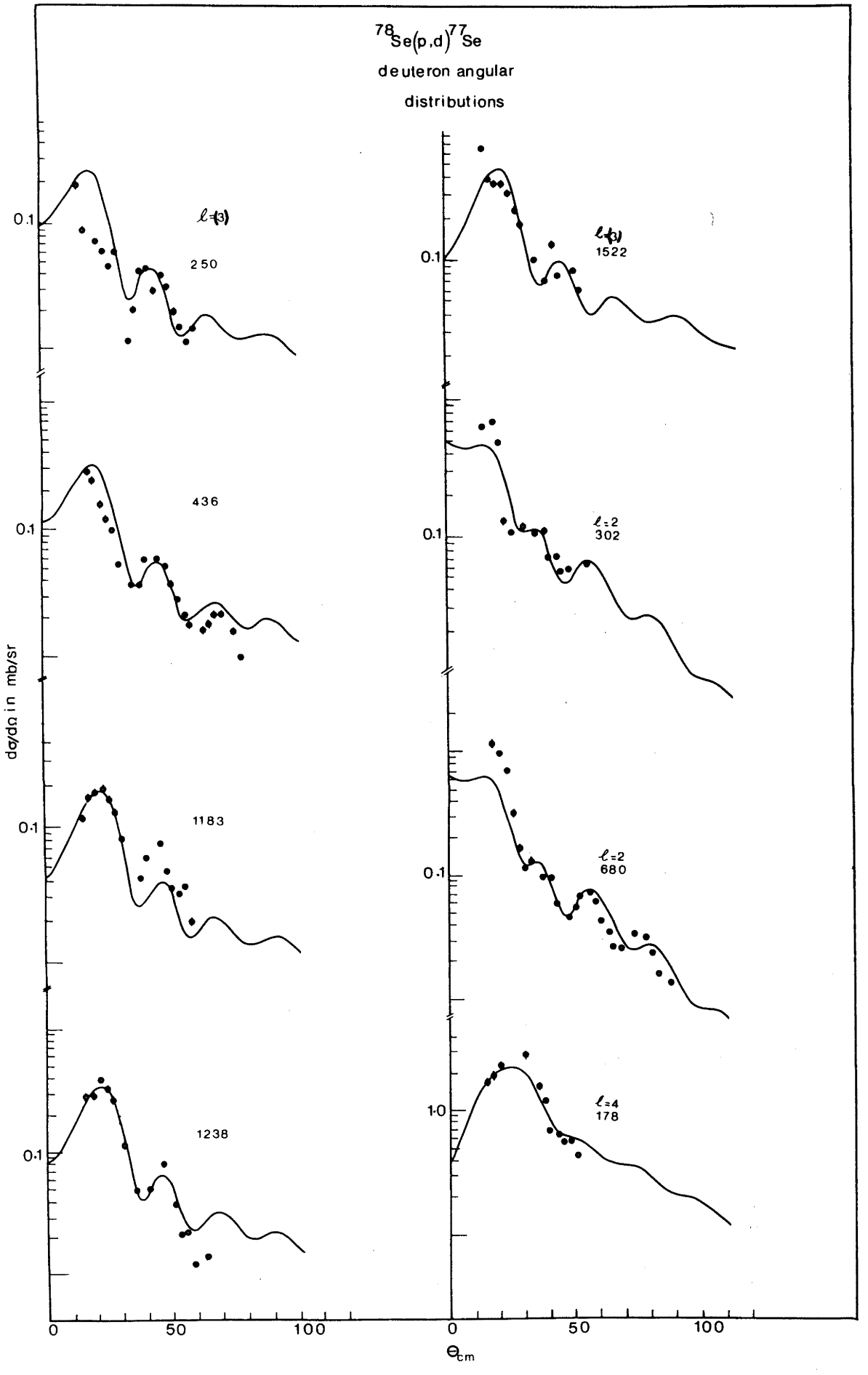

Fig.5.7. Deuteron angular distributions from the $^{78}Se(p,d)^{77}Se$ reaction compared with the DWBA predictions.

Braga and Sarantites have made a tentative spin and parity assignment of $(5/2^+)$ and Lin has fitted this state with $\ell = (2)$. Braga and Sarantites [Br 69], Rabinstein [Ra 71] and Murzin et al [Mu 73] have made a definite spin assignment of $5/2^+$ to this level.

An $\ell = 2$ assignment has been made to the level at 680 keV. As can be seen from the deuteron angular distribution in Fig. 5.7 the agreement between the predicted DWBA curve and the data at angles greater than 20° is reasonably good. An $\ell = 2$ assignment has also been made to this level by Lin [Li 65].

An $\ell = 4$ assignment has been made to the strongly excited level at 178 keV. Braga and Sarantites have made a tentative spin and parity assignment of $(9/2^+)$ and Lin fitted this level with $\ell = 1 + 4$ with a large spectroscopic factor for the $\ell = 4$ component. Braga and Sarantites have also observed a level at 161.8 keV to which a definite spin and parity assignment of $7/2^+$ was made. This level was not resolved in the present work. If the 161.8 keV level is excited in the (p,d) reaction then the angular distribution shown would be that of an unresolved doublet, both components being $\ell = 4$.

5.4 $^{80}Se(p,d)^{79}Se$

Spectroscopic information on ^{79}Se has been obtained previously from a study of the $^{78}Se(d,p)^{79}Se$ reaction by Lin [Li65]. He observed a total of 41 states, assigned ℓ values to all transitions and extracted spectroscopic factors. Lin also measured some level energies from the $^{80}Se(d,t)^{79}Se$ reaction without further study of the properties of these levels. Level energies have also been obtained from the (d,p) reaction by the MIT group [Ca 60] and also from the $^{78}Se(n,\gamma)$ reaction by Murzin et al [Mu 73] who also assigned some spins.

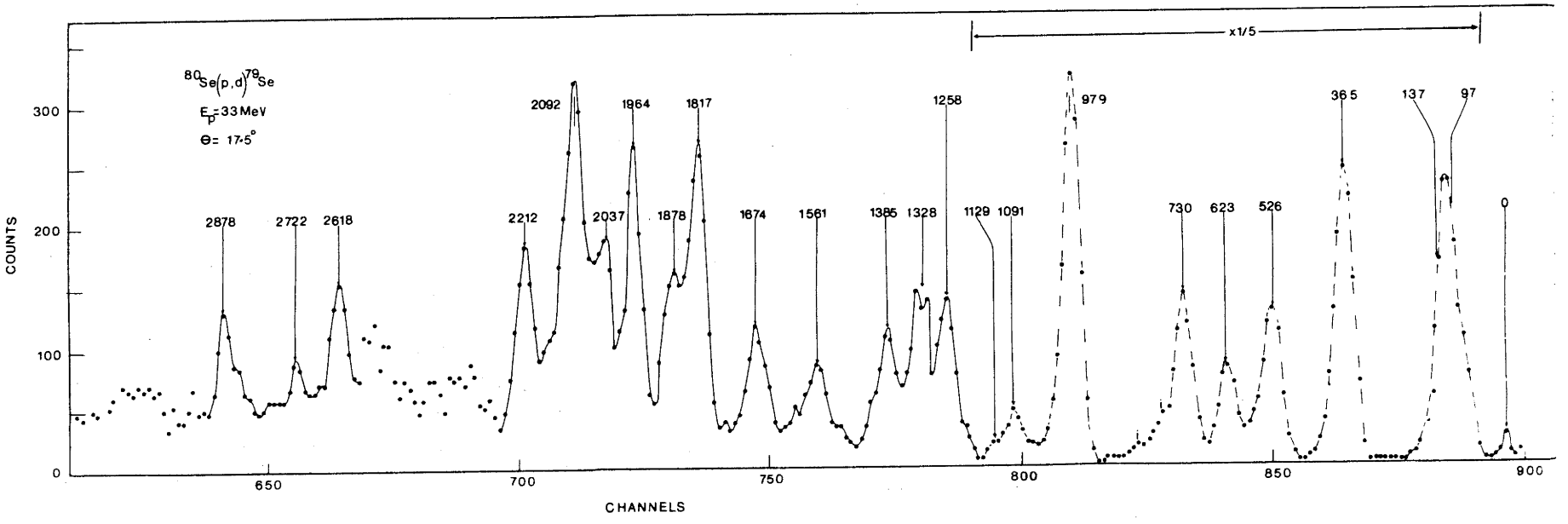

Fig.5.8. Deuteron spectrum from the $^{80}Se(p,d)^{79}Se$ reaction.

A total of 25 states were observed in the present work with angular distributions measured for 18 states. Two states were observed for the first time and six new ℓ assignments were made. Because of experimental limitations such as poor resolution and inadequate statistics, no angular distributions were measured for the remaining states. Spectroscopic factors were also extracted. A summary of the results is given in table 5.3.

5.4.1 $\ell = 1$ Transitions

Angular distributions for five $\ell = 1$ transitions together with DWBA calculations are shown in Fig. 5.9. As can be seen from the deuteron spectrum in Fig. 5.9, the $\ell = 1$ state at 97 keV is not completely resolved from the strongly excited state at 137 keV. Yields for these states were determined by forcing the program AUTOFIT to fit peaks at the above energies. Lin [Li 65] has also made an $\ell = 1$ assignment to the level at 97 keV.

An unambiguous $\ell = 1$ assignment has been made to the level at 1964 keV. This state has been reported in previous work by both Lin and the MIT group as a doubtful level. As can be seen from the deuteron spectrum Fig. 5.8 this is a strongly excited and well resolved state.

An angular distribution was obtained for the level at 1878 keV but no reasonable fit could be obtained for any value of ℓ. Lin has observed a level at 1870 keV to which he made a tentative assignment of $\ell = (1)$. He also made $\ell = 1$ assignments to levels at 2110 keV and 2280 keV. If the 2110 keV level was excited at all in the present study, our energy resolution would not be good enough to resolve it from the strongly excited $\ell = 3$ state at 2092 keV. Also the 2280 keV level, if excited at all, belongs to a group of very weakly excited states and it was not possible to identify it.

TABLE 5.3

Summary of results for states in ^{79}Se

E(keV) This Work	E(keV) Ref. [Li 65]	E(keV) Ref. [ND 66]	ℓ This Work	ℓ Ref. [Li 65]	J^{π} Ref. [ND 66]	S This Work
0[n]		0	(4)		$7/2^+$	0.08
97*	90	96	1	1	$1/2^-$	0.85
137*	130	135	4	1 + 4		2.06
365	350	367	3	3		1.6
		460				
526	520	528	1	1	$(1/2,3/2)^-$	0.39
623	620	632	2	2		0.07
720	720	727	2	2		0.1
		830				
979	970	976	1	1	$(1/2,3/2)^-$	1.15
1091[n]		1080	4			0.44
1129	1160	1158		0		
1258	1250	1254	2	2		0.03
1328[n]		1311	(3)			0.26
1385[a,n]			(3)			0.16
	1490	1495		(0)		
1561		1558				
	1600	1599		2		
1674	1670	1669	(2)	2		0.02
1743	1760	1752		2		
1817[a,n]			3			0.43
1878	1870	1861		(1)		
1964[n]	1960	1959	1	?		0.16
2037	2040	2019	1	1		0.17
2092[n]		2085	3			0.45
	2110			1		
2212	2190	2184	2	2		0.08
	2280	2262		1		
	2340	2331		2		
	2400	2387		2		
	2500	2530		2		
	2590	2594		2		
2618[a]						
2722[n]	2730	2722		(2)		
	2780			2		
2878[n]	2870			2		

a) New States

n) New ℓ assignments

* These energies were fixed in the code AUTOFIT

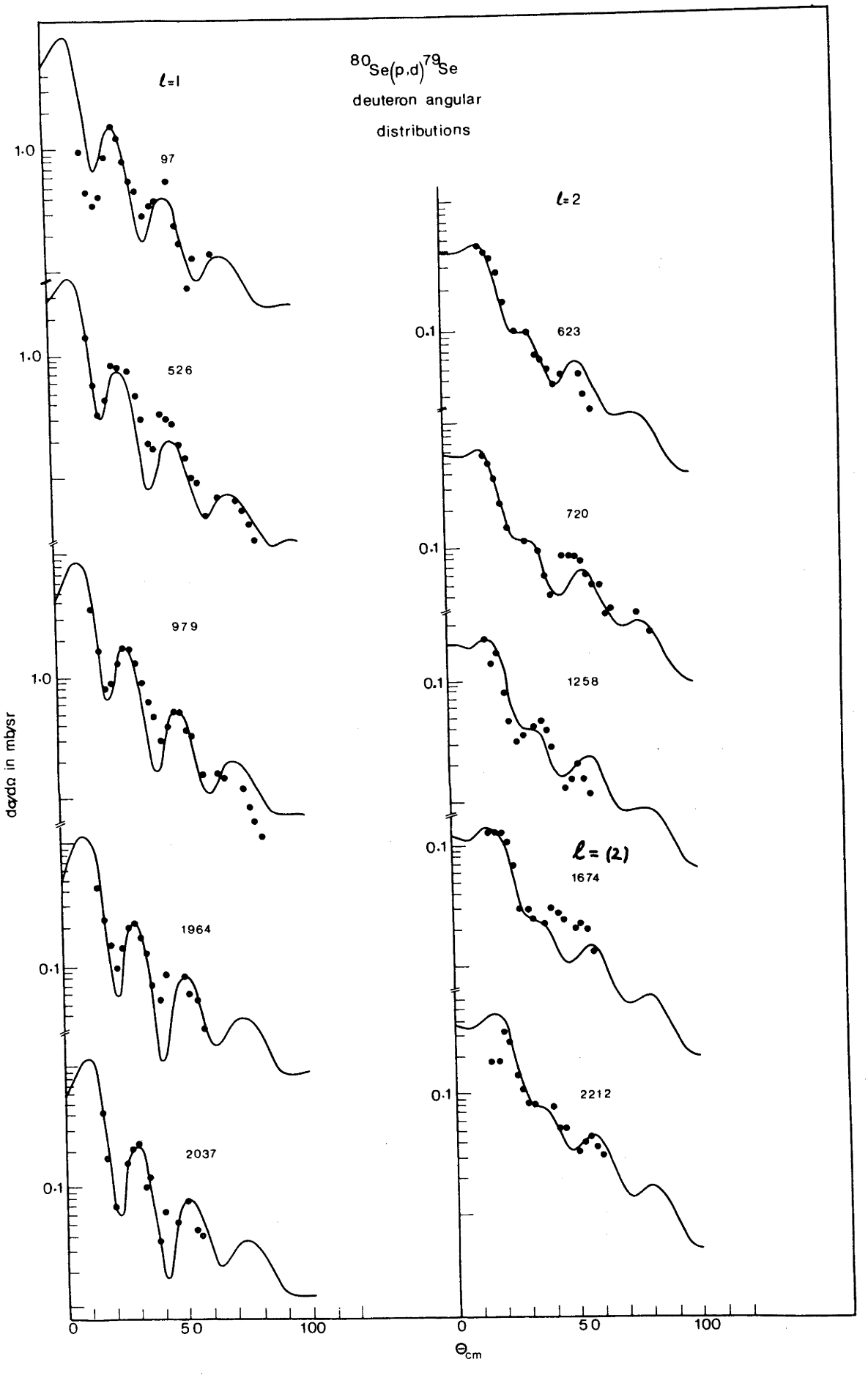

Fig.5.9 Deuteron angular distributions from the $^{80}Se(p,d)^{79}Se$ reaction compared with the DWBA predictions.

5.4.2 $\ell = 2$ Transitions

Fig. 5.9 shows angular distributions for five $\ell = 2$ transitions. The $\ell = (2)$ assignment to the level at 1674 keV is not very convincing at angles greater than 40°. There are also $\ell = 1$ and $\ell = 2$ impurities from ^{75}Se close to this state, but their contribution is estimated to be less than 1%. A tentative assignment has been made to this level to which Lin assigned an $\ell = 2$ value.

No angular distributions could be extracted for the levels at 2722 keV and 2878 keV to which Lin has made $\ell = 2$ assignments. Lin also observed an $\ell = 2$ level at 1600 keV. This level was not observed in the present work.

5.4.3 $\ell = 3$ Transitions

Angular distributions and DWBA calculations for five $\ell = 3$ transitions are shown in Fig. 5.10.

The $\ell = 3$ assignments to levels at 1328 keV, 1385 keV, 1817 keV and 2092 keV were made for the first time in the present work.

As can be seen from the deuteron spectrum in Fig. 5.8, the level at 1328 keV is partially resolved from the levels at 1258 keV and 1385 keV. Being the middle member of the triplet, it is difficult to determine the area of the peak without a large uncertainty, especially at larger angles where the statistics are poor. The best agreement between the data and the predicted DWBA shape is given for an $\ell = (3)$ transition. This should be taken as a tentative assignment.

The weakly excited state at 1385 keV in Fig. 5.8 also contains a contribution of 30% from impurities in ^{75}Se and ^{77}Se. After subtracting the impurities the deuteron angular distribution agrees reasonably well with the predicted DWBA curves. A tentative $\ell = (3)$

assignment has been made to this state which was observed for the first time in the present work.

The possible new level at 1817 keV contains a small contribution from a ^{75}Se impurity which has been subtracted. Because of the poor agreement between the predicted DWBA curve and the data at angles greater than 40° a tentative $\ell = (3)$ assignment has been made. A doubtful level at 1800 keV has been reported by the MIT group [Ca 60] which may be the same level as observed in this work.

An $\ell = 3$ assignment has been made to the level at 2092 keV. This level was not excited by Lin [Li 65] in (d,p). However he observed an $\ell = 1$ level at 2110 keV. Our good agreement between the predicted DWBA curve and the data strongly favours the $\ell = 3$ assignment for the 2092 keV level.

5.4.4 $\ell = 4$ Transitions

Fig. 5.10 presents angular distributions together with DWBA predictions for three $\ell = 4$ transitions. The ground state is known from previous work [ND 66] to be a $7/2^+$ anomalous positive parity state. The angular distribution for this state has been measured for the first time in the present work from which a tentative $\ell = (4)$ assignment has been made. The agreement between the predicted DWBA curve and the data is not very good, but there are characteristics of an $\ell = 4$ transition. As can be seen from the deuteron spectrum in Fig. 5.8, this state is very weakly excited. There is also a 20% impurity from ^{81}Se contributing to the ground state which has been subtracted.

An $\ell = 4$ assignment has been made to the strongly excited state at 137 keV. Since this state is not completely resolved from the $\ell = 1$ 97 keV state, peak areas were determined by forcing the program AUTOFIT to fit peaks at these energies. Lin made an $\ell = 1 + 4$ assignment to the 137 keV state, with a large spectroscopic factor for the $\ell = 4$

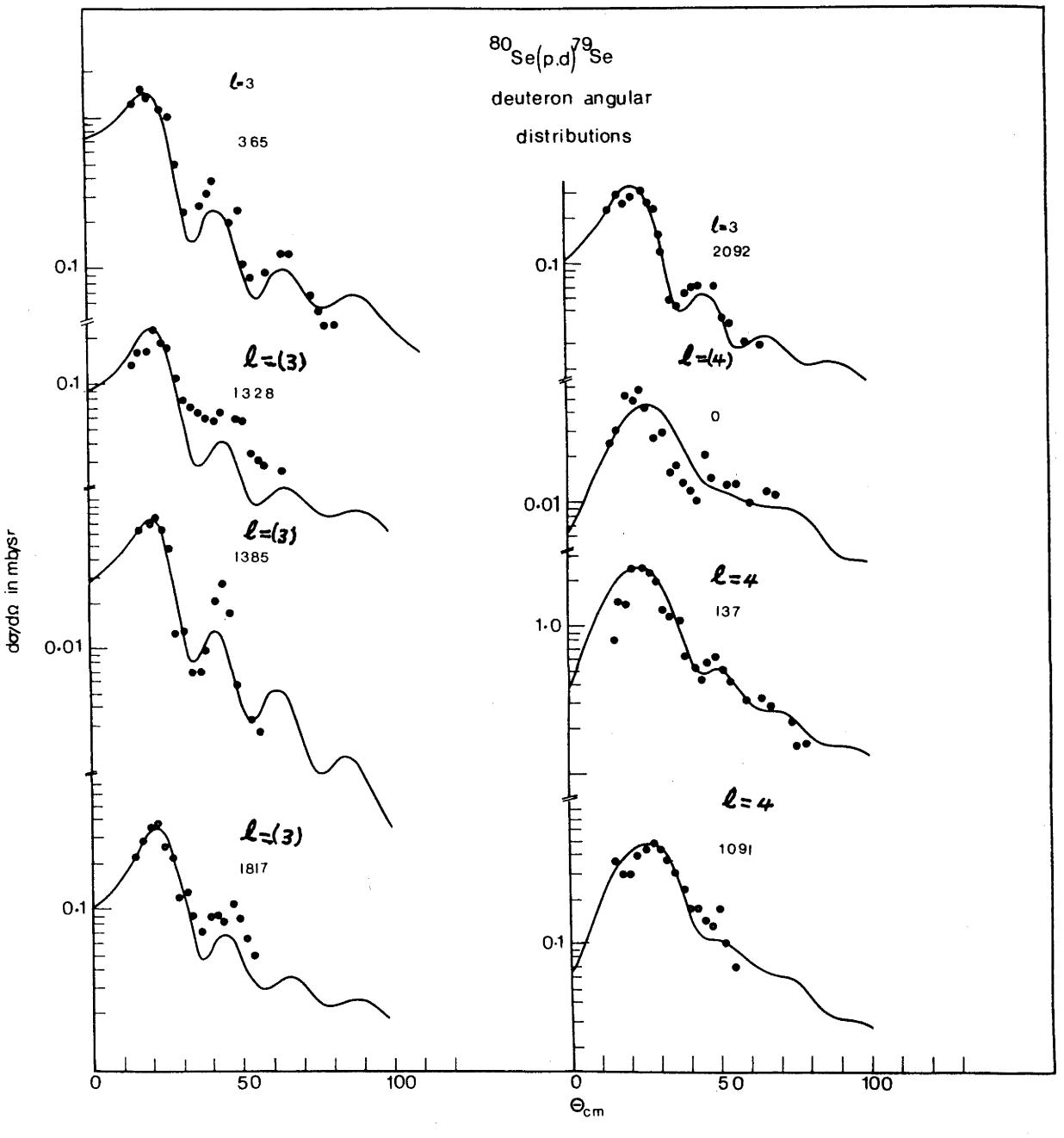

Fig.5.10. Deuteron angular distributions from the $^{80}Se(p,d)^{79}Se$ reaction compared with the DWBA predictions.

component. Murzin and Kolomiets [Mu 73] have made a spin and parity assignment of $9/2^+$ to the level at 137 keV.

The $\ell = 4$ assignment to the level at 1091 keV agrees reasonably well with the predicted DWBA curves. There is also an estimated 15% impurity from ^{77}Se contributing to the strength of this state which has been subtracted. Murzin and Kolomiets [Mu 73] observed levels at 1080 keV and 1089 keV to both of which they assigned spins and parities of $(1/2, 3/2)^-$.

5.5 ^{82}Se(p,d)^{81}Se

The odd neutron ^{81}Se nucleus has been studied previously by Lin [Li 65] through the ^{80}Se(p,d)^{81}Se reaction. He observed a total of 45 levels and measured angular distributions for 34 of these. Lin also measured 7 level energies from ^{82}Se(d,t)^{81}Se without further study of the properties of these levels. Rabinstein [Ra 71] provided energy levels and assigned some spins and parities from the ^{80}Se(n,γ)^{81}Se reaction.

In the present work a total of 30 states were observed with angular distributions measured for 29 of these states. Spectroscopic factors were extracted. There were 10 new states observed and 14 new ℓ assignments made. A summary of the results is given in table 5.4.

5.5.1 $\ell = 1$ Transitions

Fig. 5.12 shows angular distributions and the DWBA predicted curves for nine $\ell = 1$ and one $\ell = 1 + 3$ transitions, seven of which are new assignments.

The levels at 1628 keV, 2150 keV, 2603 keV and 3349 keV have been observed for the first time in the present work. From the measured deuteron angular distributions and the DWBA calculated curves $\ell = 1$ assignments have been made to these levels. $\ell = 1$

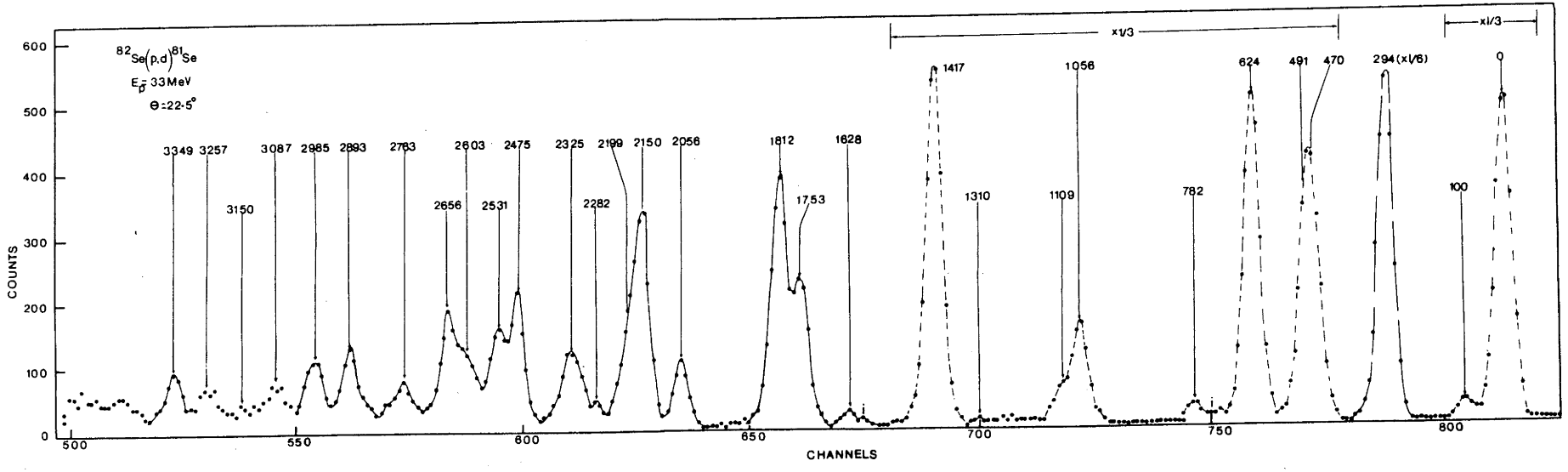

Fig.5.11 Deuteron spectrum from the $^{82}Se(p,d)^{81}Se$ reaction.

assignments have also been made to the levels at 2056 keV and 2282 keV. Lin observed levels at 2060 keV and 2260 keV, but he did not assign ℓ values. The remaining $\ell = 1$ assignments agree with Lin.

The new group of states at 3150 keV has been fitted with two ℓ values. This is because no single ℓ value gave any satisfactory DWBA fit to the data. A least squares fit was performed with possible linear combinations of ℓ values and it was found that the best fit to the data was given by $\ell = 1 + 3$. The component of each ℓ value was used to calculate spectroscopic factors shown in table 5.4.

Two levels have been observed by Rabinstein [Ra 71] at 470 keV and 491 keV to which he assigned spins and parities of $3/2^-$ and $5/2^-$ ($3/2^+$) respectively. On the basis of Rabinstein's data and the fact that at some angles there are indications of a doublet, angular distributions were extracted for both of these states. The yields were obtained by forcing the program AUTOFIT to fit peaks at the above energies. The poor agreement between the predicted DWBA curves and the experimental deuteron angular distribution has led to tentative $\ell = (1)$ and $\ell = (3)$ assignments to the 470 keV and 491 keV levels respectively. A combined angular distribution was also extracted and fitted with $\ell = 1 + 3$, but the best DWBA fit to the data is given for separate peaks at 470 keV and 491 keV.

5.5.2 $\ell = 2$ Transitions

Deuteron angular distributions for six $\ell = 2$ and one $\ell = 2 + 4$ transitions together with the DWBA calculated curves are shown in Fig. 5.13.

The $\ell = (2)$ transition at 1109 keV, which has been observed for the first time in the present work, is only partially resolved from the $\ell = 2$ transition at 1056 keV. Although the agreement between the data and the DWBA curve is reasonably good, a tentative $\ell = (2)$ assignment has been made because the angular distribution shows less

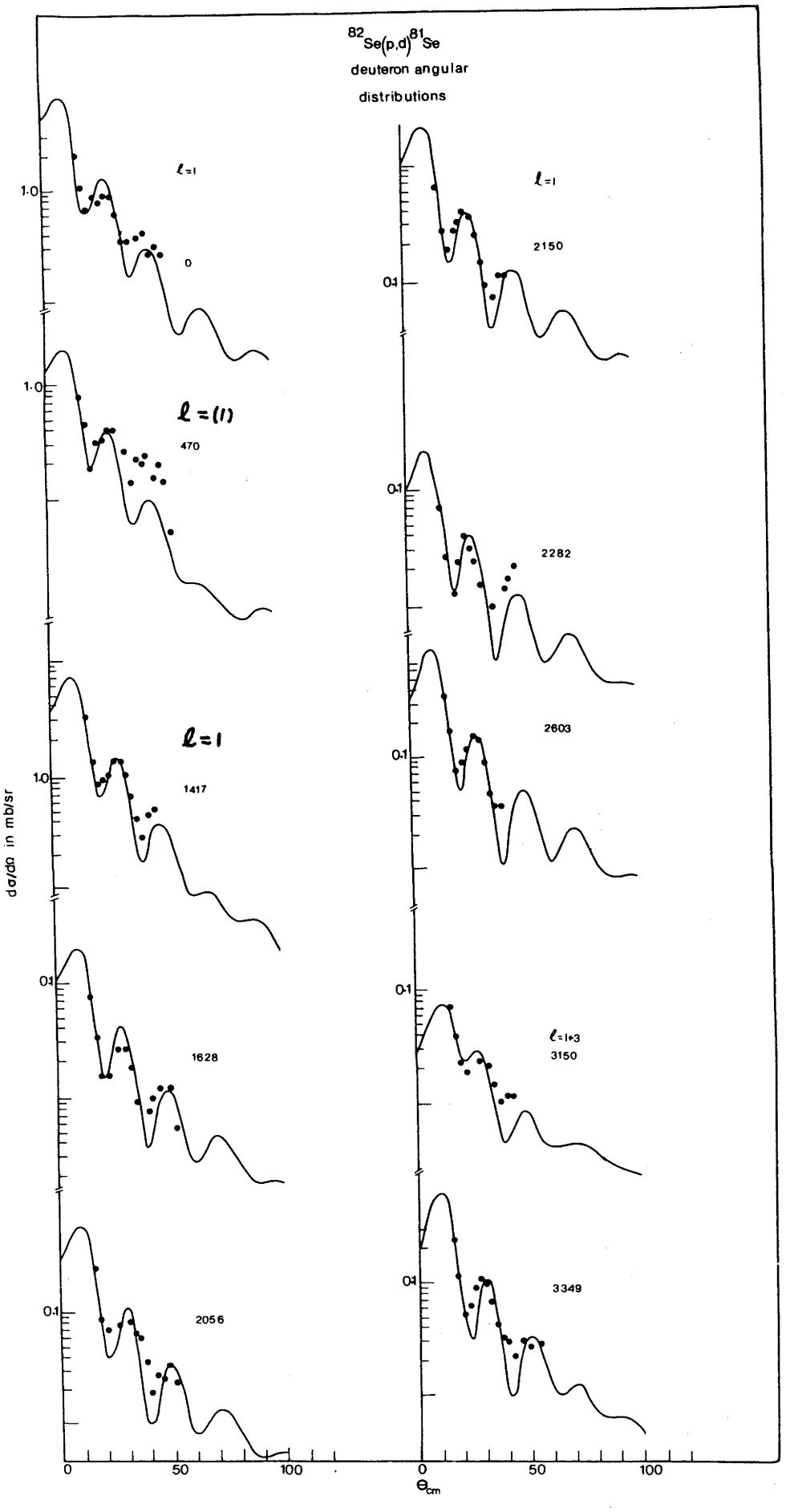

Fig.5.12 Deuteron angular distributions from the $^{82}Se(p,d)^{81}Se$ reaction compared with the DWBA predictions.

TABLE 5.4

Summary of results for states in ^{81}Se

E(keV) This Work	E(keV) Ref. [Li 65]	E(keV) Ref. [Ra 71]	ℓ This Work	ℓ Ref. [Li 65]	J^{π} Ref. [Ra 71]	S This Work
0	0	0	1	1	$1/2^-$	0.57
100	100	102.9	4	4	$7/2^+$	0.08
294	290	294.2	4	4	$9/2^+$	2.42
470*	470	467.8	1	1	$3/2^-$	0.26
491*		491.3	3		$5/2^-(3/2^+)$	0.75
		615.5				
624	640	624.6	3	3	$5/2^-$	1.02
782[a,n]			4			0.06
	900	889.6		(0)		
1056	1060	1052.5	2	2	$5/2^+$	0.09
1109[a,n]			(2)			0.02
	1250	1238.8		0		
1310	1310	1306.6	2	2	$5/2^+$	0.02
1417	1420	1406.6	1	1	$3/2^-$	0.97
1628[a,n]			1			0.02
		1702.4				
		1711.3				
1753	1730	1725	2	2		0.07
1812[n]		1828.2	4		$3/2^+$	0.46
	1840			2		
2056[n]	2060		1	?		0.07
2150[a,n]			1			0.32
2199	2180	2174	2	2		0.02
		2252.9				
2282[n]	2260		1			0.04
2325	2340	2333.3	2 + 4	2 + 3		0.03
		2383.3				0.05
2475[a,n]			3			0.20
2531[a,n]			(4)			0.15
	2550	2568.8		2		
2603[a,n]			1			0.13
2656[n]	2680		(3)	0		0.20

(cont'd)

TABLE 5.4 (cont'd)

E(keV) This Work	E(keV) Ref. [Li 65]	E(keV) Ref. [Ra 71]	ℓ This Work	ℓ Ref. [Li 65]	J^{π} Ref. [Ra 71]	S This Work
2763[n]	2790	2773.8	2 + 3	2		0.012 0.03
2893[a,n]			3 + 4			0.1 0.06
	2930			(0)		
2985[n]	2990	2953.1	3 + 4	(0)		0.09 0.07
3087	3070		(2)	2		0.07
3150[a,n]			1 + 3			0.02 0.03
3257	3240			(2)		
	3310			2		
3349[a,n]			1			0.11

* These energies were fixed in the code AUTOFIT

a) New states

n) New ℓ assignments

Angular distributions to which more than one ℓ value has been assigned correspond to unresolved multiplets, and are not the result of nuclear interference as this is not allowed by the Selection rules.

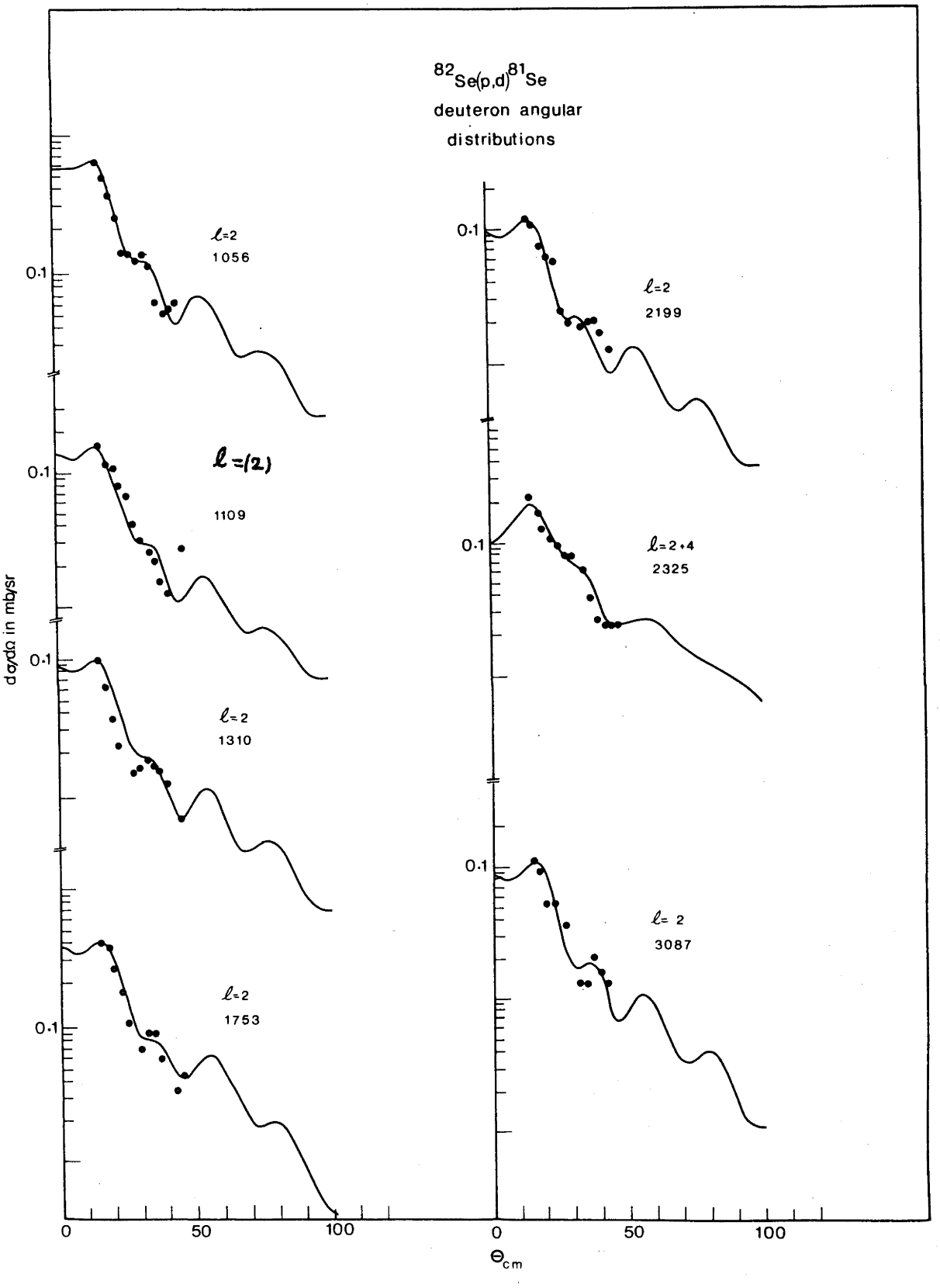

Fig.5.13 Deuteron angular distributions from the $^{82}Se(p,d)^{81}Se$ reaction compared with the DWBA predictions.

structure than other $\ell = 2$ experimental angular distributions. Lin also observed $\ell = 2$ states at 1840 keV, 2550 keV and 3310 keV which were not observed in the (p,d) reaction. All other $\ell = 2$ assignments agree with those made by Lin.

The level at 2325 keV, as can be seen from the deuteron spectrum in Fig. 5.11, corresponds to a broad peak. Because no single ℓ value gave a satisfactory DWBA fit to the data, a least squares fit was performed and it was found that the best fit to the angular distribution was given by $\ell = 2 + 4$. Lin has fitted this level with $\ell = 2 + 3$. Rabinstein also observed levels at 2333.2 keV and 2383.3 keV to which he did not make any spin and parity assignments.

5.5.3 $\ell = 3$ and $\ell = 4$ Transitions

Fig. 5.14 shows a total of twelve deuteron angular distributions and the DWBA calculations for four $\ell = 3$, one $\ell = 2 + 3$, two $\ell = 3 + 4$ and five $\ell = 4$ assignments made in the present work.

The level at 491 keV is separated by only 21 keV from another strongly excited level at 470 keV [Ra 71]. As has been discussed previously, peak areas for these transitions were obtained by fixing the peak positions in the program AUTOFIT. However the peak areas of this doublet so determined have large uncertainties. The agreement between the DWBA calculated curve and the data is not very good, but the first minimum and the second maximum occur at the same position as other $\ell = 3$ experimental angular distributions, with the first maximum slightly displaced. A tentative $\ell = (3)$ assignment has been made to this level. Rabinstein has made a spin and parity assignment of $5/2^-$ or $(3/2^+)$ and Murzin and Kolomiets [Mu 73] assigned $5/2^-$.

An $\ell = 3$ assignment has been made to the level at 2475 keV. This level has been observed for the first time in the present work. As can be seen from Fig. 5.14 there is a reasonably good agreement

between the data and the predicted DWBA curve.

The poor agreement between the experimental angular distribution and the predicted DWBA curve has led to a tentative $\ell = (3)$ assignment to the level at 2656 keV. A combination of different ℓ values was also tried but the best fit to the data was given by $\ell = (3)$. As can be seen from the energy spectrum in Fig. 5.11 this level is partially resolved from the new level at 2603 keV. No angular distribution could be extracted for the 2603 keV level.

The levels at 2763 keV, 2893 keV and 2985 keV have been fitted with two ℓ values. This is because no single ℓ value gave any satisfactory DWBA fit to the data. A least squares fit was performed with possible combinations of ℓ values and it was found that the best fit to the data was given by $\ell = 2 + 3$ for the 2763 keV level. The best fit for the levels at 2893 keV and 2985 keV was given by $\ell = 3 + 4$. The spectroscopic factors are calculated from the component of each ℓ value. The level at 2893 keV was observed for the first time. Assignments of $\ell = 0$ and $\ell = 2$ have been made by Lin [Li 65] to the states at 2680 keV and 2790 keV respectively. Lin also made an $\ell = (0)$ assignment to a level at 2990 keV.

The weakly excited level at 100 keV is known from previous work [Ra 71] to be a $7/2^+$ anomalous positive parity state. The deuteron angular distribution has been measured in the present study and an $\ell = 4$ assignment has been made. Lin also observed this state in (d,p) and made an $\ell = 4$ assignment.

The level at 294 keV is the most strongly excited state in the spectrum. From the deuteron angular distribution an unambiguous $\ell = 4$ assignment has been made. Lin also made an $\ell = 4$ assignment to this state and Rabinstein assigned a spin of $9/2^+$.

The level at 782 keV was observed for the first time in the present work. From a comparison of the deuteron angular distribution and the DWBA curve an $\ell = 4$ was assigned to this transition. A spin of $9/2^+$ has been used in the DWBA calculations. It should be also noted that the 135 keV $\ell = 4$ state from ^{79}Se appears as an impurity at 760 keV and contributes less than 50% to the strength of the 782 keV state. This impurity has been subtracted.

The $\ell = 4$ assignment to the new state at 1812 keV shows a very good agreement with the predicted DWBA curve. Rabinstein [Ra 71] has observed a level at 1828 keV to which he assigned a spin of $3/2^+$. The poor agreement between the DWBA predicted curve and the data at forward angles has led to a tentative $\ell = (4)$ assignment to the level at 2531 keV. This level has been observed for the first time in the present work. A level has also been observed by Rabinstein [Ra 71] at 2568.8 keV to which he made no spin assignment. Lin observed a level at 2559 keV to which he made an $\ell = 2$ assignment.

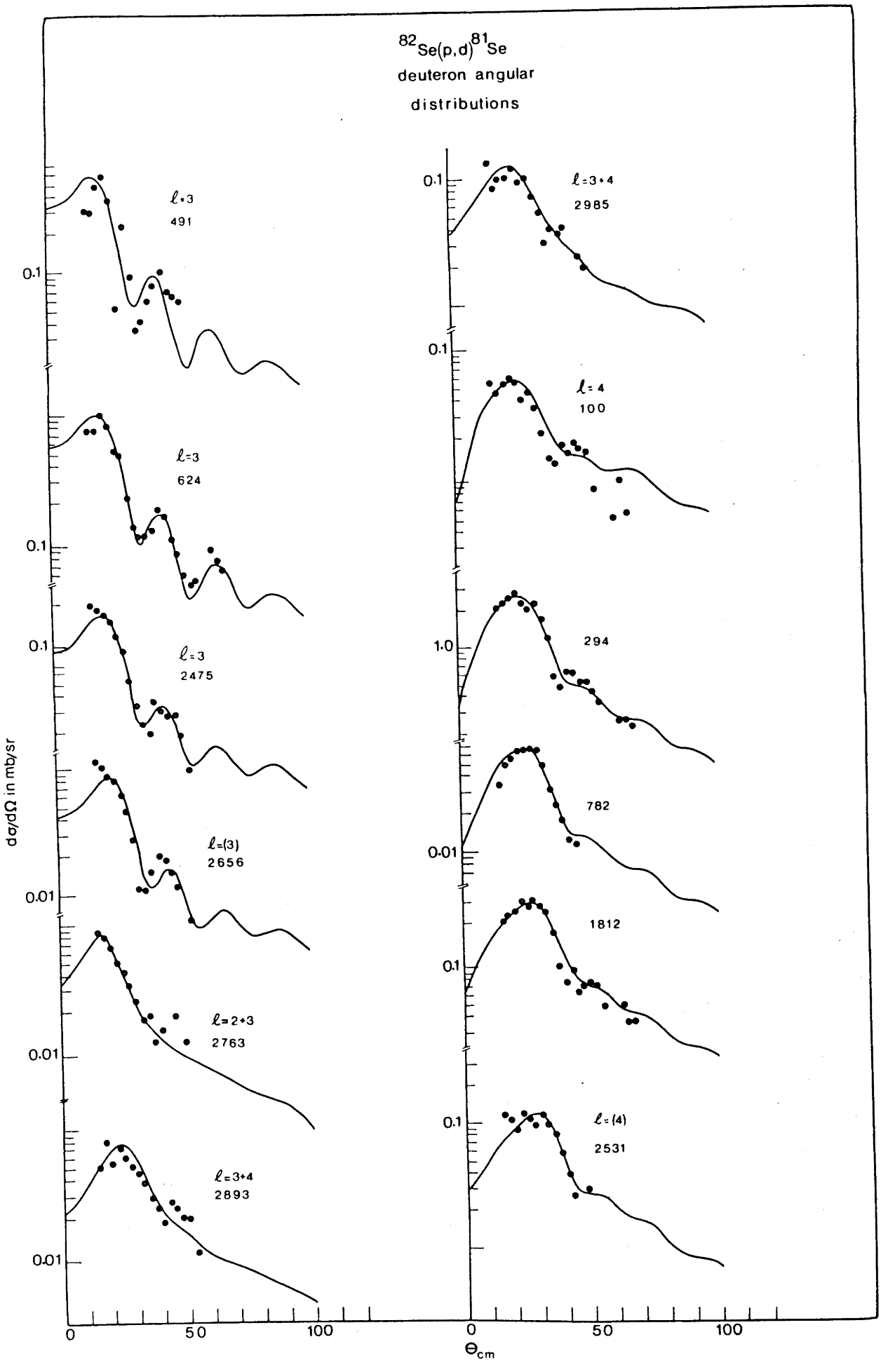

Fig. 5.14. Deuteron angular distributions from the $^{82}Se(p,d)^{81}Se$ reaction compared with the DWBA predictions.

CHAPTER 6

DISCUSSION OF RESULTS

Data from transfer reactions in this region have in the past been interpreted in terms of the shell model picture. Recent experimental evidence however indicates that the Se nuclei may be deformed, in which case an alternative approach in terms of the Coriolis coupling model is also possible. In view of this, this Chapter provides an interpretation of the (p,d) data using both the shell model approach with appropriate residual interactions and the Coriolis coupling model.

6.1 Shell Model Interpretation

According to the shell model picture in Fig. 6.1, the (p,d) reaction in the selenium region is expected to pick-up neutrons from the partially filled $2p_{3/2}$, $1f_{5/2}$, $2p_{1/2}$ and $1g_{9/2}$ orbitals. In neutron pick-up from spin-zero targets, the spin and parity of the observed low-lying levels populated by an $\ell = 3$ or 4 transitions can be assigned $5/2^-$ and $9/2^+$ respectively. However for $\ell = 3$ transitions it is still possible in the case of weakly excited states at high excitation energies to pick-up from the $1f_{7/2}$ orbital, although level systematics for nuclei in this region show that $7/2^-$ transitions are virtually unknown. It is also expected that most of the $2p_{1/2}$ spectroscopic strength should appear at low excitation, since the Fermi level is close to $2p_{1/2}$, while the $2p_{3/2}$ strength should appear at slightly higher energies. However for well known $1/2^-$ or $3/2^-$ states there seems to be no clear cut distinction in excitation energy for the Se nuclei so the ambiguity in spin for $\ell = 1$ transitions remains.

The fact that a number of $\ell = 2$ transitions have been observed in the Se nuclei in the present study and by both Sanderson and Lin in

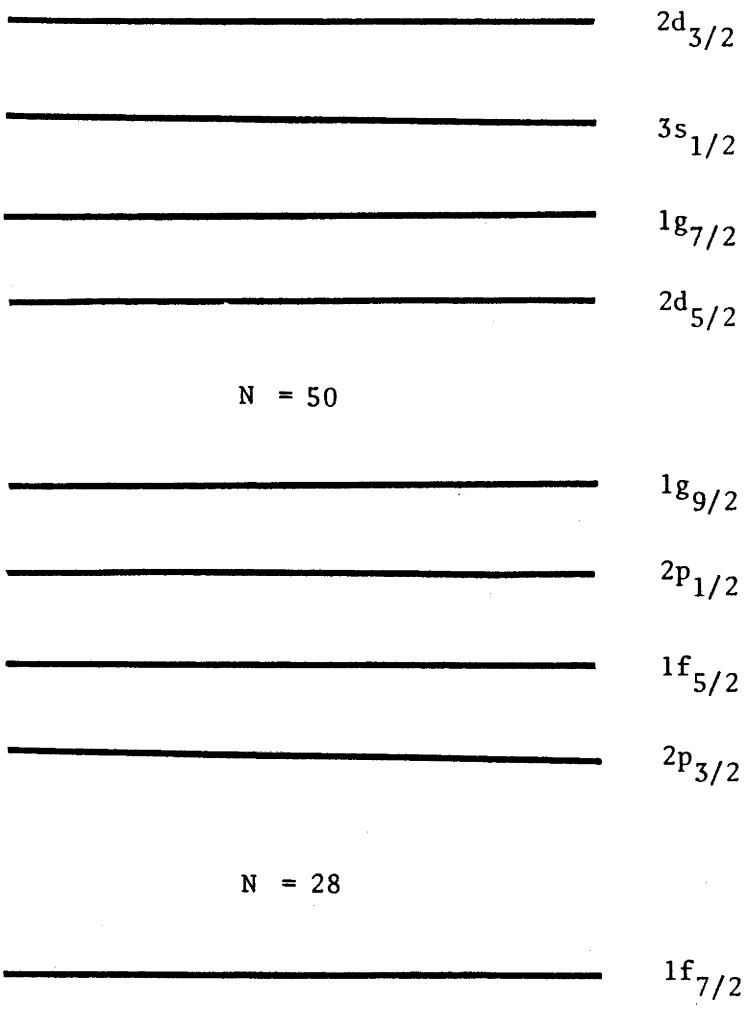

Fig. 6.1 The shell model orbitals occupied by the valence neutrons for the nuclei studied.

(d,t) seems to indicate that the $2d_{5/2}$ or $2d_{3/2}$ orbitals are surprisingly starting to fill even though the major N = 50 neutron shell is not closed. It should be noted that the energy gap between the $1g_{9/2}$ and the $2d_{5/2}$ subshells is estimated to be about 4.5 MeV. Transitions with $\ell = 2$ values which have been attributed to the $2d_{5/2}$ orbitals have also been observed in Ge(p,d) reactions by Fournier et al [Fo 73]. It is assumed in the present study that states originating from the $2d_{3/2}$ orbital should appear above the excitation energy range of about 3.5 MeV. This is based on a survey of (d,p) experimental data near A = 100 by N. Kato [Ka 73] which shows that the amount of $\underset{\sim}{\ell}.\underset{\sim}{s}$ splitting between the $2d_{5/2}$ and $2d_{3/2}$ orbitals is about 3 MeV. The special case of low-lying $7/2^+$ and $5/2^+$ states will be discussed in section 6.2.

6.1.1 Spectroscopic Factors

The spectroscopic factor $S(\ell j)$ is extracted from the data using the final expression for the differential cross-section [Ba 62]

$$\left(\frac{d\sigma}{d\Omega}\right)_{EXP} = 2.29\ S(\ell j)\ \frac{2s+1}{2} \cdot \frac{\sigma_D(\theta)}{2J+1} \qquad (6.1)$$

where $\sigma_D(\theta)$ is the theoretical cross-section calculated by the program DWUCK, $(d\sigma/d\Omega)_{EXP}$ is the experimentally measured cross-section and s and J are the spin and the total angular momentum of the transferred neutron. The numerical factor 2.29 comes from substituting for the various quantities in Eq. 2.25. The spectroscopic factor can therefore be obtained by comparing the absolute value of the experimental cross-section with the theoretical cross-section.

In the present study spectroscopic factors were extracted by matching the experimental angular distributions with the DWBA predictions over a number of forward angles for which the fits were satisfactory and the statistical errors small. The average over these angles was then taken. These angles corresponded to the first maximum where cross-sections

are largest and contain relatively small contributions from compound nucleus formation. The experimental angular distributions and the DWBA predictions presented in this thesis display the way in which they were matched in each case.

The possible error in the extracted spectroscopic factors is due to the following uncertainties, namely:

(a) the uncertainty due to matching the experimental angular distributions with the DWBA calculations;

(b) the sensitivity in the spectroscopic factor to the optical parameters used; the spectroscopic factor was extracted for a number of states using two different sets of deuteron optical parameters [Pe 66, Ch 75] and it was found that the spectroscopic factor differed by 15%;

(c) the uncertainty that arises from the error in the experimental differential cross-section.

The magnitude of the uncertainty in the spectroscopic factor is estimated to be of the order of 25%. Spectroscopic factors for the four nuclei studied in the present work are shown in tables 5.1, 5.2, 5.3 and 5.4.

Table 5.1 presents spectroscopic factors for ^{75}Se determined from the present work together with those of Sanderson [Sa 73] extracted from the ^{76}Se(d,t)^{75}Se reaction. Sanderson observed a total of 21 states up to an excitation energy of 1246 keV as compared to 14 states resolved in the present work up to the same excitation energy.

A total spectroscopic strength of 9.8 has been extracted by Sanderson, compared to 8.27 extracted for states up to the same excitation energy in the present work. Sanderson obtained a spectroscopic

factor for the ground state which is twice as large as the value obtained from the present work, and for the $\ell = 4$ state at 132 keV a value 36% larger was obtained. There is also a large discrepancy for the $\ell = 3$ state at 667 keV for which a spectroscopic factor twice as large as that of Sanderson's has been obtained in the present work. As can be seen from the deuteron spectrum in Fig. 5.1 the 667 keV state belongs to a group of partially resolved states for which a total spectroscopic factor of 0.79 has been obtained. Sanderson has obtained 0.6 (excluding the ℓ = 611 keV state) for the same group of states, a difference of 24% which is within the uncertainty in the spectroscopic factor. Sanderson was also able to resolve the group of four states at around 1050 keV. He obtained a spectroscopic factor of 0.16 for the 1048 keV $\ell = 3$ state. A spectroscopic factor of 0.44 was obtained for the state at 1050 keV, the only state observed in this region in the present work. This state is on the tail of the very strongly excited $\ell = 1$ state at 962 keV for which the spectroscopic factor of 0.40 agrees well with that of Sanderson. Spectroscopic factors for the other well-resolved states agree reasonably well.

6.1.2 Level Systematics

If we ignore pick-up from the $1f_{7/2}$ shell and below, then the total expected spectroscopic strength should be equal to the number of valence neutrons. For pick-up from a given subshell, French and Macfarlane [Fr 61] give the total spectroscopic strength as

$$\sum_{T_< = T_o - \frac{1}{2}} S = \sum S_< = \nu - \pi/(N-Z+1) \qquad (6.2)$$

where ν is the number of neutrons and π is the number of protons in the subshell, N and Z refer to the total number of neutrons and protons in the target nucleus and T_o is the isospin of the target nucleus.

States with $T_> = T_o + \frac{1}{2}$ are known [Sh 65] to be at higher excitation in this mass region and are not expected to be observed in this work.

In a (p,d) reaction the cross-section should be proportional to the average number of neutrons in the orbital from which the neutron is picked up. On the other hand, the cross-section for inserting a neutron into a given orbital should be proportional to the emptiness of that orbital. The degree of fullness V_j^2 and of emptiness U_j^2 of an orbital is defined as $V_j^2 = n_j/(2j + 1)$ and $(V_j^2 + U_j^2) = 1$, where n_j is the average number of nucleons in the j orbital.

The most important component of the residual interaction is usually the pairing force which couples together pairs of identical nucleons to total spin zero. This can cause strong configuration mixing between the available shell model states with the result that the single particle strength is spread over a number of states. The mean energy of the states over which the ℓj pure single particle state has been spread is called the centre-of-gravity energy $E_{\ell j}$ given by

$$E_{\ell j} = \frac{\sum_i S_i(\ell j) E_i(j)}{\sum_i S_i(\ell j)} \quad . \tag{6.3}$$

From the sum rule we have

$$n = K \sum_{ij} S_i(\ell j) \tag{6.4}$$

and

$$V_j^2 = K \frac{\sum_i S_i(\ell j)}{(2j+1)}$$

where $S_i(\ell j)$ is the experimental spectroscopic factor for the state i; n is the number of valence neutrons above the $1f_{7/2}$ shell and K is a normalization constant which normalizes the total experimental strength to the sum rule value.

The pairing theory developed by Kisslinger and Sorensen [Ki 60] relates the unperturbed single particle energies ε_j to the single

quasi-particle energies $E_{\ell j}$ by the expression

$$E_{\ell j} = \{(\varepsilon_j-\lambda)^2 + \Delta^2\}^{\frac{1}{2}} - C \quad . \tag{6.5}$$

Also

$$V_j^2 = \tfrac{1}{2}\left\{1 - \frac{\varepsilon_j-\lambda}{\sqrt{(\varepsilon_j-\lambda)^2 + \Delta^2}}\right\}^{\frac{1}{2}} = \frac{n_j}{2j+1}$$

where λ is the chemical potential and Δ is half the gap energy. The constant C was set equal to Δ which corresponds to setting $E_{\ell j} = 0$ for the single particle state which is half filled.

The strength of the pairing interaction G is related to Δ, λ and ε_j by the gap equation

$$\frac{G}{4} \sum_j \frac{(2j+1)}{\{(\varepsilon_j-\lambda)^2+\Delta^2\}^{\frac{1}{2}}} = 1 \ , \tag{6.6}$$

The parameters λ and Δ were determined by solving the gap equation [Ki 60] in conjunction with Eq, 6.5. A value of G = 24/A MeV was used, the value recommended by Kisslinger and Sorensen for this mass region. The single particle energies were derived using the relations given in reference [Ki 60] and the values suggested for A = 58 by Fournier et al [Fo 73]

$$\left(\varepsilon^{\circ}_{2p_{3/2}} = 0, \quad \varepsilon^{\circ}_{1f_{5/2}} = 0.3 \text{ MeV}, \quad \varepsilon^{\circ}_{2p_{1/2}} = 2.8 \text{ MeV} \quad \text{and} \right.$$

$$\left. \varepsilon^{\circ}_{1g_{9/2}} = 3.0 \text{ MeV} \right) \quad .$$

The gap parameter Δ can also be determined from the even-odd mass differences using the relation

$$\Delta \simeq \tfrac{1}{4}\left[\, |SE(N) - SE(N-1)| + |SE(N) - SE(N+1)| \,\right] \ ,$$

where N is the number of neutrons in the nucleus for which Δ is calculated and SE(N) is the separation energy of one neutron. Using the tabulated values of the mass excess Δ was calculated to be 1.5 MeV in this mass region compared to a value of approximately 1.3 MeV obtained by solving the gap equation.

The occupation probabilities V_j^2 calculated from the above relations are compared to the experimental values in Table 6.1. Because of the ambiguity in assigning spins to the $\ell = 1$ transitions, the experimental value of $K \sum_i S_i(\ell j)/6$ for the total spectroscopic strength of the $\ell = 1$ transitions is compared to the calculated value given by $(V_{1/2}^2 + 2V_{3/2}^2)/3$. The normalization constant K in Eq. 6.4 takes care of experimental uncertainties, missing spectroscopic strength from states not resolved and any variation in the spectroscopic strength due to the optical model parameters used. The value of K is not expected to change significantly from isotope to isotope. However some variation in K might be expected since the same deuteron optical parameters were used for all isotopes instead of describing them by optical wells of somewhat different geometry and depths.

As can be seen from Table 6.1 the value of K increases from 1.46 in ^{76}Se to 2.32 in ^{82}Se, indicating that the deviation from the expected spectroscopic strength increases as the number of neutrons in the Se nuclei increases. Although K is large the DWBA fits are good and the agreement between the experimental and theoretical values of V_j^2 are very good. This seems to suggest that, whatever the reason for this anomaly, all orbitals have been affected equally.

Table 6.1 gives a summary of the spectroscopic strength for the $(2p_{3/2} + 2p_{1/2})$, $1f_{5/2}$, $1g_{9/2}$ and $2d_{5/2}$ orbitals. The total spectroscopic strength for the $\ell = 1$ transitions which includes fragments of both the $2p_{3/2}$ and $2p_{1/2}$ single particle levels has a value of 2.90 in ^{76}Se, 2.49 in ^{78}Se, 2.72 in ^{80}Se and 2.51 in ^{81}Se. The sum rule prediction shows that the expected strength should be around 5.6 in ^{76}Se and should increase slightly as the number of neutrons increases. A similar observation is also made for the $\ell = 3$ transitions, where the expected total spectroscopic strength should have a value close to about six in all isotopes. However the strength decreases from 4.01 in ^{78}Se

TABLE 6.1

Comparison of experimental filling coefficients with predictions of the pairing theory.

Isotope	ℓj	$\sum_i S_i(\ell j)$	K	$V^2_{EX}(j)$	$V^2_{EX}(j)$ [Li 65]	$V^2_{Th}(j)$ b	$E_{EX}(j)$ (MeV)	$E_{Th}(j)$ (MeV)
^{76}Se	$1g_{9/2}$	2.82	1.46	0.42	0.64	0.41	0.18	0.03
	$1f_{5/2}$	3.68		0.90	0.76	0.91	0.76	1.01
	2p	2.90		0.70[c]	0.74	0.75[a]	0.70	0.96
	$2d_{5/2}$	0.2		0.05				
^{78}Se	$1g_{9/2}$	2.54	1.73	0.44	0.59	0.55	0.17	0.01
	$1f_{5/2}$	4.01		1.16	0.83	0.94	0.61	1.35
	2p	2.49		0.72[c]	0.82	0.80[a]	0.85	1.20
	$2d_{5/2}$	0.19		0.05				

(cont'd)

TABLE 6.1

(continued)

Isotope	ℓj	$\sum_i S_i(\ell j)$	K	$V^2_{EX}(j)$	$V^2_{EX}(j)$ [Li 65]	$V^2_{Th}(j)$ (b)	$E_{EX}(j)$ (MeV)	$E_{Th}(j)$ (MeV)
^{80}Se	$1g_{9/2}$	2.50	2.12	0.53	0.72	0.70	0.29	0.11
	$1f_{5/2}$	2.90		1.02	0.87	0.96	1.00	1.73
	2p	2.72		0.96[c]	0.88	0.87[a]	0.76	1.48
	$2d_{5/2}$	0.30		0.11				
^{82}Se	$1g_{9/2}$	3.26	2.32	0.76	0.76	0.76	0.76	0.26
	$1f_{5/2}$	2.47		0.96	0.94	0.99	1.24	1.99
	2p	2.51		0.97[c]	0.93	0.92[a]	1.28	1.70
	$2d_{5/2}$	0.34		0.13				

a) $V^2_{Th}(2p) = \left[2V^2_{Th}(3/2) + V^2_{Th}(1/2)\right] / 3$

b) Ref: [Ki 60] using G = 24/A for A = 76 - 82 and λ and Δ determined from solving the gap equation.

c) $V^2_{EX}(2p) = K\left[\sum S\ (3/2) + \sum S\ (1/2)\right] /6$

to 2.47 in ^{82}Se. It is unlikely that so much strength has been missed in the region of excitation below 3.5 MeV and also seems improbable that it should occur in a large number of weakly excited states at higher excitation. The former applies especially to ^{82}Se where a total of 30 states have been observed up to an excitation energy of 3.35 MeV and angular distributions missed for only one of these states. The expected total spectroscopic strength for the $\ell = 4$ transitions should increase from around 2 for ^{76}Se up to a value of 8 for ^{82}Se. The observed $\ell = 4$ spectroscopic strength varies from 2.54 in ^{78}Se to 3.26 in ^{82}Se.

No completely satisfactory explanation can be offered for these deviations from the sum rule values. No discrepancies between the low-lying $\ell = 1,2,3,4$ states could be found between the present data and that of Lin and Sanderson apart from the 1182 keV state in ^{75}Se to which Sanderson assigned $\ell = 1 + 4$ compared to $\ell = 3$ from the present work, and discrepancies in the 1878 keV, 2110 keV and 2280 keV ($\ell = 1$) states in ^{79}Se which were not resolved in the present data.

It may be possible that the DWBA overestimates the cross-sections (in which case the spectroscopic factor will be smaller) due to either the optical parameters used in the DWBA analysis or the method used (Sec. 4.5) to calculate the bound-state wave functions. The latter does not take into consideration the residual interactions between the neutrons. A number of weakly excited states were resolved below 3.5 MeV for which either no angular distributions could be obtained or angular distributions could not be fitted with any value of ℓ. There are 11 such states in ^{75}Se, 14 in ^{77}Se, 7 in ^{79}Se and only one in ^{81}Se. These states will account for some of the deviation from the sum rule, but as mentioned earlier it is unlikely that so much strength has been missed in the region of excitation below 3.5 MeV and especially in ^{81}Se which shows the largest discrepancy.

As Table 6.1 indicates the experimental values of V_j^2 exhibit the expected trend that as neutrons are added the fullness of the shell model orbitals increases. The $1g_{9/2}$ state is about 40% filled in ^{76}Se and 75% filled in ^{82}Se as expected from the pairing plus quadrupole interaction model. The values of $K(S_{(1/2)} + S_{(3/2)})/6$ and $V^2(f_{5/2})$ increase as the shell model fills up and also agree reasonably well with the predicted theoretical values which show that the 2p and $1f_{5/2}$ orbitals are close to completely full for ^{82}Se.

Experimental filling coefficients have also been extracted for the $2d_{5/2}$ orbital. As can be seen from Table 6.1 $V_j^2(2d_{5/2})$increases from 0.05 in ^{76}Se to 0.13 in ^{82}Se. Fournier et al [Fo 73] have reported $\ell = 2$ transitions with experimental filling coefficients of 0.015, 0.01, 0.075 and 0.078 from the ^{72,73,74,76}Ge(p,d) reactions respectively, with the last two values not being very reliable. They suggest that the $2d_{5/2}$ orbital may start filling without the major N = 50 shell being closed.

It is known from previous work that the odd Se nuclei also possess low-lying $7/2^+$ states. States with $\ell = 4$ values and spins of $7/2^+$ (spins known from other work) have been observed in ^{79}Se and ^{81}Se with spectroscopic strengths of 0.08 for both nuclei. This would indicate that the $1g_{7/2}$ orbital is also filling. However the fact that these states occur at low energy seems to preclude this possibility as will be discussed in section 6.3.

The experimental centre-of-gravity energies were obtained using Eq . 6.3 and as can be seen from Table 6.1, the agreement between the experimental and theoretical values is not very good. In general the experimental values are lower than the theoretical values except for $1g_{9/2}$ which are consistently larger than those predicted. The same observation was also made by Lin [Li 65]. Kisslinger and Sorensen [Ki 63]

have pointed out that the simple pairing-plus-quadrupole approximation is not adequate for nuclei in the region $N \sim 40$, $32 \leqslant Z \leqslant 36$, and suggested that both the consideration of the neutron-proton short-range interaction and a better treatment of the phonon-quasiparticle coupling are needed for a truly quantitative treatment.

A strongly excited $\ell = 1$ state is observed in ^{75}Se at 287 keV, which is known from previous work [Ag 73] to be a doublet of $J^{\pi} = 3/2^-$, $1/2^-$. As one progresses to ^{77}Se the $3/2^-$ state moves to higher excitation at 522 keV. A strongly excited $\ell = 1$ state is also observed in ^{79}Se with a spectroscopic strength of 1.15 to which no definite spin assignment has been made. On the basis of the above systematics a spin of $3/2^-$ for this state is expected. This state has also been observed by Lin in (d,p) with a small spectroscopic factor (0.09). This also favours the $3/2^-$ assignment. The nucleus ^{81}Se has a strong $\ell = 1$ transition at 1417 keV. The conclusion that can be drawn from the above discussion is that all Se nuclei possess a strongly excited $3/2^-$ state which moves progressively to higher excitation as N increases. This is what is expected as the Fermi level moves further up as the number of neutrons increases. Also a characteristic of all the Se isotopes is a strongly excited $1/2^-$ state that appears below 280 keV. Lin also observed a $1/2^-$ state in ^{83}Se at 220 keV.

More than 50% of the $\ell = 3$ spectroscopic strength is concentrated in 1 or 2 strongly excited states lying below 776 keV. The levels carrying the remainder of the strength are progressively spread over a wider range in excitation energy as N increases. ^{81}Se seems to constitute an exception to this in that only 2 levels were seen with significant strength, both below 625 keV. No further $\ell = 3$ transitions were seen below 2500 keV. This is significant in that the total $\ell = 3$ strength for this nucleus was the lowest of the four nuclei studied.

All the Se nuclei studied are characterised by a very strongly excited $\ell = 4$ level close to the ground state that carries practically all of the observed spectroscopic strength. Both ^{79}Se and ^{81}Se also have a reasonably strong $\ell = 4$ state above 1 MeV ($S \simeq 0.45$). The isotope ^{81}Se is the only one that possesses a number of weak $\ell = 4$ transitions above 1.8 MeV, some of which are tentative assignments.

A number of weak $\ell = 2$ transitions were observed in each of the nuclei studied with the strength extending to higher excitation with N especially for ^{79}Se and ^{81}Se. The low-lying $\ell = 2$ transitions together with two $\ell = 4$, $J = 7/2^+$ transitions observed in the present work will be discussed in section 6.2.

6.2 Deformed Model Picture

According to the shell model interpretation, the $1g_{9/2}$ neutron and proton odd mass nuclei should have a $9/2^+$ single particle state as either the ground state or as a low-lying excited state. Single particle states with spins of $5/2^+$ or $7/2^+$ should appear a few MeV higher in energy. However, $5/2^+$ and $7/2^+$ states have been observed either as the ground state or as low-lying states in a number of nuclei in this mass region. Table 6.2 gives a summary of the ground states and the known low-lying positive parity states in the four Se isotopes studied in the present work. It is also known that the quadrupole moment of the $5/2^+$ ground state of ^{75}Se is larger [Ze 74] than the expected value and that the $7/2^+$ ground state of ^{79}Se is almost 10 times larger than that expected from the shell model. The measured B(E2) values between low-lying states in this region are also enhanced with respect to the shell model predictions [IK 73].

J. Barrette et al [Ba 74] have shown that in spite of the fact that a $0^{+'}$, $2^{+'}$, 4^+ triplet of states have been identified in the four even-even Se nuclei studied, their characteristics do not agree with the

vibrational model since the ratios of the transition rates $(J_{tr} \rightarrow 2^+)/(2^+ \rightarrow 0^+)$ are consistently smaller than those predicted where $J_{tr} = 0^{+'}, 2^{+'}, 4^+$. For the pure vibrational model the $0^{+'}$, $2^{+'}$ and 4^+ triplet of states should occur at twice the energy of the one phonon 2^+ state and there should be no crossover transitions from the second $2^{+'}$ state to the ground state. In common with a large number of so called vibrational nuclei these criteria are not met by any of the even-even nuclei in this mass region. In ^{72}Ge for example, the second $0^{+'}$ state occurs below the first 2^+ state and in ^{78}Se the order of the triplet states is $2^{+'}$, $0^{+'}$ and 4^+. The Se nuclei also have easily observable crossover transitions from the two phonon $2^{+'}$ state to the ground state [Ba 74].

L.M. Lieder and J. Draper investigated the even selenium isotopes ^{72}Se, ^{74}Se, ^{76}Se and ^{78}Se by means of the Ge(α,2nγ)Se and Ge(α,4nγ)Se reactions. They observed quasi-rotational ground state bands up to 10^+ for ^{76}Se, up to 8^+ for ^{74}Se and ^{78}Se, and up to 6^+ for ^{72}Se. As is well known rotational bands occur in nuclei which may be described as deformed spheroids rotating about an axis perpendicular to their axis of symmetry [Bo 53]. If as indicated by Lieder and Draper, the even Se nuclei are deformed, coupling a neutron to this deformed core stabilizes the deformation and one would expect the odd Se nuclei to be also deformed. This appears to have been confirmed by Zell et al [Ze 75] who observed $5/2^-$ and $9/2^+$ rotational bands in ^{75}Se. Similar $1/2^-$ bands have also been observed in ^{77}Se by Sawa et al [Sa 74].

It should be noted that quasi-rotational bands which have been observed by heavy ion reactions can also be described by the anharmonic vibrator model. Holzwarth and Lie [Ho 72, Li75] applied this model to ^{76}Se, ^{78}Se and to a number of other even-even isotopes in this mass region. They have shown that the model can account for the discrepancies

in the pure vibrational model and can also describe the quasi-rotational bands observed by Lieder and Draper. The model gave a good description of the levels in both of these Se nuclei up to around 2.5 MeV.

There is now considerable evidence from these and other works that have found a growing list of rotational properties for Se and other nuclei in this region. These lead to the conclusion that the nuclei that fill the $1g_{9/2}$ orbital form a new and interesting region of permanent deformation.

6.3 Anomalous Positive Parity States

As shown in Table 6.2 out of the four Se nuclei studied in the present work ^{75}Se and ^{79}Se are known to have ground states of spin and parity $5/2^+$ and $7/2^+$ respectively. These states were observed in the present work. The $J^\pi = 7/2^+$ state in ^{79}Se is very weakly excited as compared to the $J^\pi = 5/2^+$ state in ^{75}Se. A $J^\pi = 7/2^+$ level at 112 keV has also been observed in the ^{76}Se(d,t)^{75}Se reaction by Sanderson [Sa 73]. This state differs by only 20 keV from a strongly excited state at 132 keV to which an unambiguous $\ell = 4$ assignment has been made from the (p,d) reaction. Strongly excited $\ell = 4$ states were also observed in the other Se nuclei. From the remaining two isotopes studied, ^{77}Se has a $7/2^+$ low-lying state at 162 keV [Ra 71]. This state was not resolved, if excited at all, from the strongly excited state at 178 keV to which an $\ell = 4$ has been assigned in the present study. A very weakly excited $\ell = 4$ state was also observed in ^{81}Se at 100 keV to which a spin of $7/2^+$ has been assigned previously by Rabinstein [Ra 71]. The lowest $\ell = 2$ transition in ^{81}Se was found at 1056 keV.

The first attempt to explain the presence of $5/2^+$ and $7/2^+$ low-lying states in the $1g_{9/2}$ odd neutron mass region was made by B. Flowers [Fl 52]. From his calculations in the $1g_{9/2}$ orbital using the seniority coupling model, he arrived at the conclusion that, "within the limits of the jj-coupling approximation, the 7/2 level of the configuration $g_{9/2}^{3,5,7}$

TABLE 6.2

Summary of the ground states and low-lying positive parity state energies in the Se isotopes. The energies are given in keV.

J^π / Isotope	$\frac{1}{2}^-$	$\frac{5}{2}^+$	$\frac{7}{2}^+$	$\frac{9}{2}^+$
^{75}Se		G.S. 625	112[b]	133
^{77}Se	G.S.	302 680	161[b]	178
^{79}Se		623 730	G.S.	137
^{81}Se	G.S.		100	294 780*

b) Not observed in the present work.

*) $\frac{9}{2}^+$ spin used to extract spectroscopic factor.

is never the ground state and would normally be expected to lie above the $9/2^+$ level of seniority one".

Calculations based on the intermediate coupling model were carried out by Kisslinger and Sorensen [Ki 63] employing a pairing plus quadrupole force. This model, known as the quasi-particle phonon coupling model (QPC), fails to predict the low-lying $5/2^+$, $7/2^+$ and $9/2^+$ states with the correct energy spacing and order of spins. Refinements of the pairing plus quadrupole model by Ikegami and Sano [Ik 66] incorporating 9 major shells in the pairing calculations, still predict the $1g_{9/2}$ nuclei to have $9/2^+$ as their lowest positive parity state. These calculations were then improved by the inclusion of quasihole-phonon coupling by Sherwood and Goswami [Sh 67] (EQPC) and by the extension of this latter approach by A. Goswami and O. Nalcioglu to include the quadrupole-quadrupole interaction. This mechanism again failed to completely explain the spectra of nuclei in the $1g_{9/2}$ mass region.

In view of the inability of these spherical model approaches to describe the low-lying positive parity states that are common to the odd neutron nuclei in the $1g_{9/2}$ mass region, together with the evidence for deformation, it is natural to look for an alternative way of describing the properties of the odd Se nuclei. Such an alternative is the Coriolis coupling model.

6.4 Coriolis Coupling Model

In this model the Hamiltonian for the odd nucleon moving in a deformed potential of the rotating core, contains a term $(\underset{\sim}{I}.\underset{\sim}{j})$which couples the motion of the single particle to that of the deformed core and it is known as the Coriolis coupling force. The vector $\underset{\sim}{I}$ is the spin of the nucleus and $\underset{\sim}{j}$ is the spin of the single particle. This force becomes important in nuclei with permanent deformation in that states of the same spin belonging to different rotational bands may be mixed by the rotation-particle coupling (RPC). This model, using a prolate deformation, has

been applied with considerable success to ^{75}Se by Sanderson [Sa 75] and to the odd mass nuclei of the $1g_{9/2}$ subshell ($73 < A < 87$) by Heller and Friedman [He 74]. The model correctly predicts $5/2^+$, $7/2^+$ and $9/2^+$ spins for the low-lying positive parity states that are in good agreement with the experimental data. It also predicts high angular momentum states which may have been observed experimentally in ^{75}Se by Zell et al [Ze 75] from a study of the ^{72}Ge(α, nγ) and ^{73}Ge(α,2nγ) reactions at 15 MeV and 22.5 MeV respectively. An outline of the theory is given in an appendix.

6.5 Coriolis Coupling Calculations

The Coriolis coupling model has been applied to all of the Se isotopes examined in the present study. The calculations were carried out using the program code SNOOPY [Ne 68].

The sequence of calculations is as follows. The Nilsson coefficients $C_{j\Omega\nu}$ and the single particle energies $E_{\Omega\nu}$ were calculated by the program from the diagonalization of the single particle Hamiltonian for a given deformation δ. The values of $\mu = 0.4$ and $\kappa = 0.065$ used, are those used by Sanderson [Sa 73]. The values of the oscillator quanta $\hbar\omega_0$ were calculated from the expression

$$\hbar\omega_0 = \frac{41}{A^{1/3}} \left[1 - \frac{4}{3}\delta^2 - \frac{16\delta^3}{27} \right]^{-1/6} .$$

The core rotational parameter $\hbar^2/2\mathcal{I}_c$ has been estimated from the neighbouring even-even 2^+ state from the expression $\Delta E = (\hbar^2/2\mathcal{I}_c)[I(I+1)]$ for $I = 2$, assuming a rotational character for this state. Since the 2^+ state of the even-even selenium nuclei is at about 600 keV, the above expression gives a value of about 100 keV for $\hbar^2/2\mathcal{I}_c$. The same rotational parameter was used for all bands in the calculations.

Calculations were carried out for deformations in the range $-0.3 < \delta < 0.3$. The deformations which best fitted the data are shown in Table 6.3. Assuming that the Nilsson orbitals shown in Fig. 6.2 are

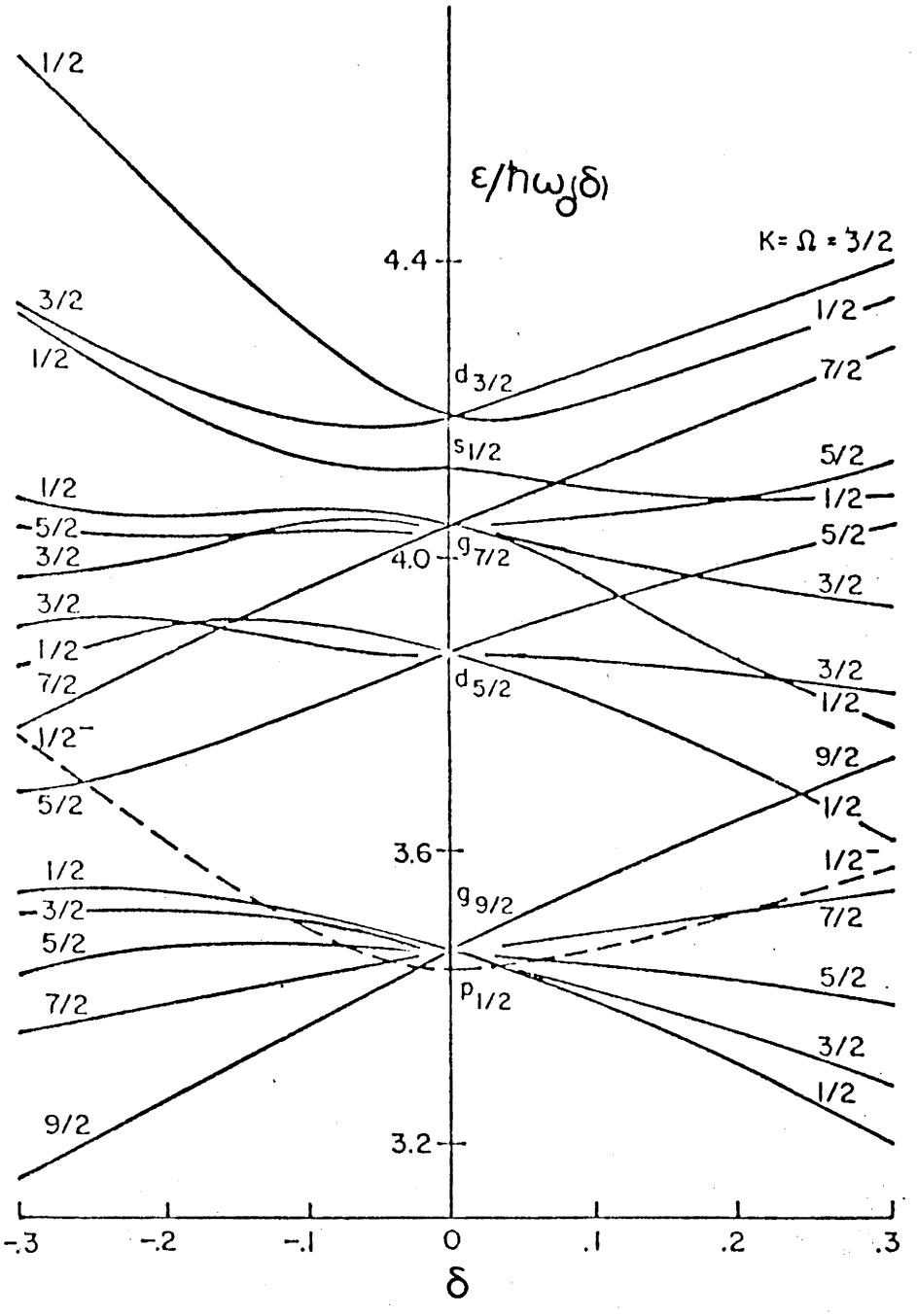

Fig.6.2. Energy-level locations predicted by the Nilsson model as a function of the deformation δ.

filling systematically, the Fermi level was initially placed at the energy corresponding to the single particle orbital in which the last odd neutron was expected to fall. In all the Se nuclei except ^{81}Se, better agreement between the model predictions and both the measured spectroscopic factors and the observed level spacing was obtained when the Fermi level was placed somewhat above the orbital of the last valence neutron. The pairing calculations were carried out for 5 Nilsson single particle orbitals arising from the $1g_{9/2}$ shell model orbital and the $1/2^+$ [431] arising from the $1g_{7/2}$ orbital using a gap parameter of about 1.5 MeV. This value was obtained from the odd-even mass difference formula.

The rotational band head energies are calculated from Eq.17A (Appendix) and added diagonally to the Coriolis coupling matrix elements of Eq.25 (Appendix). Diagonalization of Eq.25 is performed for each value of the total spin I. This gives mixing coefficients and the eigen values of $|IM\rangle$ for the rotational parameter $\hbar^2/2\mathcal{J}$ as a function of the deformation δ. The spectroscopic factor predicted by the model is calculated from the expression in brackets of Eq.31 (Appendix).

No attempt was made in this work to continuously vary all parameters in a least squares search for the best set. The aim of the present calculations was to see whether, by using parameters that were readily obtainable from other work, the Coriolis coupling model could correctly predict the various experimental quantities determined in this work. In the calculations by Heller and Friedman the success of the model was determined from its ability to correctly predict spins with level spacings that agree with the experimental data, while in the present work the additional constraint of the spectroscopic factor was also taken into consideration. Since the principal interest was in the anomalous

states no attempt was made to try and reproduce data for the negative parity states. Heller and Friedman have shown that they were also able to account for the negative parity states arising from the N = 3 orbitals.

Table 6.3 shows the deformations obtained from the present work which gave the best agreement between the model predictions and the experimental data.

	^{75}Se	^{77}Se	^{79}Se	^{81}Se
This work	0.275	0.275	0.275	0.279
[Sa 73]	0.275			
[He 74]	0.19	0.19 -0.265	0.275	0.19

Table 6.3. Comparison of deformations used in the present work with those used by other workers.

The nucleus ^{75}Se was found to have the same deformation of $\delta = 0.275$ obtained by Sanderson [Sa 73]. Heller and Friedman [He 74] obtained somewhat smaller prolate deformations for all isotopes except ^{79}Se. They found that for ^{77}Se $\delta = -0.265$ also gave excellent agreement between the model predictions and the three low-lying positive parity states. The deformations obtained in the present work are essentially constant for all isotopes even though the neutron number is approaching the major shell closure at N = 50.

6.6 ^{75}Se Calculations

The results of the Coriolis coupling calculations are shown in table 6.4. The odd neutron is expected to fall on the $K = 1/2^+$ [440] Nilsson orbital for positive deformation and $9/2^+$ [404] for negative deformation. The best agreement between the data and the spectroscopic

factors and relative energy separations predicted by the model were obtained when the Fermi level was placed in the vicinity of the $5/2^+$ [442] orbital with a deformation of $\delta = 0.275$. The same deformation was also used by Sanderson [Sa 73].

As can be seen from Table 6.4 the model predicts $9/2^+$, $5/2^+$ and $7/2^+$ as the lowest positive parity states with $9/2^+$ having a spectroscopic factor of 2.87 which compares well with the experimental value of 2.72. Experimentally ^{75}Se is observed to have a ground state of $5/2^+$ followed by $7/2^+$ and $9/2^+$ at 112 keV and 133 keV respectively. The model predicted spectroscopic factors for the $5/2^+$ states is about 5 times larger than the experimental value. Placing the Fermi level above the $5/2^+$ [422] Nilsson orbital the calculations gave results that are in good agreement with those obtained by Sanderson. However, the $9/2^+$ state is predicted to have a spectroscopic factor of 3.6 which is in disagreement with the experimental value obtained from this work.

6.7 ^{77}Se Calculations

Table 6.5 presents the results from Coriolis coupling calculations for $\delta = 0.275$. The odd neutron is expected to fall on the $K = 3/2^+$ [431] Nilsson orbital so that the Fermi level is expected to be placed at an energy approximately corresponding to the $K = 3/2^+$ [431] single particle energy. However a better agreement between the model predictions and the data was obtained when the Fermi level was placed slightly above this orbital. As can be seen from the table the agreement between the data and the model prediction for the low-lying positive parity states is very good. The model correctly predicts $7/2^+$, $9/2^+$ and $5/2^+$ states which are in very good agreement with the observed level spacing. The spectroscopic factor for the $9/2^+$ state is 57% larger than the experimental value and that for the $5/2^+$ is about 3 times larger.

TABLE 6.4

Bands included in the calculations. Predicted levels, mixing coefficients and spectroscopic factors for ^{75}Se with $\delta = 0.275$.

E (keV) Exper.	E_{Th} (keV) Theoret.	J^{π}	A_{IK}						Spect.factors	
			$\frac{1}{2}^+$ [431]	$\frac{1}{2}^+$ [440]	$\frac{3}{2}^+$ [431]	$\frac{5}{2}^+$ [422]	$\frac{7}{2}^+$ [413]	$\frac{9}{2}^+$ [404]	S_{Th}	S_{EX}
132	0	$\frac{9}{2}^+$	0.005	0.57	0.64	0.48	0.19	0.03	2.87	2.72
0	58	$\frac{5}{2}^+$	0.01	0.53	0.70	0.47			0.44	0.08
112[c]	364	$\frac{7}{2}^+$	0.35	0.22	0.66	0.67	0.24		0.03	
	815	$\frac{3}{2}^+$	0.04	0.28	0.95				0.01	
	1430	$\frac{5}{2}^+$	0.05	-0.58	-0.1	0.81			0.09	
	1722	$\frac{1}{2}^+$	-0.07	0.99					0.04	

c) Not observed in the present work, but observed by [Su 70, Sa 73]

TABLE 6.5

Bands included in the calculations. Predicted levels, mixing coefficients and spectroscopic factors for ^{77}Se with $\delta = 0.275$.

E_x (keV) Exper.	E_{Th} (keV) Theoret.	J^π	A_{IK}						Spect.factors	
			$\frac{1}{2}^+$ [431]	$\frac{1}{2}^+$ [440]	$\frac{3}{2}^+$ [431]	$\frac{5}{2}^+$ [422]	$\frac{7}{2}^+$ [413]	$\frac{9}{2}^+$ [404]	S_{Th}	S_{EX}
162[c]	162	$\frac{7}{2}^+$	0.03	0.10	0.40	0.74	0.52		0.04	
178	174	$\frac{9}{2}^+$	0.01	0.29	0.48	0.67	0.47	0.12	4.0	2.54
302	325	$\frac{5}{2}^+$	0.02	0.22	0.48	0.85			0.3	0.09
	1089	$\frac{1}{2}^+$	0.99	-0.04					0.06	
	1224	$\frac{3}{2}^+$	0.99	-0.02	0.13				0.10	
	1678	$\frac{7}{2}^+$	-0.11	-0.15	-0.46	-0.30	0.82		0.004	

c) Not observed in this work, but observed by [Ra 71]

Heller and Friedman [He 74] have shown in their calculations that the model predicts, for positive deformation, low-lying $9/2^+$, $7/2^+$ and $5/2^+$ states. They have also found that negative deformation predicts $7/2^+$, $9/2^+$ and $5/2^+$ low-lying states which are in good agreement with the observed level spacing. Calculations carried out in the present study for negative deformation gave $9/2^+$, $7/2^+$ and $5/2^+$ low-lying states. However the spectroscopic factor for the $9/2^+$ state is about 17 times smaller than the experimental value.

6.8 ^{79}Se Calculations

The results from Coriolis coupling calculations for ^{79}Se are shown in Table 6.6. The model correctly predicts the low-lying positive parity states at energies that are in good agreement with the experimental data. The $9/2^+$ state is predicted to have a 92% larger spectroscopic factor. As with the other isotopes, it was found that better agreement between the experimental data and the model calculations was obtained for $\delta = 0.275$ when the Fermi level was placed slightly above the $5/2^+$ [422] orbital. The lowest $5/2^+$ state is predicted at 569 keV with a spectroscopic factor of 0.27. Experimentally an $\ell = 2$ level is observed at 623 keV with a spectroscopic factor of 0.07.

Coriolis coupling calculations for ^{79}Se by Heller and Friedman [He 74] predict closely spaced low-lying $7/2^+$, $5/2^+$ and $9/2^+$ states for the same deformation obtained from the present studies.

6.9 ^{81}Se Calculations

Table 6.7 shows results for the first 6 positive parity states predicted by the Coriolis coupling calculations for $\delta = 0.279$. Here the Fermi level was placed at the $7/2^+$ [413] Nilsson orbital. The model correctly predicts the $7/2^+$ and $9/2^+$ low-lying states at energies that compare reasonably well with the experimental data. The spectroscopic factor for the $9/2^+$ state is 57% larger than the experimental value. As

TABLE 6.6

Bands included in the calculations. Predicted levels mixing coefficients and spectroscopic factors for ^{79}Se with $\delta = 0.275$.

E_x (keV) Exper.	E_{Th} (keV) Theoret.	J^π	A_{IK}						Spect.factors	
			$\frac{1}{2}^+$ [431]	$\frac{1}{2}^+$ [440]	$\frac{3}{2}^+$ [431]	$\frac{5}{2}^+$ [422]	$\frac{7}{2}^+$ [413]	$\frac{9}{2}^+$ [404]	S_{Th}	S_{EX}
0	0	$\frac{7}{2}^+$	0.03	0.06	0.27	0.59	0.76		0.05	0.08
137	101	$\frac{9}{2}^+$	0.02	0.18	0.35	0.59	0.66	0.23	3.95	2.06
	527	$\frac{1}{2}^+$	0.99	-0.03					0.12	
623	569	$\frac{5}{2}^+$	0.05	0.19	0.45	0.87			0.27	0.07
1258	1389	$\frac{5}{2}^+$	0.99	-0.13	0.01	-0.03			0.17	0.03
	1409	$\frac{7}{2}^+$	0.27	0.13	0.48	0.54	-0.62		0.0001	

TABLE 6.7

Bands included in the calculations. Predicted levels mixing coefficients and spectroscopic factors for ^{81}Se with $\delta = 0.279$.

E_x (keV) Exper.	E_{Th} (keV) Theoret.	J^π	A_{IK}						Spect.factors	
			$\frac{1}{2}^+$ [431]	$\frac{1}{2}^+$ [440]	$\frac{3}{2}^+$ [431]	$\frac{5}{2}^+$ [422]	$\frac{7}{2}^+$ [413]	$\frac{9}{2}^+$ [404]	S_{Th}	S_{EX}
100	100	$\frac{7}{2}^+$	0.02	0.04	0.17	0.46	0.872		0.04	0.08
294	236	$\frac{9}{2}^+$	0.02	0.10	0.23	0.49	0.759	0.338	3.79	2.42
	622	$\frac{1}{2}^+$	0.99	-0.03					0.25	
	782	$\frac{3}{2}^+$	0.99	-0.04	0.05				0.36	
1056	1238	$\frac{5}{2}^+$	0.17	0.16	0.43	0.87			0.22	0.09
1310	1520	$\frac{5}{2}^+$	0.97	-0.14	-0.03	-0.16			0.31	0.02

can be seen from the table the model can account for most of the positive parity states below 1.3 MeV. In particular the model was able to predict the movement of the lowest $5/2^+$ state to above 1 MeV in ^{81}Se. Heller and Friedman [He 74] have obtained in their calculations, for a positive deformation of $\delta = 0.19$, low-lying $7/2^+$ and $9/2^+$ states that are in good agreement with the data.

6.10 Conclusion

The Coriolis coupling calculations described in Section 6.6 have been able to give a reasonable account of the low-lying positive parity states in all of the Se isotopes studied; in particular the $5/2^+$ and $7/2^+$ anomalous states. Undoubtedly a more accurate quantitative picture could be obtained if a complete search on all model parameters were made. Nevertheless, the acceptance of the model fits in well with the presence of the other "normal" states in Se and provides a possible answer to several heretofore puzzling questions that arose from the data.

There appears to be no major discrepancies with the level systematics discussed in Section 6.1.2. It should be noted that while no $1/2^+$ or $3/2^+$ levels were observed in the present work, at least one $3/2^+$ level has been identified below 1 MeV from γ-ray work and Sanderson has seen an $\ell = 0$ transition at 611 keV in ^{75}Se with a spectroscopic factor that is well reproduced by the model. To interpret this level in terms of the shell model would require the unlikely population of the $3S_{1/2}$ orbital. In fact the Coriolis coupling model makes it unnecessary to have to assume at all that the shell above N = 50 has started to fill. In general the model predicts spectroscopic factors that are slightly larger than the experimental values.

It had been thought previously [Ka 73] that the anomalous $5/2^+$ and $7/2^+$ states contained very small if any single particle component in their wave functions and that any population of these states in a direct reaction had to be via a compound or a second order direct process.

It was therefore surprising that so many reasonably strong $\ell = 2$ transitions were observed and especially that the quality of the DWBA fits to many of these was excellent. This puzzle is now removed by the Coriolis coupling model.

Unfortunately the problem of large deviations from the expected total strength remains with this model. The Coriolis interaction does indeed push many states up out of the region of excitation studied in this work but the major portion of the strength should still be found at lower excitation. The acceptance of this model also makes it more difficult to unambiguously assign spins to levels, as in the majority of cases both $\ell \pm 1/2$ would be possible.

CHAPTER 7

SUMMARY AND CONCLUSIONS

This chapter presents a summary of the results and the main conclusions drawn from this study of the (p,d) reaction on the Se isotopes.

The following information was obtained from the study:

(a) 88 angular distributions were measured;

(b) spectroscopic factors were extracted for these states;

(c) 40 new ℓ assignments were made;

(d) 22 states were observed for the first time.

A total of 35 $\ell = 1$, 18 $\ell = 2$, 28 $\ell = 3$ and 13 $\ell = 4$ assignments were made. From the shell model picture reliable spin assignments of $5/2^+$, $5/2^-$ and $9/2^+$ respectively can be made to the $\ell = 2,3,4$ transitions observed in this work; only the $\ell = 1$ transitions remain ambiguous. However, if as is more likely, the deformed model provides a better description of these nuclei, then assigning spins becomes more difficult without more accurate calculations than those carried out in the present work.

The angular distributions measured in this study are indicative of the direct reaction mechanism. The DWBA theory is able to fit reasonably well the shapes of the angular distributions especially in the forward scattering region. Despite the good quality of the fits, the unexplained large deviations from the expected total spectroscopic strength throws some doubt on the ability of the deuteron optical parameters used to adequately describe the Se nuclei.

Spectroscopic factors were also extracted in the present study. In the case of ^{75}Se results were compared to those extracted from the

^{76}Se(d,t) reaction by Sanderson and are in reasonable agreement for most of the well resolved states.

Filling coefficients V_j^2 were extracted and compared with the calculated results from the simple pairing theory. Although the normalization constant K is large, the agreement between the theoretical predictions and the normalized V_j^2 are reasonably good. A conclusion that can be drawn is that although the shell model fails to account for the low-lying positive parity states, the simple pairing theory successfully predicts the occupational probabilities. This may be because the pairing theory depends more on the bulk properties of nuclei and is not sensitive to the fine details in the nuclear wave functions.

The spherical shell model with the appropriate residual interactions has failed to adequately describe the odd neutron nuclei in the $1g_{9/2}$ mass region. According to this model, these nuclei are predicted to have $J^\pi = 9/2^+$ as their lowest positive parity state. However low-lying $5/2^+$ and $7/2^+$ states often lie below the expected $9/2^+$ single quasi-particle state. The following models have been proposed to explain this anomaly;

(a) seniority coupling model;

(b) the quasi-particle phonon coupling model (QPC);

(c) the quasi-hole phonon coupling model (EQPC);

and the extension of this latter approach to include quadrupole-quadrupole interactions.

(d) the Coriolis coupling model.

Only the Coriolis coupling model seems capable of correctly predicting spins, parities and level spacings for the odd nuclei in this region. More recently the model has also been successful in predicting magnetic moments for both the ground and first excited states [He 75] that are in very good agreement with the experimental values. Ground state quadrupole moments are also well predicted.

Coriolis coupling calculations from the present work correctly predict the low-lying positive parity states with level spacings and spectroscopic factors that are in reasonably good agreement with the experimental data.

For all of the four Se nuclei studied in the present work the best agreement between the model predictions and the experimental data was obtained for positive deformation. These results reinforce the conclusions of Sanderson and Heller and Friedman that these nuclei have permanent deformation.

It can be concluded that this study has provided spectroscopic information in what has become lately, a very interesting region of the periodic table. A lot of progress has been made recently in understanding this region. However, further experimental work with better energy resolution and complete theoretical calculations are needed.

APPENDIX

CORIOLIS COUPLING MODEL

The Coriolis coupling model is based on the strong-coupling collective model suggested by Bohr and Mottelson. In this model all but the last odd nucleon are incorporated in the deformed core. This deformed core has angular momentum $\underset{\sim}{R}$ and the total Hamiltonian is given by

$$H = \frac{\hbar^2}{2\mathcal{I}_x} R_x^2 + \frac{\hbar^2}{2\mathcal{I}_y} R_y^2 + \frac{\hbar^2}{2\mathcal{I}_z} R_z^2 + H_{sp} + H_{pa} \qquad 1$$

where the first three terms describe the rotation of the core and H_{sp} represents the single-particle motion with respect to the core in the body-fixed coordinates. $\mathcal{I}_x$, $\mathcal{I}_y$ and $\mathcal{I}_z$ and R_x, R_y and R_z are the Cartesian components of the moment of inertia $\mathcal{I}$ and R, and H_{pa} represents the pairing interaction of the core nucleons outside the closed shell.

For spheroidally deformed nuclei with axial symmetry Z we can have (fig. below)

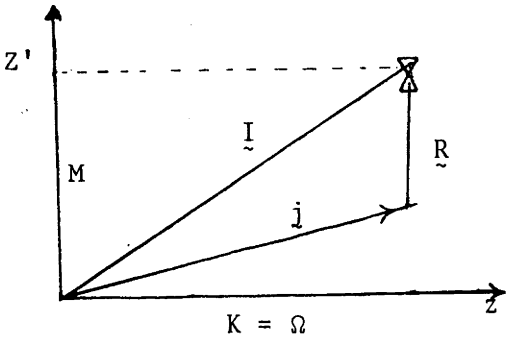

where $\underset{\sim}{I} = \underset{\sim}{R} + \underset{\sim}{j}$. This requires that both $\mathcal{I}_x = \mathcal{I}_y = \mathcal{I}$. If R is normal to z , then Ω the projection of j and K the projection of I into the z symmetry axis are equal, therefore

$$\underset{\sim}{R} = \underset{\sim}{I} - \underset{\sim}{j} \text{ and } R^2 = I^2 + j^2 - 2\underset{\sim}{I}\cdot\underset{\sim}{j} \qquad 2$$

hence

$$H_R = \frac{\hbar^2}{2\mathcal{I}} \left[\underset{\sim}{I}^2 + \underset{\sim}{j}^2 - 2\underset{\sim}{I}\cdot\underset{\sim}{j}\right] \qquad 3$$

The term $2\underset{\sim}{I}\cdot\underset{\sim}{j}$ couples the motion of the particle to the core and is

known as the Coriolis coupling force.

Using the ladder operators

$$I_{\pm} = I_x \pm iI_y, \qquad 4$$

$$j_{\pm} = j_x \pm ij_y$$

and

$$I_+j_- + I_-j_+ = 2(I_xj_x+I_yj_y) , \qquad 5$$

the term $2\underset{\sim}{I}\cdot\underset{\sim}{j}$ can be expressed as

$$2\underset{\sim}{I}\cdot\underset{\sim}{j} = (I_+j_- + I_-j_+) + 2I_zj_z . \qquad 6$$

Substituting eq.6 into eq.3 we obtain

$$H_R = H'_R + H_{pc} = \frac{\hbar^2}{2\mathcal{I}}\left[\underset{\sim}{I}^2+\underset{\sim}{j}^2-2K^2\right] - \frac{\hbar^2}{2\mathcal{I}}\left[I_+j_-+I_-j_+\right] \qquad 7$$

where I^2, j_z and I_z are good quantum numbers with eigenvalues $I(I+1)$, Ω and K respectively.

The total Hamiltonian which couples the odd neutron to the core can now be written as the sum of four terms

$$H = H'_R + H_{sp} + H_{pc} + H_{pa} \qquad 8$$

where the Coriolis coupling, H_{cp}, is the last term of eq.7. The term H_{sp} is the single particle component of the Hamiltonian in a deformed potential which is assumed to possess rotational symmetry such that two principal oscillator frequencies are equal ($\omega_x=\omega_y$). Then the Hamiltonian is given by Nilsson as

$$H_{sp} = -\frac{\hbar^2}{2M}\nabla^2 + \frac{M_r}{2}\left(\omega_x^2x^2+\omega_y^2y^2+\omega_z^2z^2\right) - \kappa\hbar\omega_{oo}(2\underset{\sim}{\ell}\cdot\underset{\sim}{s}+\mu\underset{\sim}{\ell}\cdot\underset{\sim}{\ell}) \qquad 9$$

where the first two terms correspond to a deformed harmonic-oscillator potential and M_r is the reduced mass of the last odd nucleon. The $\underset{\sim}{\ell}\cdot\underset{\sim}{s}$ term is the spin orbit coupling term, and $\underset{\sim}{\ell}\cdot\underset{\sim}{\ell}$ is introduced to reproduce the emperical fact that the high angular momentum states occur lower in energy than predicted by the simple harmonic-oscillator potential.

The frequencies ω_x, ω_y and ω_z are defined by

$$\omega_x^2 = \omega_y^2 = \omega_o^2(\delta)\left(1+\frac{2}{3}\delta\right) , \qquad 10$$

$$\omega_z^2 = \omega_o^2(\delta)\left(1-\frac{4}{3}\delta\right) , \qquad 11$$

with $$\omega_x \omega_y \omega_z = \text{constant} \qquad 12$$

which is the condition for constant volume in the nucleus. From eqs. 10, 11 and 12 the dependence of ω_o on δ is given by

$$\omega_o = \omega_o(\delta=o)\left[1-\frac{4}{3}\delta^2-\frac{16}{27}\delta^3\right]^{-1/6} . \qquad 13$$

The deformation parameter δ is related to the deformation parameter β of Bohr and Mottelson by the relation

$$\delta \approx \frac{3}{2}\left(\frac{5}{4\pi}\right)^{1/2}\beta = 0.946\beta . \qquad 14$$

In solving the eigenstates of H_{sp}, a spherical harmonic oscillator representation is employed, and the values of κ and μ are chosen in such a way that, for $\delta = o$, levels of the spherical model are reproduced. Because of nonspherical symmetry of H_{sp}, the total angular momentum j of the particle is not a good quantum number; however, its projection Ω on the symmetry axis is conserved.

The eigenfunctions of H_{sp} may be written as

$$\chi_{\Omega,\nu} \equiv \sum_j C_{j\Omega\nu}|j\Omega\rangle \qquad 15$$

where $|j\Omega\rangle$ are the wave functions of the unperturbed harmonic oscillator Hamiltonian. The extra index ν has been introduced to distinguish between different Nilsson levels with the same principal quantum number N and the same projection quantum number Ω.

The square of the expansion coefficient expresses the probability that the particle in a given Nilsson orbital has total angular momentum j. Therefore, the sum over j of the squares of the expansion coefficients for a given Nilsson state is unity.

$$\sum_j C^2_{j\Omega\nu} = 1 . \qquad 16$$

For a given (N,ℓ,j) value, the $C^2_{j\Omega\nu}$'s express how the strength has been distributed on the various deformed states. Thus, the sum of the squares times two (because of the Ω-degeneracy) for all Nilsson orbitals, equals the degeneracy, $2j + 1$, of the shell model state:

$$2\sum_{\Omega} C^2_{j\Omega\nu} = 2j + 1 \qquad 17$$

where the summation extends over all states to which the shell model state $|\, j\Omega \rangle$ contributes.

The expansion coefficients $C_{j\Omega\nu}$ and the Nilsson energy of individual nucleons $E_{\Omega i}$, are obtained by diagonalizing the single particle Hamiltonian. The total energy associated with a particular band head is given by [Ne 60]

$$E = \sum_i \frac{1}{2}\,(1+M_r/2m)E_{\Omega i} + \kappa\hbar\omega_{oo}\frac{M_r}{4m}(2\underset{\sim}{\ell}\cdot\underset{\sim}{s}+\mu\underset{\sim}{\ell}\cdot\underset{\sim}{\ell}) \qquad 17A$$

where m is the nucleonic mass and the summation runs over all occupied levels beyond the closed shell.

If we assume that there is no interaction between the rotational and single particle parts of the Hamiltonian, then the total wave function of the nucleus corresponding to a definite total angular momentum I can be written as [Sc 66]

$$\Phi = \left(\frac{2I+1}{16\pi}\right)^{1/2}\left[D^I_{MK}(\theta)\chi_{\Omega\nu}+(-1)^{I-1/2}D^I_{M-K}(\theta)\chi_{-\Omega\nu}\right]\phi^{\Omega}_c \qquad 18$$

where D is a rotational wave function describing the rotation of the system as a whole, ϕ^{Ω}_c is the wave function of the core, and $K = \Omega$ for a symmetric rotor.

When Coriolis coupling is included in the model Hamiltonian the wave function $|IM\rangle$ of the entire coupled system can be expanded in terms of Φ such that

$$|IM\rangle = \left(\frac{2I+1}{16\pi^2}\right)^{1/2}\sum_{K=\Omega\nu}\Sigma A_{K,\nu}\left[D^I_{MK}(\theta)\chi_{\Omega\nu}+(-1)^{I-1/2}D^I_{M-K}(\theta)\chi_{-\Omega\nu}\right]\phi^{\Omega}_c \qquad 19$$

where $A_{K,\nu}$ are the band mixing coefficients. The only good quantum numbers of the system are the total angular momentum I and its projection $\underset{\sim}{M}$ on the space fixed Z' axis.

The eigenvalues corresponding to $H'_R + H_{sp}$ are obtained from the solution of Schrödinger equation [Da 68]

$$H|IMK = \Omega\rangle = (H'_R+H_{sp})|IMK = \Omega\rangle = E_{I,K}|IMK = \Omega\rangle \qquad 20$$

which can be separated such that

$$H_R|IMK\rangle = \frac{\hbar^2}{2\mathcal{I}_o}\,[I(I+1) - 2K^2]|IMK\rangle \qquad 21$$

and $$H_{sp}|j\Omega\rangle = E_\Omega|j\Omega\rangle \quad . \qquad 22$$

Thus

$$E_{I,K} = \frac{\hbar^2}{2\mathcal{I}_o}\,[I(I+1) - 2K^2] + E_\Omega \quad . \qquad 23$$

The level sequence and spacing is given by

$$\Delta E(I,K) = E_{IK} - E_{KK} = \frac{\hbar^2}{2\mathcal{I}_o}\,[I(I+1) - K(K+1)] \quad . \qquad 24$$

When the Coriolis coupling term H_{pc} is considered as a perturbation term to the rotational model; for symmetric nuclei the most general expression for the matrix elements of H_{pc} are

$$\langle IMK'=\Omega'|H_{pc}|IMK=\Omega\rangle = \frac{\hbar^2}{2I_o}\sum_j C^*_{j\Omega'\nu'}C_{j\Omega\nu}\Big\{\Big[\delta_{K',K-1}+(-1)^{I-j}\delta_{K',-(K-1)}\Big] \times \Big[(I+K)(I-K+1)(j+K)(j-K+1)\Big]^{1/2} + \Big[(I-K)(I+K+1)(j-K)(j+K+1)\Big]^{1/2} \times \delta_{K',K+1}\Big\}\langle\phi^{\Omega}_{core}|\phi^{\Omega'}_{core}\rangle \quad . \qquad 25$$

The final term in eq.25 represents the overlap of the core wave functions. From pairing theory this can be reduced to the approximate form of

$$\langle\phi^{\Omega}_{core}|\phi^{\Omega'}_{core}\rangle \simeq U_\Omega U_\Omega + V_{\Omega'}V_{\Omega'} \quad . \qquad 26$$

When $K = \frac{1}{2}$ then

$$\langle IM\tfrac{1}{2}|H_{pc}|IM\tfrac{1}{2}\rangle = (-1)^{I+\frac{1}{2}}\frac{\hbar^2}{2\mathcal{I}_o}(I+\tfrac{1}{2})a_\nu \qquad 27$$

where the decoupling parameter a_ν is defined as

$$a_\nu = \sum_j (-1)^{j+\frac{1}{2}}(j+\tfrac{1}{2})|C_{j\frac{1}{2}\nu}|^2 \quad . \qquad 28$$

These diagonal contributions are to be added to the level spacing relation eq.24

$$E_I = E_K + \frac{\hbar^2}{2\mathcal{I}}\Big\{I(I+1)-K(K+1)+a_\nu\Big[1+(-1)^{I+\frac{1}{2}}(I+\tfrac{1}{2})\Big]\delta_{K,\frac{1}{2}}\Big\} \qquad 29$$

where E_K is the band head energy and $\hbar^2/2\mathcal{I}$ the rotational parameter for the band.

The decoupling parameter can have a very strong influence on the appearance of a $K = \frac{1}{2}$ rotational band. If it is very small, the band will display the usual I(I+1) spacing.

TRANSFER REACTIONS IN DEFORMED NUCLEI

In a deformed nucleus, the spectroscopic strength for a given j is spread over a number of states. The total strength 2j + 1 of the oscillator state j is shared among the $j + \frac{1}{2}$ Nilsson states, each of which can have a maximum strength of $2C^2_{j\Omega\nu}$.

If an even-even target is considered then the cross-section for a pick-up reaction can be written as

$$\left(\frac{d\sigma}{d\Omega}\right)_{\text{pick-up}} = 2C^2_{j\Omega\nu} N\sigma_D(\theta) V_j^2 \quad , \qquad 30$$

where $\sigma_D(\theta)$ is the DWBA cross-section and N = 2.29 for a (p,d) reaction. The $C^2_{j\Omega\nu}$ is the measure of the time for which the nucleon has a total angular momentum j and orbital angular momentum ℓ with projection Ω onto the symmetry axis. When the Coriolis interaction is taken into consideration, levels corresponding to rotational bands with $\Delta K = \pm 1$ mix. This gives rise to interference terms in the cross-section which can affect the intensity distributions for the rotational levels. The wave function of the entire coupled system is given by eq.19 where the $A_{K\nu}$'s are amplitudes of the individual contributions from contributing bands.

The expression for the cross-section for a pick-up reaction then becomes [El 69].

$$\left(\frac{d\sigma(\theta)}{d\Omega}\right)_{\text{pick-up}} = 2 \times 2.29\sigma_D(\theta)\left[\sum_K \sum_{\nu=1}^{n} C_{j\Omega,\nu} A_{K,\nu} V_{j\nu}\right]^2 ,$$

where n is the number of contributing bands. The expression $2\left[\sum_K \sum_{\nu=1}^{n} C_{j\Omega,\nu} A_{K,\nu} V_{j\nu}\right]^2$ is the spectroscopic factor.

REFERENCES

[Ag 73] Y.K. Agarwal, S.M. Bharathi, S.K. Bhattacherioo, B. Lal and B. Sahai, Proceedings of the International Conference on Nuclear Physics, Munich, August 27, 1973, Vol. 1, page 288.

[Ar 65] Argonne National Laboratory, Argonne, Illinois, 60439.

[AT 65] P. Spink and J.R. Erskine, A.N.L. Report 1965, PHY. 1965B.

[Au 64] N. Austern, R.M. Drisko, E.C. Halbert and G.R. Satchler, Phys.Rev. 133B (1964) 3.

[Ba 62] R. Bassel, R.M. Drisko and G.R. Satchler. The Distorted-Wave-Theory of Direct Reactions, ORNL-3240.

[Ba 68] J.B. Ball and C.B. Fulmer, Phys.Rev. 172 (1968) 1199.

[Ba 74] J. Barrette, M. Marrette, G. Lamoureux, S. Monara and S. Markiza. Nucl.Phys. A235 (1974) 154.

[Be 70] R.W. Bercaw and R.E. Warmer, Phys.Rev. C2 (1970) 297.

[Be 69] F.D. Becchetti and G.W. Greenlees, Phys.Rev. 182 (1969) 1190.

[Bh 74] S.M. Bharathi, Y.K. Agarwal, B. Lal, C.V. Baba, submitted to Pramana.

[Bo 55] A. Bohr and B.R. Mottelson, Mat.Fys.Meddr. 27, No.16 (1953).

[Br 74] R.A. Braga and D.G. Sarantites, Phys.Rev. 9C (1974) 1493.

[Bu 64] P. Buttler, Proc.Phys.Soc. 83 (1964) 701.

[Ca 60] C.F. Carter Jr. MIT-LNS.Prog. Report, p.90 (May 1960).

[Ch 75] J. Childs and N.W. Daechnic, University of Pittsburgh-75.

[Co 72] A. Coban, J.C. Willmott, J.C. Lisle and G. Murray. Nuc.Phys. A182 (1972) 385.

[Da 68] J.P. Davidson. Collective Models of the Nucleus, Academ. Press 1968.

[Di 72] F. Dickmann, V. Metag and R. Repnow, Phys.Lett. 38B (1972) 207.

[Du 70] G.G. Dussel and D. Bes, Nucl.Phys. A143 (1970) 623.

[El 69] B. Elbek and P.O. Tjom. Advances in Nuclear Physics, Vol.3, page 259.

[En 71] J.B.A. England, A.N.U.-P/1514.

[En 70] J.B.A. England, A.N.U.-P/1534.

[Fi 70] E. Finckh, V. Jahnke, B. Schreiber and A. Weidingner, Nucl.Phys. A144 (1970) 67.

[Fl 52] B.H. Flowers, Proc.Roy.Soc. 215 (1952) 398.

[Fo 73] R. Fournier, J. Kroon, T.H. Hsu, B. Hird and G.C. Ball, Nucl.Phys. A202 (1973) 1.

[Fr 61] J.B. French and M.H. Macfarlane, Nucl.Phys. 26 (1961) 168.

[Gn 69] G. Gneuss, V. Mosel and W. Greiner, Phys.Lett. 30B (1969) 397.

[Go 68] A. Goswami and O. Nalcioglu, Phys.Lett. 26B (1968) 353.

[Go 73] A. Goswami, D.K. McDaniels and O. Nalcioglu, Phys.Rev. C7 (1973) 1263.

[He 74] S.L. Heller and J.N. Friedman, Phys.Rev. C10 (1974) 1509.

[He 75] S.L. Heller and J.N. Friedman, Phys.Rev. C12 (1975) 1006.

[Ho 72] G. Holzwarth and S.G. Lie, Z.Phys. 249 (1972) 332.

[IM 69] N. Imamishi, M. Sakisaka and Fukuzawa, Nucl.Phys. A125 (1969) 626.

[Jo 70] R.C. Johnson and P.J. Soper, Phys.Rev. C4, 976 (1970).

[Ik 73] H. Ikegami and M. Sano, Jour.Phys.Soc. Japan, Vol. 34, Supplementary 1973.

[Ik 66] H. Ikegami and M. Sano, Phys.Lett. 21 (1966) 323.

[Ki 60] L.S. Kisslinger and R.A. Sorensen, Mat.Fys.Meddr. 9,(1960) 32.

[Ka 73] Norihisa Kato, Nucl.Phys. A203 (1973) 97.

[Ki 63] L.S. Kisslinger and R. Sorensen, Rev.Mod.Phys. 35 (1963) 853.

[Ku 66] P.D. Kunz, University of Colorado Report Coo-535-606 (1966).

[Li 65] E.K. Lin, Phys.Rev. 139B (1965) 340.

[Li 75] S.G. Lie and G. Holzwarth, Phys.Rev. 12C (1975) 1035.

[Li 70] R. Liede and J. Draper, Phys.Rev. C2 (1970) 531.

[Ma 63] E. Marshal, L.W. Person and R.K. Sheline, Rev.Mod.Phys. 35 (1963) 108.

[Ma 67] J. Marion and S. Zimmerman, Nucl.Inst. and Meth. 51 (1967) 94.

[Mc 66] L.C. McIntyre, Phys.Rev. 152 (1966) 1013.

[Mc 71] D.G. McCauley and J.E. Draper, Phys.Rev. C4 (1971) 475.

[McD66] F.A. McDonald and M.H. Hull, Phys.Rev. 143 (1966) 838.

[Me 71] J.J.H. Menet, E.E. Gross, J.J. Malenefy and A. Zucker, Phys. Rev. C4 (1971) 1114.

[ND 66] Nuclear Data B1-4-50, 1966.

[ND 70] Nuclear Data B3-3 (1970) 4.

[Ne 68] GAP 15-16 Niels Bohr Institute Computer Centre Report, R. Casten and C.S. Newton.

[No 70] E. Nolte, W. Kutschera, Y. Shida and H. Morinaga, Phys.Lett. 33B (1970) 294.

[No 75] E. Nolte and P. Vogt, Z.Physik A275 (1975) 33.

[Pe 66] C.M. Perey and F.G. Perey, Phys.Rev. 152 (1966) 923.

[Pr 73] C. Protop, K.O. Zell, H.G. Friedricks, B. Heits and P. vonBrentano, Proc.Int.Conf.Nucle.Phys. 216 (1973) München.

[Ra 71] D. Rabenstein and H. Vona, Z.Naturf.Phys. 26A (1971) 458.

[Ro 74] Robert A, Braga and D.G. Sarantites, Phys.Rev. 4C (1974) 1493.

[Sa 58] G.R. Satchler, Ann.Phys. 3 (1958) 275.

[Sa 69] D.G. Sarantites, Phys.Rev. 4, 177 (1969) 1631.

[Sa 64] G.R. Satchler, Nucl.Phys. 55 (1964) 1.

[Sa 73] N. Sanderson, Nucl.Phys. A216 (1973) 173.

[Sc 66] W. Scholz and F.B. Malik, Phys.Rev. 147 (1966) 836.

[Sc 68] W. Scholz and F.B. Malik, Phys.Rev. 176 (1968) 1355.

[Sc 55] G. Scharff and J. Weneser, Phys.Rev. 98 (1955) 212.

[Sh 65] S. Sherr, B. Bayman, E. Rost, M.E. Rickey and C.G. Hoot, Phys.Rev. 139B (1965) 1272.

[Sh 67] A. Sherwood and A. Goswami, Nucl.Phys. 89 (1967) 465.

[Sk 67] D.J. Skyrme, Nucl.Inst. and Meth. 57 (1967) 61.

[St 58] R.H. Stokes, R. Bock, P. David, H.H. Duhm and T. Tamura, Rev.Sc.Inst. 29 (1958) 61.

[Sa 74] Z.P. Sawa, K. Forssten, F. Ingebretson and F. Walrus, Zagrebe Conference 1974.

[Su 74] T. Sugimitsu, Nucl.Phys. A224 (1974) 199.

[Wy 73] W.G. Wyckhoff and J.E. Draper, Phys.Rev. C8 (1973) 796.

[Ze 75] K.O. Zell, H.G. Friederichs, B. Heits and P. vonBrentano, Z.Phys. A272 (1975) 27.